Compressive Spectrum Sensing in Cognitive IoT

by

Xingjian Zhang

Doctor of Philosophy

School of Electronic Engineering and Computer Science
Queen Mary University of London
United Kingdom

June 2018

Abstract

With the rising of new paradigms in wireless communications such as Internet of things (IoT), current static frequency allocation policy faces a primary challenge of spectrum scarcity, and thus encourages the IoT devices to have cognitive capabilities to access the underutilised spectrum in the temporal and spatial dimensions. Wideband spectrum sensing is one of the key functions to enable dynamic spectrum access, but entails a major implementation challenge in terms of sampling rate and computation cost since the sampling rate of analog-to-digital converters (ADCs) should be higher than twice of the spectrum bandwidth based on the Nyquist-Shannon sampling theorem. By exploiting the sparse nature of wideband spectrum, sub-Nyquist sampling and sparse signal recovery have shown potential capabilities in handling these problems, which are directly related to compressive sensing (CS) from the viewpoint of its origin.

To invoke sub-Nyquist wideband spectrum sensing in IoT, blind signal acquisition with low-complexity sparse recovery is desirable on compact IoT devices. Moreover, with cooperation among distributed IoT devices, the complexity of sampling and reconstruction can be further reduced with performance guarantee. Specifically, an adaptively-regularized iterative reweighted least squares (AR-IRLS) reconstruction algorithm is proposed to speed up the convergence of reconstruction with less number of iterations. Furthermore, a low-complexity compressive spectrum sensing algorithm is proposed to reduce computation complexity in each iteration of IRLS-based reconstruction algorithm, from cubic time to linear time. Besides, to transfer computation burden from the IoT devices to the core network, a joint iterative reweighted sparse recovery scheme with geo-location database is proposed to adopt the occupied channel information from geo-location database to reduce the complexity in the signal reconstruction. Since numerous IoT devices access or release the spectrum randomly, the sparsity levels of wideband spec-

trum signals are varying and unknown. A blind CS-based sensing algorithm is proposed to enable the local secondary users (SUs) to adaptively adjust the sensing time or sampling rate without knowledge of spectral sparsity. Apart from the signal reconstruction at the back-end, a distributed sub-Nyquist sensing scheme is proposed by utilizing the surrounding IoT devices to jointly sample the spectrum based on the multi-coset sampling theory, in which only the minimum number of low-rate ADCs on the IoT devices are required to form coset samplers without the prior knowledge of the number of occupied channels and signal-to-noise ratios. The models of the proposed algorithms are derived and verified by numerical analyses and tested on both real-world and simulated TV white space signals.

Acknowledgments

Foremost, I would like to express my sincere gratitude to my supervisor, Dr. Yue Gao, for his continuous support, patience, and guidance throughout my entire PhD. His immense knowledge, enthusiasm, and encouragement provided me a great opportunity to gain expertise in my area of research. I would like to convey my special thanks to him for spending so much time discussing my work in details and helping me improve my work. His valuable feedback helped shape much of the work in this thesis. Dr. Yue Gao has been my source of courage and inspiration when I hurdle all the obstacles throughout my research work and life in this foreign country. He definitely is the best supervisor I could have during my PhD study.

I would also like to express my appreciation to Professor Clive G. Parini and Professor Andrea Cavallaro for their valuable advice and insightful comments throughout my research work. I am very grateful for all our discussions on my research and scientific writing. I would also like to thank Professor Shuguang Cui (University of California, Davis) and Professor Wei Zhang (University of New South Wales) who gave me lots of constructive comments and suggestions on cognitive radio and compressive sensing.

I also wish to thank and offer my blessings to all the friends in the network, antenna group and WMC lab for creating an enthusiastic and dynamic research environment, especially to those who supported me in any respect during the completion of the research work. I enjoyed all our discussions every day in the lab. You guys made my life in Queen Mary full of happy and unforgettable moments.

Finally, with my love and gratitude, I would like to thank my family, especially my parents and girlfriend, who are always there for me and giving me enormous love, support, and never-ending encouragement. To them I dedicate this thesis.

Table of Contents

List of Figures

List of Tables

List of Abbreviations

ADC   Analog-to-Digital Conversion

AIC   Analog-to-Information Converter

APGL   Accelerated Proximal Gradient Line

AWGN   Additive White Gaussian Noise

AR-IRLS Adaptively-Regularized Iterative Reweighted Least Square

BP   Basis Pursuit

BPDN   Basis Pursuit Denoising

BPF   Band Pass Filter

CBRS   Citizens Broadband Radio Service

CDF   Complementary Distribution Function

CoSamp Compressive Sampling Matching Pursuit

CS   Compressive Sensing

CSS   Cooperative Spectrum Sensing

CP   Cyclic Prefix

CG   Conjugate gradient

DFT   Discrete Fourier Transform

DSA   Dynamic Spectrum Access

DOMP   Distributed Orthogonal Matching Pursuit

DTT   Digital Terrestrial Television

EFT	Exponential Fitting Test
ESC	Environmental Sensing Capability
FCC	Federal Communications Commission
FFT	Fast Fourier Transform
FOCUSS	FOCal Underdetermined System Solver
FPCA	Fixed-Point Continuation with Approximate
GAA	General Authorized Access
IA	Incumbent Access
IHT	Iterative Hard Thresholding
IRLS	Iterative Reweighted Least Squares
JSON	Javascript Object Notation
LASSO	Least Absolution Shrinkage and Selection Operator
LAN	Local Area Network
LP	Linear Programming
MDL	Minimum Description Length
MJD	Multi-channel Joint Detection
MMV	Multiple Measurement Vector
MSE	Mean Squared Error
M2M	Machine-to-Machine
MUSIC	MUltiple SIgnal Classification
MWC	Modulated Wideband Converter
NPRM	Notice of Proposed Rule Making
NI	National Instruments
Ofcom	Office of Communications
OFDM	Orthogonal Frequency Division Multiplexing
OMP	Orthogonal Matching Pursuit
PAL	Priority Access License

PFMJD	Permuted and Filtered Multi-channel Joint Detection
PMSE	Programme Making and Special Events
PSD	Power Spectrum Density
PU	Primary User
PCG	Preconditioned Conjugate Gradient
GAA	Generalized Authorized Access
QMUL	Queen Mary University of London
RF	Radio Frequency
RIP	Restricted Isometry Property
ROC	Receiver Operating Characteristic
r-MSE	Relative Mean Square Error
RREVD	Rank-Revealing Eigenvalue Decomposition
SA-SOMP	Subspace-Augmented Simultaneous Orthogonal Matching Pursuit
SMV	Single Measurement Vector
SNR	Signal to Noise Ratio
SOMP	Simultaneous Orthogonal Matching Pursuit
StOMP	Stagewise OMP
SU	Secondary User
SVT	Singular Value Thresholding
SAS	Spectrum Access System
TVWS	TV White Space
UHF	Ultra High Frequency
U-NII	Unlicensed National Information Infrastructure
WSD	White Space Device

List of Symbols

$\mathbf{A}$	Matrix
$\mathbf{a}_i$	i-th column of $\mathbf{A}$
$\mathbf{A}[i]$	i-th row of $\mathbf{A}$
$\mathbf{A}_{ij}$	ij-th entry of $\mathbf{A}$
$\mathbf{A}^T, \mathbf{A}^H$	The transpose and Hermitian transpose of $\mathbf{A}$
$\mathbf{A}^\dagger$	Pseudo-inverse of the matrix $\mathbf{A}$
$\mathbf{A}_{\mathcal{S}}$	The matrix made of the columns of $\mathbf{A}$ with indices from $\mathcal{S}$
$\|\mathbf{A}\|_{p,q}$	$\ell_{p,q}$ norm of $\mathbf{A}$: $\|\mathbf{A}\|_{p,q} \triangleq (\sum_{i=1}^{L} \|A[i]\|_p^q)^{\frac{1}{q}}$
$\mathcal{I}(\mathbf{A})$	Support of $\mathbf{A}$: $\mathcal{I}(\mathbf{A}) = \{i|\mathbf{A}[i] \neq 0\}$ indicates the indices of rows containing nonzero entries
$\mathcal{W}$	The whole bandwidth of the spectrum of interest
$\mathcal{B}_0$	Bandwidth of each sub-channel
$\mathcal{C}$	Sampling pattern in the multicoset sampling
f_{NYQ}	Nyquist sampling rate
f_s	sub-Nyquist sampling rate
H_0	Hypothesis of PU absent
H_1	Hypothesis of PU present
J	Number of secondary users in the cooperative cognitive radio network
k	Number of non-zero dominant frequency components over the spectrum of interest

k_l^m	Lower bin index of the m-th sub-channel
k_u^m	Upper bin index of the m-th sub-channel
L	Number of samples on each sub-channel
M	Dimension of compressive samples
N	Number of samples over the whole spectrum at Nyquist rate
$n(t)$	White Gaussian noise
N_{sig}	Number of uncorrelated primary signals
P_d	Probability of detection
P_f	Probability of false alarm
p	The number of cosets in the multicoset sampling
$\mathbf{R}$	Correlation matrix of the samples
$\mathcal{S}$	The set of the indices of the occupied channels over the spectrum of interest
$s(t)$	Primary signal in time domain
T_m	Test statistics of the m-th sub-channel
T_s	Sensing time
$\mathbf{\Lambda}$	Diagonal matrix of eigenvalues
$\mathbf{U}$	Matrix whose columns are the eigenvectors so that $\mathbf{RU} = \mathbf{U\Lambda}$.
$\mathcal{W}$	Noise sets containing the indices of the unoccupied spectral components
$\boldsymbol{w}$	Weight vector in IRLS algorithm
$x(t)$	Continuous-time signal with finite energy
$\widehat{\boldsymbol{x}}$, $X(f)$	Fourier transform of $\boldsymbol{x}$
$X_m(f)$	The pieces of the spectrum in the m-th sub-channel
α	Spectrum occupation ratio
β	Extraction ratio in the permutation and filtering scheme
η	Noise uncertainty
κ	Number of occupied sub-channels over the spectrum of interest
λ	Penalty parameter

μ Eigenvector of $\mathbf{R}$

σ_n^2 Noise variance

τ Time offset

ρ Compressive ratio

$\mathbf{\Phi}$ Sensing matrix

$\boldsymbol{\xi}$ Noise perturbation in samples

δ Upper bound of noise perturbation in samples

Ω_ϵ Regularizer in AR-IRLS algorithm

φ_d Predefined threshold in energy detection

Chapter 1

Introduction

The recent developments of Internet of things (IoT) has drawn world-wide attention of both academia and industry with the vision of extending Internet connectivity to a vast number of "things" in our physical world [7]. With turning IoT paradigm into a reality, the amount of IoT devices is expected to grow in large numbers, which leads to difficulty in allocating sufficient spectrum resource to these devices. Therefore, it is the vision that smart IoT devices should have cognitive capabilities to enable spectrum sharing over wideband spectrum [8, 9]. With cognitive capabilities, interference among the IoT devices can be alleviated by seeking for vacant channels through dynamic spectrum access. Spectrum sensing, as one of the vital important technologies in cognitive radio (CR), was proposed to efficiently explore the underutilized spectrum [10]. However, it is unrealistic to directly acquire the wideband signals by conventional Nyquist sampling scheme, especially in the energy-constrained IoT devices, since that requires high sampling rates (double or more than the bandwidth of the signal in frequency domain), resulting in high power consumption in the analog-to-digital converter (ADC) or low sampling rates in sequential manner but introducing large sensing latency.

Therefore, compressive sensing (CS) [11] was applied to to realize wideband spectrum sensing without the high-rate signal sampling and processing. It enables fast and

accurate spectrum detection with sub-Nyquist sampling by exploiting the sparse nature of underutilized wideband spectrum in practice [12, 13]. This thesis will present several algorithms that implement wideband spectrum sensing with CS, aiming to invoking the efficient usage of the underutilized spectrum in cognitive IoT scenarios.

1.1 Motivations and Contributions

The specific motivations and contributions of my Ph.D. research are summarised in the following.

1.1.1 Adaptively-Regularized Compressive Sensing in Cognitive Radio Networks

For implementing compressive spectrum sensing in IoT scenario, accurate signal reconstruction of the wideband signals with less requirements on the signal sparsity and the number of compressive samples is of critical importance to achieve reliable spectrum detection. However, conventional reconstruction algorithms which satisfy the above conditions lead to relatively high computational complexity and need to run through many iterations to achieve the desired signal recovery, which incurs a large latency and is difficult to be implemented in IoT scenario.

In this thesis, an adaptively-regularized iterative reweighted least squares (AR-IRLS) algorithm has been proposed to implement the sparse signal reconstruction, which speeds up the convergence of the signal reconstruction by reducing the required iterations (up to 70%) and provides high fidelity guarantees to cope with the varying bandwidths and power levels over the occupied channels. To further reduce the computational complexity of signal reconstruction, a low-complexity compressive spectrum sensing algorithm is proposed. It could keep the fast convergence speed of previous algorithms such as [14] and AR-IRLS with reduced computational complexity by exploiting the diagonally dominant

feature in the square of measurement matrix. Moreover, to eliminate the impact of noise uncertainty and reconstruction errors, a practical descent-based algorithm for decision threshold setting is proposed. Both the simulation and real-time experiments show that the proposed algorithm outperforms the conventional IRLS algorithms in terms of convergence speed, reconstruction accuracy, and compressive ratio.

1.1.2   Blind Compressive Sensing Augmented Spectrum Sensing

Since increasing number of IoT devices would access the spectrum, the sparsity of target spectrum is fluctuate and unknown. Conventionally, prior knowledge of signal sparsity is adopted or estimated for sparse signal sampling and reconstruction. However, if the signal sparsity is unknown, most of CS approaches assume a high sparsity level and choose the excess number of compressive samples to guarantee the quality of reconstruction. It turns out that these approaches require more sensing time or higher sampling rates to collect compressive samples.

This thesis proposes a blind CS-based sensing algorithm that enables the local SUs to automatically choose the minimum sensing time without knowledge of spectral sparsity or channel characteristics. The compressive samples are collected block-by-block in time and SUs can adaptively adjust the sensing time or sampling rate afterwards. Furthermore, a CS-based blind cooperating user selection algorithm is proposed to select the cooperating SUs via indirectly measuring the degeneration of signal-to-noise ratio (SNR) experienced by different SUs. Numerical and real-world test results demonstrate that the proposed algorithms achieve high detection performance with reduced sensing time and number of cooperating SUs in comparison with the conventional compressive spectrum sensing algorithms.

1.1.3 Distributed Compressive Sensing Augmented Wideband Spectrum Sharing for Cognitive IoT

Most IoT devices are difficult to perform wideband spectrum sensing using either conventional Nyquist sampling system or sub-Nyquist sampling system since both the power-hungry sampling components and intricate sub-Nyquist sampling hardware are unrealistic in the power-constrained IoT paradigm.

In this paper, we propose a distributed sub-Nyquist sensing scheme by utilizing the surround IoT devices to jointly sample the spectrum based on multi-coset sampling theory. Thus, only low-rate ADCs on the IoT devices are required to form coset samplers and minimum number of coset samplers are adopted without the prior knowledge of the number of occupied channels and signal-to-noise ratios. Moreover, to further reduce the number of coset samplers and transfer part of the computational burden from the IoT devices to the core network, we adopt the data from geo-location database when applicable. The experimental results on both the simulated and real-world signals verify the theoretical results and the effectiveness of the proposed scheme. At the meanwhile, it is shown that the adaptive number of coset samplers could be adopted without causing degradation of the detection performance and the number of coset samplers could be further reduced with the assists from geo-location database even when the obtained information is partially incorrect.

1.2 Publication List

Journal Paper

- **X. Zhang**, Y. Ma, Y. Gao and S. Cui, "Real-time Adaptively-Regularized Compressive Sensing in Cognitive Radio Networks", *IEEE Transactions on Vehicular Technology*, vol. 67, no. 2, pp. 1146-1157, Sep. 2017.

- **X. Zhang**, Y. Ma, Y. Gao and W. Zhang, "Autonomous Compressive Sensing Augmented Spectrum Sharing", *IEEE Transactions on Vehicular Technology* (Accepted).

- **X. Zhang**, Y. Ma, H. Qi and Y. Gao, "Low-Complexity Compressive Spectrum Sensing for Large-Scale Real-Time Processing", *IEEE Wireless Communications Letter* (Accepted).

- **X. Zhang**, Y. Ma, H. Qi, Y. Gao and et al, "Distributed Compressive Sensing Augmented Wideband Spectrum Sharing in Cognitive IoT", *IEEE Internet of Things Journal* (Accepted).

- Y. Ma, **X. Zhang**, and Y. Gao, "Joint Sub-Nyquist Spectrum Sensing Scheme with Geolocation Database over TV White Space", *IEEE Transactions on Vehicular Technology*, vol. 67, no. 5, pp. 3998-4007, May 2018.

- H. Qi, **X. Zhang**, and Y. Gao, "Channel Energy Statistics Learning in Compressive Spectrum Sensing", *IEEE Transactions on Wireless Communications* (Major Revision).

- L. Bedogni, A. Trotta, M. Felice, Y. Gao, **X. Zhang**, Q. Zhang, F. Malabocchia, L. Bononi, "Dynamic Adaptive Video Streaming on Heterogeneous TVWS and Wi-Fi Networks", *IEEE/ACM Transactions on Networking*, vol. 25, no. 6, pp. 3253-3266, Aug. 2017.

Conference Paper

- **X. Zhang**, Y. Ma and Y. Gao, "Blind Compressive Spectrum Sensing in Cognitive Internet of Things", *IEEE Global Communications (GLOBECOM)*, Singapore., Dec. 2017, pp. 1-6.

- **X. Zhang**, Y. Zhang, Y. Ma and Y. Gao, "Blind Cooperating User Selection for Compressive Spectrum Sensing in Cognitive Radio Networks", *IEEE/CIC Inter-*

national Conference on Communications in China (ICCC), Qingdao, China, Oct. 2017, pp. 1-6.

- **X. Zhang**, Y. Zhang, Y. Ma and Y. Gao, "RealSense: Real-time Compressive Spectrum Sensing Testbed over TV White Space", *IEEE World of Wireless, Mobile and Multimedia Networks (WoWMoM)*, Macau, China, Jun. 2017, pp. 1-3.

- **X. Zhang**, Y. Ma and Y. Gao, "Autonomous Compressive Spectrum Sensing Approach for 3.5 GHz Shared Spectrum", *IEEE Global Conference on Signal and Information Processing (GlobalSIP)*, Washington, D.C., Dec. 2016, 1378-1382.

- **X. Zhang**, Y. Ma and Y. Gao, "Adaptively Regularized Compressive Spectrum Sensing From Real-time Signals to Real-time Processing", *IEEE Global Communications (GLOBECOM)*, Washington, D.C., Dec. 2016, pp. 1-6.

- **X. Zhang**, Z. Qin and Y. Gao, "Dynamic Adjustment of Sparsity Upper Bound in Wideband Compressive Spectrum Sensing", *IEEE Global Conference on Signal and Information Processing (GlobalSIP)*, Atlanta, GA, Dec. 2014, , pp. 1214-1218.

- Y. Gao, **X. Zhang** and Y. Ma, "Hybrid sub-Nyquist Spectrum Sensing with Geolocation Database in M2M Communications", *Vehicular Technology Conference (VTC) 2017 Fall*, Toronto, Canada, Sep. 2017, pp. 1-5.

- Y. Ma, **X. Zhang** and Y. Gao, "An Efficient Joint Sub-Nyquist Spectrum Sensing Scheme with Geolocation Database over TV White Space", *IEEE International Conference on Communications (ICC)*, Paris, France, May 2017, pp. 1-6.

- Y. Ma, **X. Zhang** and Y. Gao, "Sub-Nyquist Cooperative Wideband Spectrum Sensing based on Multicoset Sampling for TV White Spaces", *IEEE/CIC International Conference on Communications in China (ICCC)*, Chengdu, China, Jun. 2016, pp. 1-6.

- Q. Zhang, **X. Zhang**, Y. Gao, O. Holland, M. Dohler, P. Chawdhry, J. Chareau,

"TV White Space Network Provisioning with Directional and Omni-directional Terminal Antennas", *IEEE Vehicular Technology Conference (VTC) 2016 Fall*, Montréal, Canada, Sep. 2016, pp. 1-5.

- H. Qi, **X. Zhang** and Y. Gao, "Mixture Model-Based Channel Energy Statistics Modeling in Compressive Spectrum Sensing", *IEEE Global Communications (GLOBECOM)*, Abu Dhabi, Dec. 2018 (Accepted).

- H. Qi, **X. Zhang** and Y. Gao, "Channel Energy Statistics Modeling and Threshold Adaption in Compressive Spectrum Sensing", *IEEE International Conference on Communications in China (ICCC)*, Beijing, Aug. 2018 (Accepted).

1.3 Outline of the Thesis

Chapter 2 provides an overview of the background knowledge including cognitive radio in IoT, dynamic spectrum sharing and spectrum sensing.

Chapter 3 proposes an adaptively-regularized CS based spectrum sensing scheme to implement the fast convergence signal recovery in CS-based wideband spectrum sensing. The numerical analyses of the proposed scheme are presented on both simulated and real-world TVWS signals.

Chapter 4 mainly proposes an blind CS-based sensing algorithm that enables the local SUs to adaptively adjust the sensing time and a CS-based blind cooperating user selection algorithm for selecting the cooperating SUs.

Chapter 5 presents a blind joint sub-Nyquist sensing scheme by utilizing the surround IoT devices to jointly sample the spectrum based on the multi-coset sampling theory. Moreover, to further reduce the number of coset samplers and transfer part of the computational burden from the IoT devices to the core network, the data from geo-location database is adopted when applicable.

Chapter 6 draws the conclusion and a plan for the future work.

Chapter 2

Background

In this chapter, Section 2.1 presents the motivations for using cognitive radio (CR) in IoT. Section 2.2 introduces the definition of dynamic spectrum access, which is the key technology for enabling CR, and its structure and the functionalities. Section 2.3 provides a literature review on wideband spectrum sensing. Wideband spectrum sensing can be broadly categorized into two types: Nyquist wideband spectrum sensing and sub-Nyquist wideband spectrum sensing. The former acquires the signals at or above the Nyquist rate, whereas the latter processes signals lower than the Nyquist rate. This section first discusses Nyquist wideband spectrum sensing techniques, i.e., multiband joint detection, wavelet detection, sequential scanning, and filter bank detection in Section 2.3.1. Sub-Nyquist wideband spectrum sensing algorithms are then analysed in Section 2.3.2. Section 2.4 concludes this chapter.

2.1 Cognitive Radio in IoT

The recent developments of IoT has drawn world-wide attention of both academia and industry with the vision of extending Internet connectivity to a vast number of "things" in our physical world [7, 15]. IoT will enable real-world objects to exchange their infor-

mation, interact with people and co-create knowledge. Effective deployment of IoT systems will lead to significant cost savings, new revenues, and employee productivity enhancements. With turning IoT paradigm into a reality, the amount of IoT devices is expected to grow in large numbers. It is projected that there will be approximately 11.6 billion mobile devices and connections by 2020, among which 7.4% are low-power devices [16], which leads to difficulty in allocating sufficient spectrum bands to these devices. Additionally, transmission performance degeneration will be caused due to the overcrowding in the unlicensed industrial, scientific and medical (ISM) bands [17]. CR has been considered as one of the promising solutions to tackle the spectrum scarcity in future wireless networks, i.e., 5G and beyond. CR can sense the surrounding spectrum environment and accordingly adapt radio parameters such as the centre frequency, bandwidth, transmit power, and waveform to utilize spectrum bands currently not used by primary users (PUs). These tasks can be implemented by a basic cognitive cycle: *spectrum analysis, modelling and learning, spectrum sensing, and spectrum management* [18]. In the *spectrum analysis, modelling and learning* step, the secondary user (SU) analyses the spectrum, estimates the PU's transmission parameters, and models the PU's transmission structure through observations over a long time period. This information can then be used to formulate the threshold, noise statistics, etc. in the *spectrum sensing* step. Finally, in the *spectrum management* step, SU adapts itself to transmit in the open bands, potentially changing its carrier frequency, transmit power, modulation type, and packet length. Therefore, it is the vision that smart IoT devices should have cognitive capabilities to enable spectrum sharing over wideband spectrum [8, 9]. With cognitive capabilities, interference among the IoT devices can be alleviated by seeking for the vacant channels through dynamic spectrum sharing.
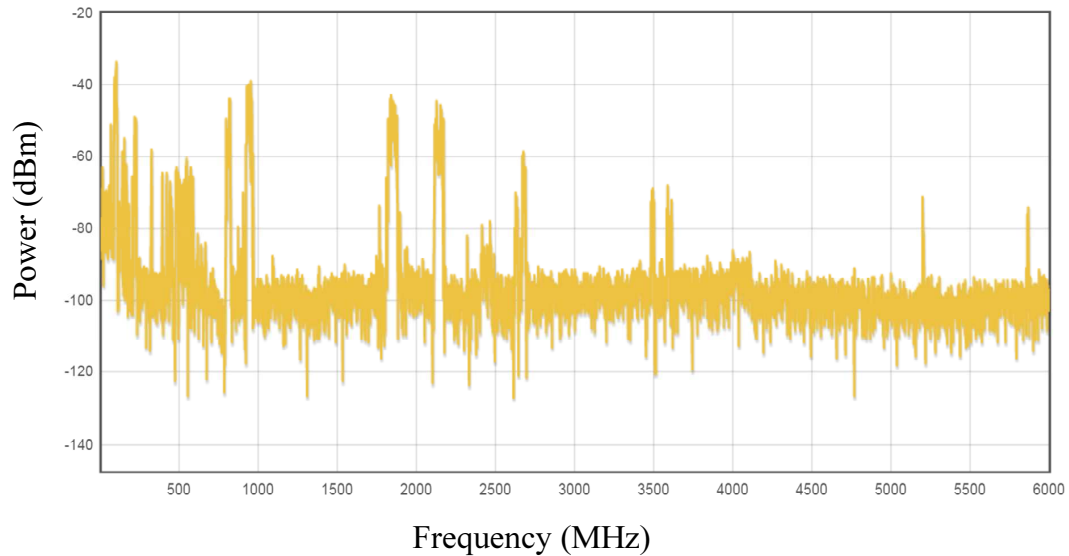
Figure 2.1: The real-time spectrum occupancy recorded at QMUL (51.523021°N 0.041592°W) on November 10th, 2017 and the averaging sampling time is $10s$, where the figure shows that the spectrum is sparsely occupied on $\mathcal{F} = [0, 6000]$ MHz.

2.2   Dynamic Spectrum Sharing

Static spectrum access is the main policy for the current wireless communication technologies, where fixed channels are assigned to licensed users for exclusive use while unlicensed users are prohibited from accessing those channels even when they are unoccupied. Nowadays, regulatory bodies worldwide are facing that the rapid growth of wireless communication industry is overwhelming current static spectrum supply, and thus encourages an urgent need for improved spectrum assignment strategy to mitigate the gap between the available spectrum and the demand [19, 20]. A key finding of the U.S. 2012 President's Council of Advisers on Science and Technology (PCAST) report [21] is that advanced spectrum sharing technologies have the potential to "transform spectrum scarcity into abundance" based on the observation that not every channel in every portion of the spectrum is fully utilized all the time even for the 'busy' spectrum below 6 GHz in the urban areas, as shown in Fig. 2.1. This observation has encouraged the standardization bodies such as Federal Communications Commission (FCC) in U.S. and Office of Communications (Ofcom) in U.K. to release the underutilized licensed bands

such as TV white space (TVWS) [22] and 3.5GHz shared spectrum [23] for temporary secondary access through the use of dynamic wideband spectrum sharing. For example, It has shown that over 50% of locations in the UK are likely to have more than 150 MHz of vacant TV spectrum and that even 90% of locations might have around 100 MHz of spectrum available [22]. Moreover, the superior penetration propagation characteristic over Ultra High Frequency (UHF) spectrum enables TVWS to have longer communication distance and better penetration through obstacles [24], which makes TVWS be an ideal candidate for the long-range wide-area IoT network, especially for the smart agriculture in rural area. Recently, the 3550-3700 MHz (referred to as 3.5 GHz band) Citizens Broadband Radio Service (CBRS), is considered for the spectrum sharing by FCC in the US. Meanwhile, UK Ofcom has published the call for input [25] which considers the 3.8 GHz to 4.2 GHz as the first band where they apply the spectrum sharing framework. In order to share the spectrum efficiently and limit the interference among users, three-tiered spectrum access framework was introduced in the above-mentioned shared spectrums [26, 27], where the incumbent users as the PUs operate at the top tier, while the CBRS users as SUs operate at the second or third tiers holding priority access license (PAL) or generalized authorized access (GAA), respectively. Each tier accepts interference from tiers above and is protected from tiers below. In addition, Ofcom recently issued a *call for inputs*, which tried to gauge interests and assess the potential for enabling enhanced spectrum sharing in the 3.8 GHz to 4.2 GHz band [25]. To put these shared spectrum to good usages, we need fast and reliable occupancy detection of the surrounding spectrum such that no harmful interference caused to the surrounding licensed services, including Digital Terrestrial Televisions (DTT), Programme Making and Special Events (PMSE) users, e.g., wireless microphone systems, and other future incumbent users [27]. Two classes of solutions for addressing these challenges are being considered from engineering and regulatory viewpoints:

- *Spectrum Sensing.* Spectrum sensing [5] is the process that is responsible for detecting the spectrum holes by measuring signal levels cross time and frequency as well

as the potential PUs in a geographical area. Also, it is required for the SU to quickly vacate the channel once the PU reappears such that the harmful interference effect on the licensed users is reduced. For instance, spectrum sensing was an initial ingredient in the standards discussion for the establishment of secondary access to vacated TV channels provided no harmful interference is caused to incumbent services, which requires sensitivity of -120 dBm over 8 MHz for TV channels and -126 dBm over a 200 kHz bandwidth for wireless microphones [22].

- *Geolocation Database.* The other is through a geo-location database that calculates the interference generated in wireless communication systems through theoretical propagation models and then outputs the maximum allowable equivalent isotropic radiated power (EIRP) for each vacant TVWS channel at a specific location and time [28]. The secondary device, also named as white space device (WSD), determines its location and queries the central database that will return a list of available frequency channels and their associated maximum transmit powers at current location. So far, several geo-location database providers, such as Google, Nominet, Spectrum Bridge, etc., have been approved by Ofcom in UK [28].

However, the geo-location database is static method and the dynamics of this scheme depends on how fast the primary spectrum usage information is updated in the database. Besides, it only records the information of the licensed PUs. Consequently, unpredictable dynamic changes of the wireless propagation environment could pose significant challenges to this approach. As the core component of dynamic spectrum access, spectrum sensing aims to obtain awareness about the spectrum usage and the existence of PU in a certain geographical area at a particular duration of time. It allows the SU to detect spectral holes and opportunistically use these under-utilized frequency bands [29]. According to the bandwidth of the spectrum of interest, spectrum sensing can be categorized into two types, narrowband spectrum sensing and wideband spectrum sensing. The term "narrowband" implies that the bandwidth of interest is less than the coherence bandwidth of the channel such that the channel frequency response can be considered as

flat [30]. Therefore, narrowband spectrum sensing only decides whether a particular slice of the spectrum is a hole or not.

Many narrowband spectrum sensing algorithms have been developed in literature, including matched filtering [31], energy detection [32], eigenvalue-based detection [33], feature detection [34], etc.

2.3   Wideband Spectrum Sensing

While traditional narrowband spectrum sensing schemes have focused on exploiting spectral opportunities over narrow frequency range, CR in IoT will eventually be required to exploit spectral opportunities over a wide frequency range from hundreds of megahertz to several gigahertz for achieving higher opportunistic throughput [2] since more and more IoT devices will be online. For instance, to exploit spectrum opportunities in the whole UHF TV band, wideband spectrum sensing techniques should be adopted, which aim to sense a frequency bandwidth that exceeds the coherence bandwidth of the channel. Narrowband spectrum sensing approach cannot be directly used for wideband sensing as it make a single binary decision for the whole spectrum and thus cannot identify individual channel occupancy state that lie within the wideband spectrum.

Wideband spectrum sensing can be broadly categorized into two types in terms of the sampling system: Nyquist wideband spectrum sensing and sub-Nyquist wideband spectrum sensing. The Nyquist wideband sensing utilizes the Nyquist sampling system which require the sampling rate to be at least twice the bandwidth of the signal at baseband according to the Nyquist-Shannon sampling theorem. The common challenge in these approaches is the high implementation complexity due to the required ultra high sampling rates, the high computational complexity of the solutions, and the required sensing time especially when practical considerations are taken into account such as the Automatic-Gain-Control (AGC) settling time, the switching time for the Phase-Locked-Loop (PLL), and the processing delay [35].

The sub-Nyquist wideband spectrum sensing approach acquires signals using a sampling rate below the Nyquist rate by exploring the sparsity nature of the wideband signals which has attracted more and more attention to implement a more flexible and faster wideband spectrum sensing system.

2.3.1   Nyquist Wideband Spectrum Sensing

Wideband spectrum sensing can be simply implemented by a standard ADC to directly acquire the signal and then use the back-end digital signal processing components such as FPGA or CPU to detect the spectrum occupation status.

In [1], a wavelet-based wideband spectrum sensing algorithm was proposed, which formulates the wideband sensing as a spectral edge detection problem and exploits wavelet transform to scan over the wide bandwidth to identify all piecewise smooth subbands. In this algorithm, the power spectral density (PSD) of the wideband spectrum is modelled as a train of consecutive frequency subbands, where the PSD is smooth within each subband but exhibits discontinuities on the border of two subbands. By controlling the smoothing function, the wavelet-based wideband spectrum sensing approach is adaptive to the dynamic spectrum in which the wavelet transform is then used to characterize the edges exhibited in the wideband PSD. Furthermore, in [2], a multiband joint detection
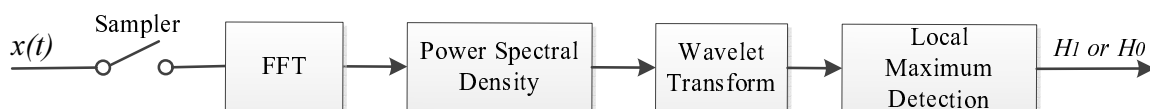
Figure 2.2: Block diagram of wavelet detectionn [1].

(MJD) algorithm was proposed that can sense the PUs over multiple frequency bands jointly. As demonstrated in Fig. 2.3, the wideband signal is firstly sampled by a standard high-rate ADC, after which a serial-to-parallel conversion is utilized to divide sampled data into parallel data sequences. Fast Fourier transform (FFT) is then implemented to convert the received signals into frequency domain. The wideband spectrum is then divided into a series of narrowband spectra $X_f^{(1)}, X_f^{(2)}, ..., X_f^{(M)}$. Finally, spectral occu-

pancy of each narrowband is determined by using the binary hypotheses tests, where H_0 denotes the absence of PUs and H_1 denotes the presence of PUs.
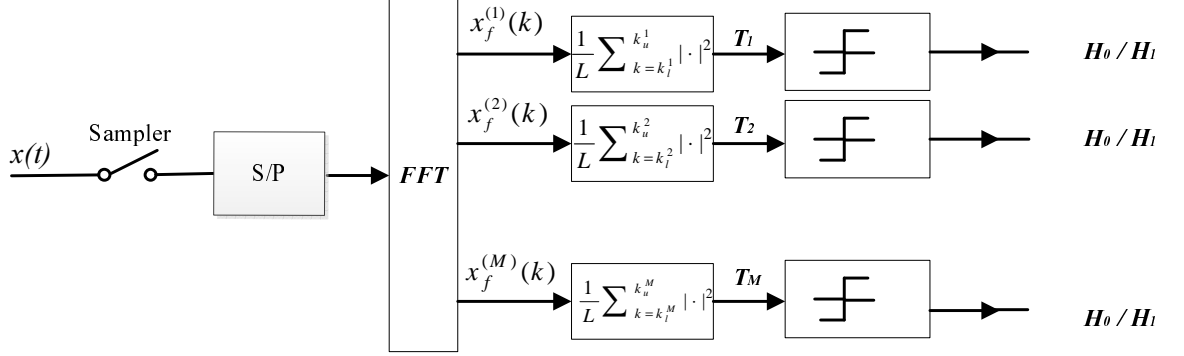
Figure 2.3: Block diagram of multiband joint detection [2].

However, in the wideband regime, a major challenge arises from the stringent requirements on the high sampling rate at the ADC to transform the received signals into digital signals by sampling at the Nyquist rate, which presents significant challenges in the high-speed sampling hardware and signal processing algorithms.

A simple approach to relax the high sampling rate requirement in the wideband spectrum is sequential scanning, which investigates all of the narrow channels one by one to detect the existence of licensed PU transmission [3]. In order to implement this, a tunable narrowband Bandpass Filter (BPF) at the RF frond-end is used to scan one narrowband frequency for every sensing interval. The occupancy of each channel can be determined by measuring the energy of the signal at the output of each filter. However, the BPFs involve with a variable number of RF components and the tuning range of each BPF should be pre-selected. The sequential nature of such a scheme is also slow and inflexible, which could result in missed opportunities or causing interferences to the existing users.

Another solution is the filter bank detection [36]. As shown in Fig. 2.5, the wideband signal to be monitored is passed through a bank of filters with different shifted central frequencies, and the output power of each filter is measured as an estimate of the spectral
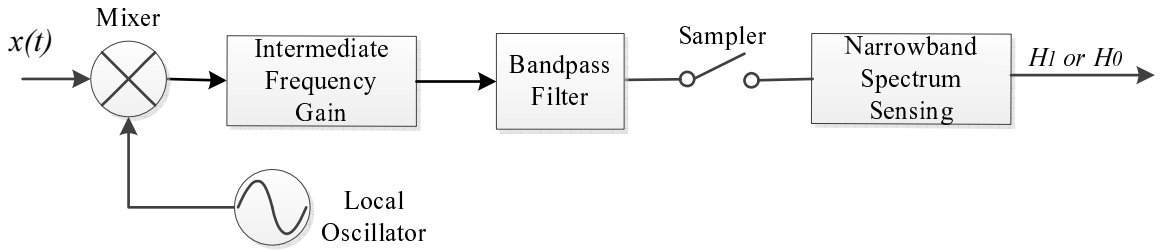
Figure 2.4: Block diagram of sequential scanning [3].

power over the associated subband. This algorithm can therefore capture the dynamic nature of wideband spectrum by using low sampling rates. However, it requires a great number of RF front-end components, e.g., BPFs, ADCs, etc., whose range of and amount are always preset, and are assumed to be a pair of matched root-Nyquist filters [4]. Therefore, it is not practical in the cognitive radio networks.
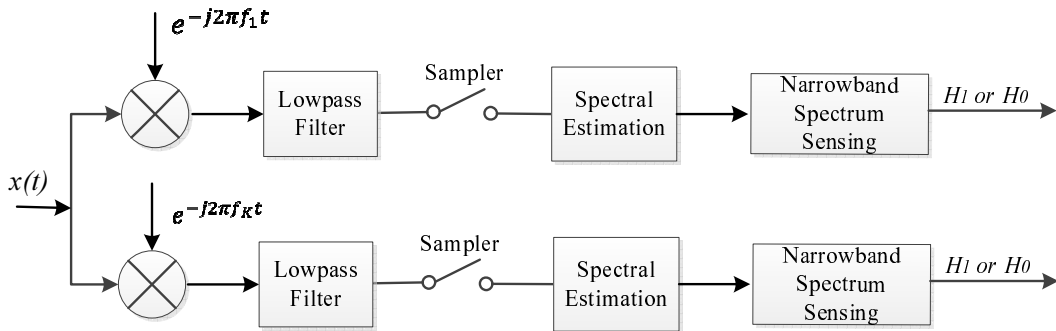
Figure 2.5: Block diagram of filter bank algorithm [4].

2.3.2 Sub-Nyquist Wideband Spectrum Sensing

Due to the major challenges of high sampling rate or high implementation complexity in Nyquist wideband spectrum sensing, sub-Nyquist approaches are drawing more and more attention for fast, efficient, and in-expensive signal processing algorithms, applications, and devices. It was shown in [37] that an arbitrary wideband signal can be perfectly reconstructed if being sampled at a rate no less than the total bandwidth of occupied spectrum, which is also known as Landau rate.

Exploiting the sparse nature of the underutilized wideband spectrum as shown in

Fig. 2.1, sparse representation techniques have shown huge potential capabilities in handling these problems, which are directly related to CS from the viewpoint of its origin [10, 38]. CS theory indicates that if a signal has the sparse structure, i.e., the intra-signal correlation, that signal can be reconstructed by exploiting a few samples, which are much less than the ones suggested by previously used theories such as Nyquist-Shannon's sampling theorem. The entire process of CS consists of three parts: signal sparse representation; measurement collection (linear encoding); sparse reconstruction (nonlinear decoding). These three parts will be discussed as follows.

2.3.2.1 Signal Sparse Representation

Many signals of interest can often be well-approximated by a linear combination of only a few elements from a specific basis due to the sparsity nature. The traditional strategy to exploit this sparsity is to first acquire the signal in a high-dimensional space and then apply a compression method to capture the dominant part in the appropriate basis, such as MP3 for audio signals and JPEG for images. The research area of compressed sensing challenges this strategy by suggesting merging compression and sampling, so that a compressed representation can be obtained directly.

The sparsity of a signal can be often quantified by the l_0-quasinorm in the CS literature, i.e., the number of nonzero elements in the signal under certain domain [39], i.e., Frequency domain. For example, a k-sparse vector in $\mathbb{C}^N$, which can be defined as

$$||\boldsymbol{x}||_0 = |\text{supp}(\boldsymbol{x})| = |\{j : x_j \neq 0\}| \leq k. \tag{2.1}$$

We call the set of indices corresponding to the nonzero entries the *support* of $\boldsymbol{\theta}$ and denote it by $\text{supp}(\boldsymbol{\theta})$. Normally, the signals we are dealing with in the time domain are not sparse. Suppose $\boldsymbol{x}$ can be expressed as a linear combination of $\boldsymbol{\theta} \in \mathbb{C}^N$ in some orthonormal basis $\boldsymbol{\Psi} \in \mathbb{C}^{N \times N}$, e.g., Fourier or wavelet basis, that is $\boldsymbol{x} = \boldsymbol{\Psi}\boldsymbol{\theta}$, we still refer to $\boldsymbol{x}$ as *k-sparse* if $||\boldsymbol{\theta}||_0 \leq k$.

However, the sparse signals are an idealization that we do not encounter in practical applications, e.g., the wideband signals always contain noises. In practice, the original signals tend to be compressible, rather than sparse, where a compressible signal has a representation whose entries decay rapidly when sorted in the decreasing order of magnitude. As a result, compressible signals are well approximated by sparse signals.

2.3.2.2   Compressive Samples Collection

Theoretically, the process of collecting compressive measurements can be viewed as the action of a *sampling matrix* $\boldsymbol{\Phi}$ on the target signal. If we take M measurements, or samples, of a signal in $\mathbb{C}^N$, then the sampling matrix $\boldsymbol{\Phi}$ has dimensions $M \times N$. Therefore, the compressive samples acquisition can be expressed by the following analytical model:

$$\boldsymbol{y} = \boldsymbol{\Phi}\boldsymbol{x} \quad \text{subject to } ||\boldsymbol{x}||_0 \leq k, \tag{2.2}$$

It turns out that the real-world sampling always leads to noise. Thus, (2.2) could be modified to a revised model incorporating the small noise perturbation as

$$\boldsymbol{y} = \boldsymbol{\Phi}\boldsymbol{x} + \boldsymbol{\xi} \quad \text{subject to } ||\boldsymbol{x}||_0 \leq k, \tag{2.3}$$

where $\boldsymbol{\xi} \in \mathbb{R}^M$ is the noise perturbation, whose magnitude is constrained by an upper bound δ, i.e., $||\boldsymbol{\xi}||_2 < \delta$.

A compressive sample is a linear function applied to the signal. Our goal is to push M as close as possible to the signal sparsity k in order to perform as much signal "compression" during acquisition as possible.

For the unique signal reconstruction, the sampling matrix must not map two different k-sparse signals to the same set of samples. A key sampling matrix condition, which used to ensure the accurate signal reconstruction, is known as the restricted isometry property (RIP) [39–41].

Although it is computationally difficult to check the RIP for a given matrix, a striking fact is that many types of random sampling matrices satisfy RIP with high probability, which includes the sampling matrices whose entries following the i.i.d. Gaussian distribution, Bernoulli distribution, and the partial Fourier matrix [39]. For these matrices, the order $2k$ RIP condition is satisfied with overwhelming probability if the number of measurements satisfies the inequality

$$M \geq Ck\log(N/k), \tag{2.4}$$

where C is a constant depending on the specific measurement matrix instance. Therefore, for the above mentioned matrices, there exists a stable algorithm with which the exact sparse signal reconstruction is achievable with overwhelmingly high probability.

An alternative approach to guarantee the stability of CS recovery is to ensure that the sampling matrix $\mathbf{\Phi}$ is incoherent with the sparsifying matrix $\mathbf{\Psi}$. More specifically, incoherence property requires that the rows of $\mathbf{\Phi}$ cannot sparsely represent the columns of $\mathbf{\Psi}$ and vice versa. The mutual coherence between the sampling matrix $\mathbf{\Phi}$ and the representation basis $\mathbf{\Psi}$ is defined as:

$$\mu(\mathbf{\Phi}, \mathbf{\Psi}) = \sqrt{N} \cdot \max_{1 \leq j,k \leq N} |\langle \phi_j, \psi_k \rangle|. \tag{2.5}$$

The coherence measures the largest correlation between any two elements of $\mathbf{\Phi}$ and $\mathbf{\Psi}$. It follows from linear algebra that $\mu(\mathbf{\Phi}, \mathbf{\Psi}) \in [1, \sqrt{N}]$. Within the CS framework, low coherence between $\mathbf{\Phi}$ and $\mathbf{\Psi}$ leads to fewer samples required for signal reconstruction [42].

As the wideband spectrum is normally under-utilized in reality, the received signal $x(t)$ bears a spectrally sparse property in the frequency domain such that all (or most) of its energy is concentrated in one or more disjoint frequency bands, i.e., its spectral measure is small relative to the overall signal bandwidth. This motivates to apply the idea of sub-Nyquist sampling to wideband spectrum sensing that would bring substantial saving in terms of the sampling rate. However, CS has concentrated on finite-length and

discrete-time signals. Thus, innovative technologies are required to extend compressive sensing to the analog domain.

To realize the analog compressive sensing, Tropp et al. proposed a new type of signal acquisition system, called *random demodulator* [43], constructed from low-power, readily available components, which is a good basis for the translation of compressive sampling from theory into practice. The random demodulator employs structured sensing matrices for the acquisition of periodic multitone analog signals. Random demodulator consists of a pseudo-random number generator, a mixer, an accumulator, and a low-rate sampler. The pseudo-random number generator produces a sign waveform that alternates randomly at the Nyquist rate W. Then, the mixer multiplies the continuous-time input signal $x(t)$ by this pseudonoise sequence, which smears the frequency spectrum of the original signal across the entire spectrum. Subsequently, the demodulated signal is intergraded by the accumulator and then sampled using a low-rate sampler for every $1/R$ seconds, where R is the sub-Nyquist sampling rate which is much lower than the Nyquist rate W. The sparse signal can then be reconstructed from the resulting compressive measurements. However, analog signals require a great number of harmonics to approximate them well in the discrete model, which makes the reconstruction computationally infeasible and precludes processing at a low rate.

In [5], Mishali and Eldar proposed another hardware implementation system, named as modulated wideband converter (MWC). The main difference between MWC and random demodulator is that MWC has multiple sampling channels, with the accumulator in each channel replaced by a general low-pass filter. As shown in Fig. 2.6, the analog signal is firstly multiplied with a bank of periodic waveforms, whose period corresponds to the multiband model parameters. Subsequently, the product is low-pass filtered and sampled uniformly at a low rate. One significant advantage of MWC is that it is robust against the noise and model mismatches. Furthermore, the dimension of the measurement matrix is reduced in the proposed framework, efficiently reducing the computation complexity of the spectral reconstruction. However, the implementation is specifically

designed for MWC, and difficult to extend to make it match well with the other existing compressive sensing algorithms.
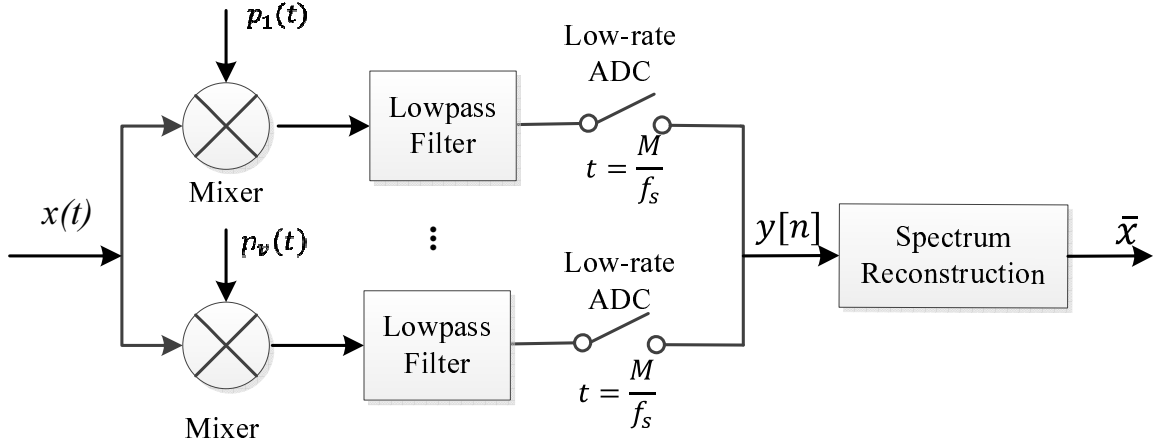
Figure 2.6: Block diagram of modulated wideband converter [5].

An alternative multichannel sub-Nyquist sampling approach is multicoset sampling. Multicoset sampling selects a subset of samples from a uniform grid, which is obtained using a sampling rate f_s at or above the Nyquist rate. The uniform grid is then divided into blocks of M consecutive samples, and in each block only p $(p \leq M)$ samples are retained, while the rest are skipped. Multicoset sampling can be implemented by using p sampling channels with sampling rate of f_s/M and different time offsets on each sampling channel, as shown in Fig. 2.7. The advantage of multicoset sampling is that the sampling rate in each channel is M times lower than the Nyquist rate. Furthermore, the number of measurements is only p/M of that in the Nyquist sampling case. In [44], wideband spectrum sensing scheme based on multicoset sampling was proposed. In addition, a low-speed sub-Nyquist multicoset sampling strategy was proposed in [45] for wideband spectrum sensing without the need of analog front-end processing. However, it requires the knowledge of the spectral support to allow for the perfect reconstruction. In [6], the proposed multicoset sampling based blind multiband signal reconstruction approach only assumes the number of bands and their widths without any other limitations on the support. The major drawback of the multicoset sampling is that accurate time offsets between sampling channels are required to ensure the overall non-uniform sampling.

Another alternative multichannel model for sub-Nyquist sampling in analog domain is
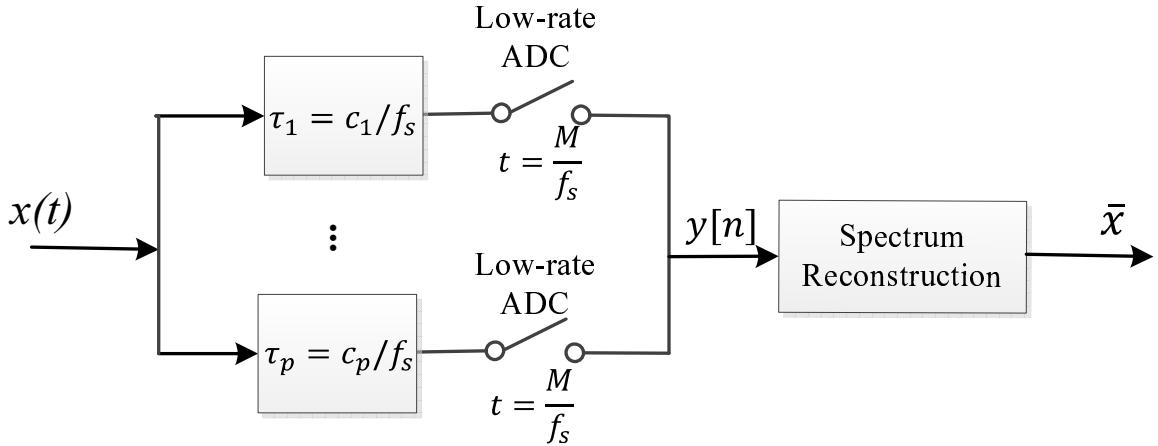
Figure 2.7: Block diagram of multicoset sampler [6].

the multirate sampling. In [46] and [47], Asynchronous multirate sampling (MRS) and synchronous multirate sampling (SMRS) are proposed for reconstructing sparse multi-band signals. However, both of them have high implementation complexity due to its stringent requirements on optical devices. In [48], instead of electro-optical devices, low-rate ADCs are employed in Multi-rate asynchronous sub-Nyquist sampling (MASS). The advantage of multicoset sampling is that it has the robustness against the lack of time synchronisation among channels.

2.3.2.3 Sparse Reconstruction

The major algorithmic challenge in CS is to recover the sparse or compressible signal from the given compressive samples $\boldsymbol{y}$ and sampling matrix $\boldsymbol{\Phi}$, find a signal $\boldsymbol{x}$ such that $\boldsymbol{y} = \boldsymbol{\Phi}\boldsymbol{x}$ exactly or approximately. Specifically, to find the unknown signal $\boldsymbol{x}$ as well as preserve its sparsity from the compressive samples, it is intuitive to consider the following optimization problem

$$\min \|\boldsymbol{x}\|_0 \ \text{ subject to } \ \boldsymbol{y} = \boldsymbol{\Phi}\boldsymbol{x}. \tag{2.6}$$

There exists a wide variety of approaches to solving this problem. We now briefly review four typical types of methods in the literature.

1) Convex Relaxation: In the presence noise, the optimization problem (2.6) can be formulated as

$$\underset{\boldsymbol{x}\in\mathbb{R}^N}{\arg\min}\,||\boldsymbol{x}||_0 \quad \text{subject to } ||\boldsymbol{\Phi}\boldsymbol{x}-\boldsymbol{y}||_2^2 \leq \delta, \tag{2.7}$$

which aims to seek a maximally sparse representation of $\boldsymbol{y}$, or

$$\underset{\boldsymbol{x}\in\mathbb{R}^N}{\arg\min}\,||\boldsymbol{\Phi}\boldsymbol{x}-\boldsymbol{y}||_2^2 \quad \text{subject to } ||\boldsymbol{x}||_0 \leq k, \tag{2.8}$$

which finds the possible minimum reconstruction error at a given sparsity k. In practice, the original signals tend to be compressible, rather than sparse, where a compressible signal has a representation whose entries decay rapidly when sorted in the decreasing order of magnitude. Although compressible signals can be well approximated by sparse signals, the reconstruction errors can only be diminished but not vanished [49]. Therefore, according to the Lagrange multiplier theorem, a proper constant parameter $\lambda > 0$ could be introduced to balance the objective of minimizing the reconstruction error and the solution sparsity, such that problems (2.7) and (2.8) could be equivalently solved by solving the following unconstrained minimization problem:

$$\underset{\boldsymbol{x}\in\mathbb{R}^N}{\arg\min}\,\frac{1}{2}||\boldsymbol{\Phi}\boldsymbol{x}-\boldsymbol{y}||_2^2 + \lambda||\boldsymbol{x}||_0. \tag{2.9}$$

However, problems (2.7), (2.8) and (2.9) are known to be NP-hard in general, which cannot be solved efficiently. It was shown in [50, 51] that the solution via the l_1-norm minimization with sufficient sparsity can be equivalent to the solution obtained by the l_0-norm minimization, where the l_1-norm optimization problem can be solved in polynomial time. This adaption leads to the following minimization problem, known as *Basis Pursuit (BP)*.

Therefore, problems (2.7), (2.8) and (2.9) can be efficiently and approximately solved by solving the following problems:

$$\underset{\boldsymbol{x}\in\mathbb{R}^N}{\arg\min}\,||\boldsymbol{x}||_1 \quad \text{subject to } ||\boldsymbol{\Phi}\boldsymbol{x}-\boldsymbol{y}||_2^2 \leq \delta, \tag{2.10}$$

or equivalently,

$$\arg\min_{\boldsymbol{x}\in\mathbb{R}^N} \frac{1}{2}||\boldsymbol{\Phi}\boldsymbol{x} - \boldsymbol{y}||_2^2 + \lambda||\boldsymbol{x}||_1. \tag{2.11}$$

It is known as the *Least Absolution Shrinkage and Selection Operator (LASSO)* [52] problem, where λ is the penalty parameter for balancing the reconstruction accuracy and the sparsity of the minimization result. Since $||\boldsymbol{\Phi}\boldsymbol{x} - \boldsymbol{y}||_2^2$ is a convex quadratic function, (2.11) is shown to be efficient under certain conditions in finding a sparse representation to achieve a small $||\boldsymbol{\Phi}\boldsymbol{x} - \boldsymbol{y}||_2^2$ [53].

In summary, this class of algorithms solves a convex optimization problem to reconstruct the signal. The number of measurements required for exact reconstruction is small but these methods are computationally complex. So it may not be very efficient for the large-scale problems.

2) Greedy Algorithm: Another class of CS reconstruction algorithms is the greedy algorithm. These methods are iterative in nature and select columns of $\boldsymbol{\Phi}$ based on their correlation with the measurements $\boldsymbol{y}$ determined by an appropriate inner product. They solve the reconstruction problem by making locally optimal choices at each step until a convergence criterion is met. Examples include orthogonal matching pursuit (OMP) [54], stagewise OMP (StOMP) [55], compressive sampling matching pursuit (CoSaMP) [56]. The major advantages of this algorithm are its high speed of recovery and its ease of implementation. Taking CoSaMP as an example, given the measurement vector $\boldsymbol{y}$ and the measurement matrix $\boldsymbol{\Phi} = [\phi_1, ..., \phi_N]$, the algorithm can be summarized as follows:

- Initialize the residual $\boldsymbol{r}_0 = \boldsymbol{y}$, the index set $\Lambda_0 = \emptyset$, $J_0 = \emptyset$, and the iteration counter $t = 1$.

- Find the $2k$ indices corresponding to the largest magnitude entries and store them in J_0 by solving the optimization problem:

$$\arg\max_{n=1,...,N} |\langle \boldsymbol{r}_{t-1}, \phi_n \rangle|. \tag{2.12}$$

- Augment the index set and the matrix of chosen atoms: $\Lambda_t = \Lambda_{t-1} \cup J_0$ and $\boldsymbol{\Phi}_t = [\boldsymbol{\Phi}_{t-1} \ \ \phi_{\lambda_t}(\text{for all} \ \ \lambda_t \in J_0)]$.

- Solve a least square problem to obtain a new signal estimate:

$$\boldsymbol{x}_t = \arg\min_{\boldsymbol{x}} ||\boldsymbol{y} - \boldsymbol{\Phi}_t \boldsymbol{x}||_2 = (\boldsymbol{\Phi}_t^T \boldsymbol{\Phi}_t)^{-1} \boldsymbol{\Phi}_t^T \boldsymbol{y}. \tag{2.13}$$

- Select the k largest elements from $\boldsymbol{x}_t$ as $\boldsymbol{x}_{tk}$ and the corresponding atoms in $\boldsymbol{\Phi}_t$ as $\boldsymbol{\Phi}_{tk}$ and the index set $\Lambda_t = \Lambda_{tk}$.

- Calculate the new approximation of the data and the new residual:

$$\boldsymbol{a}_t = \boldsymbol{\Phi}_{tk} \boldsymbol{x}_{tk}, \quad \boldsymbol{r}_t = \boldsymbol{y} - \boldsymbol{a}_t. \tag{2.14}$$

- If the stopping condition is achieved, stop the algorithm. Otherwise, increment t, and return to Step 2.

3) Non Convex Minimization Algorithm: Another reconstruction approach is to relax the ℓ_0-norm to l_ν-quasinorm $(0 < \nu < 1)$, defined as $||\boldsymbol{x}||_\nu = (\sum_{j=1}^{N} |x_j|^\nu)^{1/\nu}$, which is possible to achieve the exact reconstruction with substantially fewer measurements [57] and could be formulated as

$$\arg\min_{\boldsymbol{x} \in \mathbb{C}^N} ||\boldsymbol{x}||_\nu \quad \text{subject to} \ ||\boldsymbol{\Phi}\boldsymbol{x} - \boldsymbol{y}||_2^2 \leq \varsigma. \tag{2.15}$$

As the l_ν norm minimization provides a closer approximation to the l_0 norm minimization, it is a more efficient solution to exactly reconstruct the original signals with less requirements on the signal sparsity and the number of measurements. The l_ν norm minimization is nonconvex but could be solved by iteratively reweighted least squares (IRLS) algorithm [58]. Each iteration of the IRLS algorithm corresponds to a weighted least-squares problem which can be efficiently solved by standard convex optimization methods.

Sparse Bayesian framework: Besides the aforementioned convex and non-convex minimization and greedy algorithms, there are a number of computational approaches for solving the original sparse recovery problem. Recently, sparse Bayesian learning framework has been derived to find robust solutions in sparse signal recovery [59]. Sparse Bayesian framework formulates the CS problem via the Bayesian rule, and its close relationship to the non-convex l_ν-norm ($0 < \nu < 1$) minimization problem is derived in [60]. Different from the traditional convex relaxation algorithms [52], whose global minimum is generally not the sparsest solution [61], the global minimum of sparse Bayesian framework is always the sparsest one. More specifically, in sparse Bayesian framework, a prior distribution for the unknown vector is assumed to find the posterior probability $p(\boldsymbol{x}|\boldsymbol{y};\boldsymbol{\theta})$ based on Bayesian algorithm, which have superior recovery performance, especially in the presence of high correlation of rows in the measurement matrix, high noise level, or poor signal sparsity [59]. The more details of sparse Bayesian framework based CS model can be found in [62].

4) Joint Sparse Recovery: In practice, the common sparse support among the SUs enables an efficient reconstruction algorithm to recover all of the signals *jointly*. Specifically, multiple SUs acquire the same primary signal but with different phase shifts or attenuations caused by different signal propagations. Thus the primary signals received at all SUs share a common sparse support with different amplitudes, known as *joint sparsity* [63].

Suppose that J ($J > 1$) SUs are performing sub-Nyquist sampling individually to collect their low-rate measurements $\boldsymbol{y}^{(j)}$, which can be expressed as $\boldsymbol{y}^{(j)} = \boldsymbol{\Phi}^{(j)}\boldsymbol{x}^{(j)}$. The vector model has been extended to a finite set of sparse vectors sharing a common sparsity pattern. The SUs share their compressive measurements, rather than original Nyquist samples to reduce communication overhead, with a fusion centre that will recover the underlying joint support. The overhead in delay and energy caused by cooperative sensing is mitigated by processing sub-Nyquist samples. In this setting, rather than trying to recover a single sparse vector $\boldsymbol{x}$ seperately, the goal is to jointly recover a set

of vectors $\boldsymbol{x}(j)$, $j = 1, ..., J$ that share a common support. Stacking these vectors into the columns of a matrix $\boldsymbol{X}$, there will be at most k non-zero rows in $\boldsymbol{X}$. The support of $\boldsymbol{X}$ denotes the union of the supports of the columns of $\boldsymbol{X}$, or equivalently, the set of indices of non-zero rows. This class of algorithm is known as the *multiple measurement vectors* (MMVs) problem [64].

In order to determine the support of $\boldsymbol{x}(j)$, $j = 1, ..., J$, joint sparse property in the frequency domain is exploited. There are existing algorithms for recovering jointly sparse signals in the literature [65, 66]. In [67], Tropp and Gilbert have proposed an iterative algorithm, called Simultaneous Orthogonal Matching Pursuit (SOMP), which can be readily applied in this joint sparse recovery framework. To adapt the SOMP algorithm to the cooperative spectrum sensing setting, it is first extended to cover a different sampling matrix $\boldsymbol{\Phi}^{(j)}$ for each received signal $\boldsymbol{x}^{(j)}$ at the SU. Then, in each iteration, the column index $n \in \{1, 2, ..., N\}$ is selected that accounts for the greatest amount of residual energy across all SUs [68]:

$$\lambda_t = \underset{n=1,...,N}{\arg \max} \sum_{j=1}^{J} |\langle \boldsymbol{r}_{t-1}^{(j)}, \phi_n^{(j)} \rangle|. \qquad (2.16)$$

It's important to notice that joint spectrum recovery requires much less samples for each SU comparing with separate recovery scheme, which further reduces power and bandwidth for communication and memory size for storage.

2.4 Summary

This chapter presents current development on cognitive IoT, dynamic spectrum access, spectrum sensing, and wideband spectrum sensing, as well as the fundamental concepts of compressive sensing. From the literature, there are three major challenges when implementing sub-Nyquist wideband spectrum sensing in cognitive IoT. First is the high computational burden. For the sub-Nyquist spectrum sensing, signal reconstruction is

required before the decision making. In other words, It looks like part of implementation complexity of Nyquist wideband spectrum sensing is transfer to computational complexity in the signal reconstruction, therefore, how to reduce the computational complexity with reconstruction performance guarantee is a challenge for implementing Cognitive IoT. Secondly, in conventional CS, these methods tend to require more sensing time or higher sampling rate because of high sparsity level assumption. Thirdly, most sub-Nyquist sampling scheme need special sampling hardware, which is difficult to be added on the commercial IoT devices.

Chapter 3

Adaptively-Regularized Compressive Sensing in Cognitive Radio Networks

Wideband spectrum sensing is regarded as one of the key functional blocks in cognitive radio systems to enable cognitive IoT, where compressive sensing (CS) has become one of the promising techniques to deal with the Nyquist sampling rate bottleneck. However, the implementation of CS over real-world signals and real-time processing poses significant challenges due to the high computational burden and reconstruction errors against noise. In this chapter, an adaptively-regularized CS based spectrum sensing scheme is proposed to implement the real-time signal recovery in CS-based wideband spectrum sensing. Specifically, the related work on CS-based wideband spectrum sensing and main contributions of this chapter are firstly reviewed in Section 3.1. In Section 3.2 and 3.3, each block of the proposed adaptively-regularized CS scheme and low-complexity reconstruction algorithm are illustrated. In Section 3.4, the real-time compressive spectrum sensing testbed are presented. The simulations for the performance evaluation of the proposed sensing scheme are demonstrated in Section 3.5 on the simulated and real-world

TV white space (TVWS) signals. Finally, Section 3.6 concludes this chapter.

3.1 Introduction

3.1.1 Related Work

To overcome the Nyquist sampling rate bottleneck of the conventional wideband spectrum sensing, several new compressive sampling based spectrum sensing methods have been proposed [69–74], where the sampling rate could be reduced by exploiting some specific features of the spectrum. In [69], a compressive spectrum sensing approach over wide spectrum was proposed by utilizing the embedded sparsity of the edge spectrum. In [70, 71], power spectrum estimation over the compressive samples has been proposed by concentrating on the autocorrelation of the compressive samples instead of the original signal itself. In [72–75], sub-Nyquist sampling approaches have been developed based on multicoset sampling to estimate the spectrum by recovering the frequency support of the multiband signals. Although these algorithms can reduce the sampling requirement and computational complexity, they depend on prior spectral assumptions such as fixed channel bandwidth and power levels and concentrate on the partial signal reconstruction.

In recent years, as the secondary spectrum market has been opened for spectrum sharing, an increasing number of programme making and special event (PMSE) users are joining for public access, which cover a wide range of radio systems, e.g., wireless microphones, continuous talkback systems, high-quality audio links, remote controllers, etc [76]. As PMSE users have varying channel bandwidths and radiated levels (up to 200kHz and 10mW respectively), accurate detection of the PMSE users and other PUs with varying power levels challenges the traditional compressive spectrum sensing algorithms [69–71]. Therefore, the full reconstruction of the wideband signals with the high fidelity guarantee is of critical importance to work with real-world signals in achieving reliable spectrum detection.

To find the optimal solution that best matches the compressive projections, the original wideband signals can be reconstructed using certain optimization strategies based on l_0-norm minimization [49]. Since l_0-norm minimization is an NP-hard problem, l_1-norm minimization is usually utilized to find an equivalent solution based on the restricted isometry property (RIP) [11]. To further improve the recovery performance with less requirements on the signal sparsity and the number of compressive samples, the weighted l_ν-norm $(0 < \nu < 1)$ minimization is proposed to replace the l_1-norm minimization, which is nonconvex but could be solved by iterative reweighted least squares (IRLS) algorithm [58]. As the l_ν-norm minimization provides a closer approximation to the l_0-norm minimization, the weighted l_ν-norm minimization is a more efficient solution to exactly reconstruct the original signals [57, 61, 77, 78]. However, without any prior information on the original signals, conventional IRLS algorithms could lead to relatively high computational complexity and need to run through many iterations to achieve the desired signal recovery, which incurs a large latency and is difficult to be implemented in real-time processing [57].

In addition, the performance of spectrum sensing greatly depends on the detection methods over the reconstructed signal. Energy detection is the most widely used detection method since it is simple, to implement and does not require any prior information about the spectral, features of primary signals [79, 80]. Most conventional energy detection algorithms adopt a fixed or adaptive decision threshold to distinguish PU signals from the noise [81], which is calculated via prior knowledge over the noise power. However, it is difficult to guarantee the detection and false alarm probabilities with the traditional threshold setting algorithms when the noise power is unknown or fluctuates in real-time wideband spectrum sensing. In [82], the decision threshold setting is based on the noise power measured in the vacant channels. However, it is difficult to distinguish which channels contain noise only without related prior information in practice. Moreover, the power level of noise is likely to change after the reconstruction process [13]. Besides, we notice that most of the existing compressive wideband spectrum sensing

schemes do not specify the reconstruction errors from the compressive samples, which inevitably exists and interferes the detection. Therefore, a practical and effective reconstruction strategy that can dynamically eliminates the influence of CS reconstruction errors and distorted noise floors is critical to enable accurate real-time wideband spectrum sensing.

3.1.2 Contributions

Motivated by the above challenges, the contribution of this paper is four-fold.

1. Firstly, an adaptively-regularized CS scheme is proposed to implement the real-time wideband spectrum sensing in this chapter. Specifically, the proposed adaptively-regularized iterative reweighted least squares (AR-IRLS) reconstruction algorithm moves the estimated solutions along an exponential-linear path by regularizing weights with a series of nonincreasing penalty terms and the penalty parameter which balances the reconstruction accuracy and the sparsity is adaptive to the varying noise levels. The proposed scheme significantly speeds up the convergence of the signal reconstruction by reducing the required iterations (up to 70%) and provides high fidelity guarantees to cope with the varying bandwidths and power levels over the occupied channels.

2. Secondly, to further reduce the computational complexity in the signal reconstruction, a low-complexity IRLS-based reconstruction algorithm is proposed. It could keep the fast convergence speed of the previous algorithms such as [14] and AR-IRLS with reduced computational complexity by exploiting the diagonally dominant feature in the square of measurement matrix.

3. Thirdly, a descent-based decision threshold setting algorithm is proposed to distinguish the primary signals from the mixture of the reconstruction errors and unknown noises.
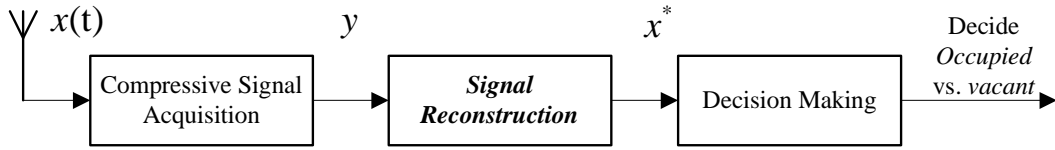
Figure 3.1: Block diagram of CS-based wideband spectrum sensing scheme.

4. Finally, to verify the CS-based spectrum sensing scheme in real-world scenarios, a real-time compressive spectrum sensing testbed is proposed to process the real-time data collected from the TVWS spectrum. From the evaluation of the reconstruction performance, it is shown that the proposed AR-IRLS algorithm is able to deal with real-world signals in real-time wideband spectrum sensing, with improvements over the convergence speed as well as sensing cost when compared with conventional iterative l_ν-norm minimization approaches.

3.2 Adaptively-regularized CS Based Spectrum Sensing

The proposed adaptively-regularized CS-based wideband spectrum sensing scheme can be presented as a typical three-step framework: compressive signal acquisition, signal reconstruction by the proposed AR-IRLS algorithm and decision making by the proposed descent-based threshold setting algorithm, as shown in Fig. 3.1.

3.2.1 Compressive Signal Acquisition

The basic idea of CR is spectrum sharing, which allows the unlicensed users, i.e., SUs, to communicate over licensed spectrum when the bands are not fully utilized by PUs. The received signal $x(t)$ at the CR is usually assumed to be bandlimited and continuous, which consists of N_{sig} uncorrelated primary signals in addition to the noise. The primary signals are superposed in the time domain but occupied the different region of the spectrum, such that

$$x(t) = \sum_{i=1}^{N_{\text{sig}}} s_i(t) + n(t), \tag{3.1}$$

where $s_i(t)$ is the i-th primary signal and $n(t)$ refers to additive white Gaussian noise with zero mean and variance σ_n^2. Since the wideband spectrum is practically underutilized [83], $x(t)$ typically bears a sparse property in the frequency domain such that its discrete Fourier transform $\boldsymbol{x} \in \mathbb{R}^N$ is a k-sparse vector, i.e., $|\{x_i \ : \ x_i \neq 0\}| \leq k$. The compressive samples acquisition at each SU can be expressed by the following analytical model:

$$\boldsymbol{y} = \boldsymbol{\Phi}\boldsymbol{x} + \boldsymbol{\xi} \quad \text{subject to } ||\boldsymbol{x}||_0 \leq k, \tag{3.2}$$

where $\boldsymbol{\Phi} \in \mathbb{R}^{M \times N}$ is the sensing matrix to generate the compressive samples $\boldsymbol{y} \in \mathbb{R}^M$ from the original signal, $M \in \mathbb{Z}$ (with $k < M < N$) refers to the dimension of $\boldsymbol{y}$ and $||\cdot||_0$ represents the number of nonzero elements in the vector, which is also treated as the measure of sparsity. Since the real-world sampling always leads to noise, vector $\boldsymbol{\xi} \in \mathbb{R}^M$ represents the noise perturbation, whose magnitude is constrained by an upper bound δ, i.e., $||\boldsymbol{\xi}||_2 < \delta$. Incidentally, the compressive ratio in this sub-Nyquist signal acquisition is given by $\rho = M/N < 1$.

3.2.2 Signal Reconstruction

Under certain assumptions including the RIP on $\boldsymbol{\Phi}$ and the signal sparsity bound [11], robust signal reconstruction with respect to model (3.2) at each SU can be achieved as

$$\underset{\boldsymbol{x} \in \mathbb{R}^N}{\arg\min} ||\boldsymbol{x}||_0 \quad \text{subject to } ||\boldsymbol{\Phi}\boldsymbol{x} - \boldsymbol{y}||_2^2 \leq \delta, \tag{3.3}$$

which aims to seek a maximally sparse representation of $\boldsymbol{y}$, or

$$\underset{\boldsymbol{x} \in \mathbb{R}^N}{\arg\min} ||\boldsymbol{\Phi}\boldsymbol{x} - \boldsymbol{y}||_2^2 \quad \text{subject to } ||\boldsymbol{x}||_0 \leq k, \tag{3.4}$$

which finds the possible minimum reconstruction error at a given sparsity k. In practice, the original signals tend to be compressible, rather than sparse, where a compressible signal has a representation whose entries decay rapidly when sorted in the decreasing

order of magnitude. Although compressible signals can be well approximated by sparse signals, the reconstruction errors can only be diminished but not vanished [49]. Therefore, according to the Lagrange multiplier theorem, a proper constant parameter $\lambda > 0$ could be introduced to balance the objective of minimizing the reconstruction error and the solution sparsity, such that problems (3.3) and (3.4) could be equivalently solved by solving the following unconstrained minimization problem:

$$\arg\min_{\boldsymbol{x} \in \mathbb{R}^N} \frac{1}{2} ||\boldsymbol{\Phi}\boldsymbol{x} - \boldsymbol{y}||_2^2 + \lambda ||\boldsymbol{x}||_0. \tag{3.5}$$

However, problems (3.3), (3.4) and (3.5) are known to be NP-hard in general, which cannot be solved efficiently. It was shown in [50, 51] that the solution via the l_1-norm minimization with sufficient sparsity can be equivalent to the solution obtained by the l_0-norm minimization, where the l_1-norm optimization problem can be solved in polynomial time. Thus, problems (3.3), (3.4) and (3.5) can be efficiently and approximately solved by solving the following problems:

$$\arg\min_{\boldsymbol{x} \in \mathbb{R}^N} ||\boldsymbol{x}||_1 \quad \text{subject to } ||\boldsymbol{\Phi}\boldsymbol{x} - \boldsymbol{y}||_2^2 \le \delta, \tag{3.6}$$

or equivalently,

$$\arg\min_{\boldsymbol{x} \in \mathbb{R}^N} \frac{1}{2} ||\boldsymbol{\Phi}\boldsymbol{x} - \boldsymbol{y}||_2^2 + \lambda ||\boldsymbol{x}||_1. \tag{3.7}$$

Since $||\boldsymbol{\Phi}\boldsymbol{x} - \boldsymbol{y}||_2^2$ is a convex quadratic function, (3.7) is shown to be efficient under certain conditions in finding a sparse representation to achieve a small $||\boldsymbol{\Phi}\boldsymbol{x} - \boldsymbol{y}||_2^2$ [53]; but it may not be the optimal solution to problem (3.5) since the l_1-norm optimization problem usually requires much more compressive samples [57]. Therefore, this poses challenges when the signal dimension is high, i.e., when we have wideband spectrum signals. Thus, we propose to replace the l_1-norm in (3.7) with the l_ν-norm, for $0 < \nu < 1$, which is possible to achieve the exact reconstruction with substantially fewer samples [57, 78].

The basic idea of the proposed algorithm is to find a surrogate function based on the

l_ν-norm to majorize the objective function in (3.5), and then to minimize the surrogate function to drive the objective function downward until a global optimum is reached. In particular, we conduct the relaxation of the l_0-norm problem by utilizing the l_ν-norm instead of the l_1-norm in (3.7). In contrast to the l_1-norm, the l_ν-norm with $0 < \nu < 1$ is nonconvex. As convex optimization techniques are no longer applicable, the l_ν-norm makes the solution uniqueness and convergence analysis more complicated. However, fewer samples are usually required for the l_ν-norm approach compared with the l_1-norm approach [57]. Moreover, it was shown in [57, 84] that the l_ν-norm regularization leads to better sparsity approximation performance than l_1-norm. This is because l_ν-norm not only enforces stronger sparsity than l_1-norm, but it also better preserves edges [85], which is capable of yielding a sparser solution with higher fidelity than the l_1-norm regularization.

Given a function f that is convex, the l_ν-norm regularized problem can be presented as

$$\underset{\boldsymbol{x}\in\mathbb{R}^N}{\arg\min}\ f(\boldsymbol{x}) + \lambda||\boldsymbol{x}||_\nu^\nu \quad 0 < \nu < 1. \tag{3.8}$$

As $||\boldsymbol{\Phi x} - \boldsymbol{y}||_2^2$ is a convex quadratic function and therefore a valid choice for f in (3.8), we can transform (3.5) into the following unconstrained regularization problem:

$$\underset{\boldsymbol{x}\in\mathbb{R}^N}{\arg\min}\ \frac{1}{2}||\boldsymbol{\Phi x} - \boldsymbol{y}||_2^2 + \lambda||\boldsymbol{x}||_\nu^\nu \quad 0 < \nu < 1. \tag{3.9}$$

Since problem (3.9) is intermediate in the sense of norm minimization between problems (3.5) and (3.7), one can expect that it is also capable of seeking out a solution to (3.5) under certain conditions. Here, as discussed before, $\lambda > 0$ is the penalty parameter that balances the reconstruction accuracy and the sparsity of the minimization result. In addition, the choice of λ depends on the noise level of the original signal, e.g., the value of λ should be increased when the noise is larger [86]. Therefore, for the varying wideband spectrum signal in a real-time processing environment, the choice of λ greatly influences the behaviour of the spectrum reconstruction, such that we need to find the

most suitable value of λ for difference signals. Some approaches have been proposed for determining λ. However, these approaches are based on some extra algorithms [87, 88], which leads to increased computational complexity. In our work, we optimize λ along with the signal reconstruction process and λ is defined as a function of the target signal such that the problem in (3.9) can be transformed into the following form:

$$\operatorname*{arg\,min}_{\boldsymbol{x}\in\mathbb{R}^N} \left\{F(\boldsymbol{x}) = \frac{1}{2}||\boldsymbol{\Phi}\boldsymbol{x} - \boldsymbol{y}||_2^2 + \lambda(\boldsymbol{x})||\boldsymbol{x}||_\nu^\nu\right\} \quad 0 < \nu < 1, \tag{3.10}$$

where $\lambda(\boldsymbol{x})$ projects the signal $\boldsymbol{x}$ as a positive real number. In order to retain the numerical property of the original problem, $\lambda(\boldsymbol{x})$ should be a function of the smoothing functional, e.g., we could set it in general as $\lambda(\boldsymbol{x}) = g(F(x))$, where $g(\cdot)$ is a monotonically increasing function. Moreover, the objective function in each iteration should preserve its convexity and exhibits only a global minimizer regardless of the value of $\lambda(\boldsymbol{x})$. Therefore, we utilize the linear function of the form: $F(x) = \varrho\lambda(\boldsymbol{x})$ [89], where ϱ is the coefficient representing the slope of the line and also controls convexity. It is straightforward to show that this linear form could keep the numerical property of the original problem unchanged. Therefore, from (3.10), $\lambda(\boldsymbol{x})$ can be expressed as

$$\lambda(\boldsymbol{x}) = \frac{\frac{1}{2}||\boldsymbol{\Phi}\boldsymbol{x} - \boldsymbol{y}||_2^2}{\varrho - ||\boldsymbol{x}||_\nu^\nu} \quad 0 < \nu < 1 \tag{3.11}$$

However, it is general computationally hard and not guaranteed to obtain its global minimum due to the nonconvexity of the l_ν-norm. An alternative approach is to solve a sequence of the approximation subproblems, named as IRLS [57, 58, 78]. It is shown in [57] that under certain assumptions such as the null space property (NSP) on $\boldsymbol{\Phi}$, the solution sequence generated by the IRLS algorithm converges to the local minimum as the sparsest solution that is also the actual global l_ν-norm minimizer. Therefore, this IRLS method could be utilized to solve the unconstrained l_ν-norm minimization problem in (3.10).

In particular, each iteration of the IRLS algorithm corresponds to a weighted least

squares subproblem that can be efficiently solved by standard convex optimization methods. Let the weight $\boldsymbol{w} \in \mathbb{R}^N$ be a vector with each element being a positive number, i.e., $w_i > 0$ for all $i = 1, 2, ..., N$. The corresponding weighted inner product and weighted l_2-norm, are defined as

$$
\langle \boldsymbol{a}, \boldsymbol{b} \rangle_{\boldsymbol{w}} := \sum_{i=1}^{N} w_i a_i b_i
$$

$$
||\boldsymbol{a}||_2^{2(\boldsymbol{w})} := \langle \boldsymbol{a}, \boldsymbol{a} \rangle_{\boldsymbol{w}}.
$$

(3.12)

Without knowing apriori the spectral support of the original signal, the procedure for selecting weights is iterative in nature. A typical approach updates the weights at each iteration by using the solution of the weighted least squares problem from the previous iteration, i.e., $\boldsymbol{w}^{(l)} := |\boldsymbol{x}^{(l-1)}|^{-1}$ [58]. Specifically, the IRLS algorithm generates a sequence $\{\boldsymbol{x}^{(l)}\}_{l=1}^{\infty}$ which are the iterative estimates of $\boldsymbol{x}$ and given by

$$
\boldsymbol{x}^{(l)} := \underset{\boldsymbol{x} \in \mathcal{J}(\boldsymbol{x})}{\arg\min} \ \frac{1}{2}||\boldsymbol{\Phi}\boldsymbol{x} - \boldsymbol{y}||_2^2 + \lambda(\boldsymbol{x}^{(l-1)})||\boldsymbol{x}||_2^{2(\boldsymbol{w}^{(l)})},
$$

$$
\boldsymbol{w}^{(l)} := (w_1^{(l)}, ..., w_N^{(l)}),
$$

(3.13)

where $w_j^{(l)} := |x_j^{(l-1)}|^{-1}$, and the set $\mathcal{J}(\boldsymbol{x}) = \{\boldsymbol{x} \mid ||\boldsymbol{\Phi}\boldsymbol{x} - \boldsymbol{y}||_2^2 \leq \delta\}$ represents the set of feasible points to (3.3). Therefore, the weighted least squares problem in each iteration of the IRLS algorithm works over a closed convex set $\mathcal{J}(\boldsymbol{x})$, and can be efficiently solved using standard convex optimization methods.

However, if one of the elements $x_j^{(l)}$ vanishes at some iteration l, i.e., $x_j^{(l)} \to 0$, the corresponding weight component $w_j^{(l+1)} \to \infty$, which leads to $x_j^{(l+1)} = 0$ at the next iteration as well and persists in all sequential iterations, resulting in certain loss of information. As such, a small fixed regularizer $\epsilon > 0$ [78] could be adopted to regularize the optimization problem in order to provide stability and ensure that a zero-valued component in $\boldsymbol{x}^{(l)}$ does not strictly prohibit a nonzero estimate at the next iteration, as shown below:

$$
w_i^{(l)} = \left(\left(x_i^{(l-1)} \right)^2 + \epsilon \right)^{\frac{\nu}{2} - 1} \qquad 0 < \nu < 1.
$$

(3.14)

Following the arguments in [61], the l_ν-norm ($0 < \nu < 1$) could closely approximate the l_0-norm by setting a small enough ϵ, where a large fixed ϵ leads to inaccurate results. Unfortunately, as $\epsilon \to 0$, the regularizing functionality of ϵ becomes weak. That would cause the loss of certain information during the optimization as we discussed before. Thus, fixing ϵ relatively small or high would not be an optimal choice. A scheme where ϵ is dynamically decreased in each step is suggested in [58], which is based on the knowledge over anticipated accuracy for arbitrary signal recovery. Although this approach provides the l_ν-norm with a better l_0-norm approximation, ϵ would get to zero and some of the weights would be infinite since the reconstructed signals in some iterations could be sparser than the original signal. Therefore, it does not offer theoretical guarantees and would lead to some wrong local solutions.

To speed up the convergence and prevent getting trapped into the wrong local solutions, we propose to start with a relatively large regularizer which is given as Ω_ϵ for $\boldsymbol{w}^{(0)}$, and then quickly update the weights at each iteration by exponentially decreasing Ω_ϵ in the first few iterations, as a smaller regularizer allows the optimization process go deeper to achieve higher reconstruction accuracy [90]. We then let Ω_ϵ descend slowly in order to prevent $\Omega_\epsilon \to 0$ while keeping Ω_ϵ sufficiently small. Finally the decrement of Ω_ϵ tends to be 0 when the iterations move towards the end. As the result of regularizing weights by the proposed algorithm, the estimated solutions is moved along an exponential-linear path. Even early iterations may get inaccurate reconstruction results, the primary elements in signal would be likely identified as nonzero values, such that their influences are diminished to provide chances for the algorithm to locate the remaining small but nonzero signal elements in later iterations.

To illustrate how the proposed algorithm works, a generalizing function Γ_ν is defined as

$$\Gamma_\nu(\boldsymbol{x}, \boldsymbol{w}, \Omega_\epsilon) := \left[\frac{1}{2} ||\boldsymbol{\Phi}\boldsymbol{x} - \boldsymbol{y}||_2^2 + \lambda(\boldsymbol{x}) \sum_{i=1}^{N} w_i x_i^2 \right], \qquad (3.15)$$

where $\boldsymbol{x} \in \mathbb{R}^N$, $\boldsymbol{w} \in \mathbb{R}_+^N$, and $\Omega_\epsilon \in \mathbb{R}_+$. We initialize the parameters by setting $\boldsymbol{w}^0 =$

Algorithm 1 Adaptively-regularized iterative reweighted least squares

---

Require: samples vector $\boldsymbol{y} \in \mathbb{R}^N$, sensing matrix $\boldsymbol{\Phi} \in \mathbb{R}^{M \times N}$, $\Omega_\epsilon^{(0)} = 1$, $\boldsymbol{w^{(0)}} = 1, \ldots, 1$.
Ensure: Practical solution $\boldsymbol{x}^*$

1: **for** $l = 0, 1, \cdots, l_{\max}$ **do**
2:      Constrained weighted least square minimization:

$$\boldsymbol{x^{(l)}} := \arg\min \; \Gamma_\nu(\boldsymbol{x}^{(l-1)}, \boldsymbol{w}^{(l)}, \Omega_\epsilon^{(l)})$$

3:      Weights update: $\boldsymbol{w}^{(l+1)} = O(\boldsymbol{x}^{(l)}, \Omega_\epsilon^{(l)})$
4:      Penalty parameter update:

$$\lambda(\boldsymbol{x}^{(l)}) = \frac{\frac{1}{2}\|\boldsymbol{\Phi}\boldsymbol{x}^{(l)} - \boldsymbol{y}\|_2^2}{\varrho - \sum_{i=1}^{N} w_i^{(l+1)}(x_i^{(l)})^2}$$

5:      Regularizer update:
6:         **if** $\|\Delta\boldsymbol{x}^{(l)}\| \leq \frac{\epsilon^\nu}{100}$

$$\Omega_\epsilon^{(l+1)} = \left(1 + \frac{e^{-2l}}{h(\boldsymbol{x}^{(l)})_{k+1}}\right) h(\boldsymbol{x}^{(l)})_{k+1}$$

7:         **else**
8:             $\Omega_\epsilon^{(l+1)} = \Omega_\epsilon^{(l)}$
9: **end for**
10: **return** $\boldsymbol{x}^* = \boldsymbol{x}^{(l+1)}$;

$1, \ldots, 1$ and $\Omega_\epsilon^{(0)} = 1$. Therefore, (3.13) is equal to

$$\boldsymbol{x^{(l)}} := \arg\min \; \Gamma_\nu(\boldsymbol{x}^{(l-1)}, \boldsymbol{w}^{(l)}, \Omega_\epsilon^{(l)}), \tag{3.16}$$

which requires solving a weighted least squares problem that can be expressed in the matrix form:

$$\boldsymbol{x}^{(l)} = \boldsymbol{W}^{(l)}\boldsymbol{\Phi}^T \left(\boldsymbol{\Phi}\boldsymbol{W}^{(l)}\boldsymbol{\Phi}^T + \lambda(\boldsymbol{x}^{(l-1)}) * \boldsymbol{I}\right)^{-1} \boldsymbol{y}, \tag{3.17}$$

where $\boldsymbol{W}^{(l)}$ is the $N \times N$ diagonal matrix with $1/w_i^{(l)}$ as the i-th diagonal element and $\boldsymbol{\Phi}^T$ refers to the transpose of the sensing matrix $\boldsymbol{\Phi}$. Once $\boldsymbol{x}^{(l)}$ is obtained, we then

update the parameters as

$$w_j^{(l+1)} := O(\boldsymbol{x}^{(l)}, \Omega_\epsilon^{(l)}) = \left((x_j^{(l)})^2 + \Omega_\epsilon^{(l)}\right)^{\frac{\nu}{2}-1},$$

$$j = 1, ..., N,$$

$$\Omega_\epsilon^{(l+1)} := \begin{cases} \left(1 + \frac{e^{-2l}}{h(\boldsymbol{x}^{(l)})_{k+1}}\right) h(\boldsymbol{x}^{(l)})_{k+1}, & \text{if } ||\Delta\boldsymbol{x}^{(l)}|| \leq \frac{\epsilon^\nu}{100} \\ \Omega_\epsilon^{(l)}, & \text{otherwise,} \end{cases} \tag{3.18}$$

where $h(\boldsymbol{x})_i$ is the i-th largest element of the set $\{|\boldsymbol{x}|_j, j = 1, ..., N\}$, k refers to the sparsity of the signal, and $\Delta\boldsymbol{x}^{(l)} = \boldsymbol{x}^{(l)} - \boldsymbol{x}^{(l-1)}$. From (3.15), we have

$$\lambda(\boldsymbol{x}) := \frac{\Gamma_\nu(\boldsymbol{x}, \boldsymbol{w}, \Omega_\epsilon) - \frac{1}{2}||\boldsymbol{\Phi}\boldsymbol{x} - \boldsymbol{y}||_2^2}{\sum_{i=1}^N w_i x_i^2}. \tag{3.19}$$

We then substitute $\Gamma_\nu(\boldsymbol{x}, \boldsymbol{w}, \Omega_\epsilon) = \varrho \cdot \lambda(\boldsymbol{x})$ into (3.19), and obtain

$$\lambda(\boldsymbol{x}) = \frac{\frac{1}{2}||\boldsymbol{\Phi}\boldsymbol{x} - \boldsymbol{y}||_2^2}{\varrho - \sum_{i=1}^N w_i x_i^2}. \tag{3.20}$$

In each iteration, to guarantee that the convexity of the function $\Gamma_\nu(\boldsymbol{x}, \boldsymbol{w}, \Omega_\epsilon)$ is unchanged, the penalty parameter should smaller than 1, i.e., $\lambda(\boldsymbol{x}) < 1$ [91]. From the convexity perspective, we have $\varrho > 1/2||\boldsymbol{\Phi}\boldsymbol{x} - \boldsymbol{y}||_2^2 + ||\boldsymbol{x}||_2^{2(\boldsymbol{w})}$ by substituting $\lambda(\boldsymbol{x}) < 1$ into (3.20). Since $||\boldsymbol{x}||_2^{2(\boldsymbol{w})}$ could be approximated by $||\boldsymbol{x}||_2^\nu$ and $||\boldsymbol{x}||_2^\nu \simeq ||\boldsymbol{y}||_2^\nu$ according to [89] and

$$\frac{1}{2}||\boldsymbol{\Phi}\boldsymbol{x} - \boldsymbol{y}||_2^2 = ||\boldsymbol{\xi}||_2^2 \leq ||\boldsymbol{y}||_2^2, \tag{3.21}$$

where $||\boldsymbol{y}||_2^2 = ||\boldsymbol{\Phi}\boldsymbol{x} + \boldsymbol{\xi}||_2^2$, the constraint $\lambda(\boldsymbol{x}) < 1$ could be obtained by setting $\varrho \geq \frac{1}{2}||\boldsymbol{y}||_2^2 + ||\boldsymbol{y}||_2^\nu$. Therefore, the value of control parameter ϱ is determined by the proposed algorithm according to the samples vector $\boldsymbol{y}$ in practice.

This whole process of reconstruction terminates when it converges or l reaches a specified maximum number of allowed iterations $l_{\max}$. The outline of the proposed algorithm is summarized in Algorithm 1.

3.2.3 Decision Making

When the recovered signal $\boldsymbol{x}^*$ is obtained by the proposed algorithm discussed above, energy detection could be applied to determine the spectrum occupancy by comparing the energy density of the recovered signal against a predefined threshold φ_d, which for example could be set as [92]

$$\varphi_d = \sigma_n^2 \left(1 + \frac{Q^{-1}(P_f)}{\sqrt{N/2}} \right), \tag{3.22}$$

where σ_n^2 is the noise variance and P_f refers to the target probability of false alarm. If the energy of the reconstructed signal is higher than the threshold, the corresponding channel is determined as occupied by PU, and SUs are forbidden to access. Otherwise, the corresponding channel is determined as vacant, and SUs could access to transmit unlicensed signals. It should be noted that the detection performance would benefit from higher CS reconstruction accuracy. If the original signal is noise-free and the number of samples M is large enough, the threshold φ_d for decision making could be set as the magnitude of the smallest element in the reconstructed signals, to ensure zero miss and low false alarms. However, in real-time processing, the reconstruction error increases as M is reduced, and it is further mixed with the noise whose variance is unknown and varying. Therefore, the traditional noise variance based methods for threshold setting as in (3.22) are not applicable anymore.

The rule of the proposed descent-based algorithm for φ_d setting is to locate the "first significant change" in the sorted sequence as illustrated by Fig. 3.2. Specifically, this algorithm first divides the reconstructed signal $\boldsymbol{x}^* \in \mathbb{R}^N$ into L sub-bands and therefore each sub-band contains $b = N/L$ elements. The average value of each sub-band is used to form the sequence:

$$\boldsymbol{p} = \{p_i\}_{i=1}^L \text{ where } p_i = E\left[\sum_{j=(b\cdot i+1)}^{b\cdot(i+1)} x_j^* \right] \tag{3.23}$$
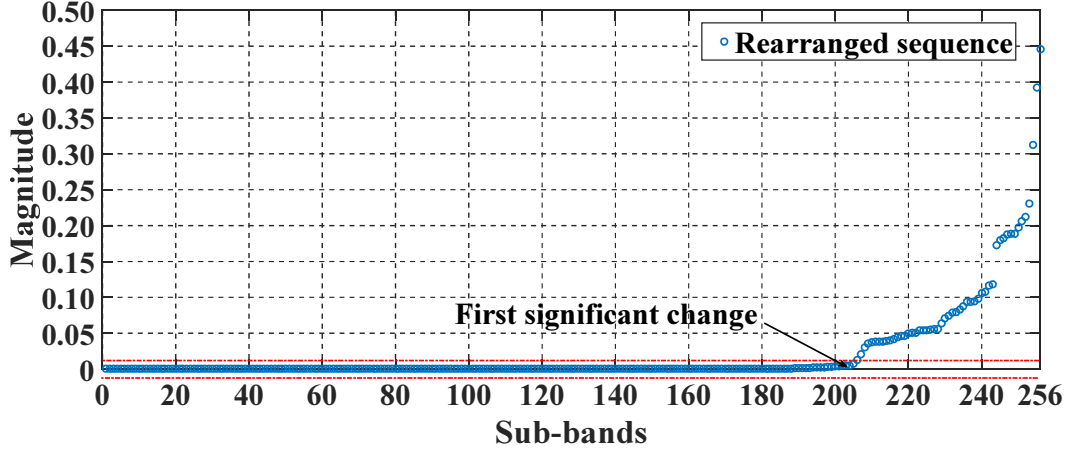
Figure 3.2: The sorted sequences of the sub-bands and their first significant change.

Then we sort all elements of $\boldsymbol{p}$ in an ascending order in term of their magnitudes, which is donated by the sequence $\boldsymbol{p}^s = \{p_i^s\}_{i=1}^L$, i.e., p_1^s is the smallest element and p_L^s is the largest element in $\boldsymbol{p}$. Then we define the increment value between two adjacent elements in $\boldsymbol{p}^s$ by $\nabla p_i^s = (p_i^s + p_{i+1}^s)/2$. Since the original signal contains noise, which means that the reconstructed signal contains both the reconstruction error and noise, φ_d should be set equal to or slightly larger than the magnitude of the smallest element in the set of the largest $\tau\%$ elements so that the influence of the possible noise fluctuation could be diminished, where τ should be chosen to be large enough, such that the primary components in the signal $\boldsymbol{x}^*$ can not be missed.

The algorithm compares ∇p_i^s with the values from ∇p_1^s to ∇p_{i-1}^s. If p_i^s belongs to the largest $\tau\%$ part of $\boldsymbol{p}^s$ and ∇p_i^s is larger than ∇p_1^s to ∇p_{i-1}^s, we locate p_i^s as the "first significant change"; otherwise we increase i until the "first significant change" is obtained. We adopt this value as the threshold to distinguish the primary components and the combination of noise and reconstruction errors. It should be noted that the larger the sub-band, the simpler the algorithm becomes since less increment calculations and iterations are required. But the performance may be degraded if L is too small. The "first significant change" exists since in the reconstructed signal $\boldsymbol{x}^*$, the true nonzeros are large in magnitude and small in number, while the noise and false ones are large in number and small in magnitude due to the nature of the IRLS algorithm [14]. There-

fore, the magnitudes of the true nonzeros are spread out, while those of the noise and reconstruction errors ones are clustered.

3.2.4 Theoretical Guarantees

Theorem 1. *(Null Space Property) From [58], we shall say that the matrix $\mathbf{\Phi}$ has the ν-Null Space Property (ν-NSP) of order S for $\gamma > 0$ if*

$$||\eta_T||_\nu^\nu \leq \gamma ||\eta_{T^c}||_\nu^\nu \tag{3.24}$$

for all sets T of cardinality not exceeding L and all $\eta \in \mathcal{N}$, where $\mathcal{N}$ is the null space of $\mathbf{\Phi}$ as we defined before and T^c denotes the complement of the set T. In addition, η_T is the vector obtained from η by setting all coordinates $\eta_i = 0$ for $i \neq T \subset \{1, 2, \ldots, N\}$.

It is stated in [57] that in order to guarantee that a k-sparse vector $\boldsymbol{x}^*$ is the unique l_ν-norm minimizer of $\mathcal{J}(\boldsymbol{x})$, it is sufficient that $\mathbf{\Phi}$ has the ν-NSP ($0 < \nu < 1$) of order $s \leq S$ with $\gamma \in (0, 1)$. Thus, we can extend this result to our weighted l_ν-norm minimization in (3.13).

3.2.4.1 Convergence

Theorem 1 ensures that, under certain conditions, the proposed algorithm has a unique exact solution according to [58], as established by the following theorem.

Theorem 2. *Fix $\boldsymbol{y} \in \mathbb{R}^M$, define $\Gamma_\nu^n = \Gamma_\nu(\boldsymbol{x}^n, \boldsymbol{w}^n, \Omega_\epsilon^n)$ and let S be chosen such that $\mathbf{\Phi}$ satisfies the ν-NSP of order K. Then the sequence $\{\Gamma_\nu^n\}_{n=1}^\infty$ converges to a fixed point of the algorithm.*

Proof. We first show that the sequence $\{\Gamma_\nu^n\}_{n=1}^\infty$ decreases monotonically over n, as we

have the following monotonicity property hold for all $n \geq 0$:

$$\Gamma_\nu(\boldsymbol{x}^{n+1}, \boldsymbol{w}^{n+1}, \Omega_\epsilon^{n+1}) \leq \Gamma_\nu(\boldsymbol{x}^{n+1}, \boldsymbol{w}^n, \Omega_\epsilon^{n+1})$$
$$\leq \Gamma_\nu(\boldsymbol{x}^{n+1}, \boldsymbol{w}^n, \Omega_\epsilon^n) \leq \Gamma_\nu(\boldsymbol{x}^n, \boldsymbol{w}^n, \Omega_\epsilon^n). \tag{3.25}$$

Here, the first inequality follows from the minimization property that defines $\boldsymbol{w}^{n+1}$, the second inequality from $\Omega_\epsilon^{n+1} \leq \Omega_\epsilon^n$, and the last inequality from the minimization property that defines $\boldsymbol{x^{n+1}}$. For a given n, $\boldsymbol{x}^{n+1}$ is completely determined by $\boldsymbol{w}^n$; for $n = 0$, in particular, $\boldsymbol{x}^1$ is determined solely by $\boldsymbol{w}^0$, and independent of the choice of $\boldsymbol{x}^0 \in \mathcal{J}(\boldsymbol{x})$. Next, we prove that the sequence $\{\Gamma_\nu^n\}_{n=1}^\infty$ is bounded as $||\boldsymbol{x}^n||_\nu^\nu \leq \Gamma_\nu(\boldsymbol{x}^1, \boldsymbol{w}^0, \Omega_\epsilon) := L$. First,

$$2\left[\Gamma_\nu^n(\boldsymbol{x}^n, \boldsymbol{w}^n, \Omega_\epsilon^n) - \Gamma_\nu^{n+1}(\boldsymbol{x}^{n+1}, \boldsymbol{w}^{n+1}, \Omega_\epsilon^{n+1})\right] \geq$$
$$2\left[\Gamma_\nu^n(\boldsymbol{x}^n, \boldsymbol{w}^n, \Omega_\epsilon^n) - \Gamma_\nu^{n+1}(\boldsymbol{x}^{n+1}, \boldsymbol{w}^n, \Omega_\epsilon^n)\right]$$
$$= \langle \boldsymbol{x}^n, \boldsymbol{x}^n \rangle_{\boldsymbol{w}^n} - \langle \boldsymbol{x}^{n+1}, \boldsymbol{x}^{n+1} \rangle_{\boldsymbol{w}^n}$$
$$= \langle \boldsymbol{x}^n + \boldsymbol{x}^{n+1}, \boldsymbol{x}^n - \boldsymbol{x}^{n+1} \rangle_{\boldsymbol{w}^n} \tag{3.26}$$
$$= \langle \boldsymbol{x}^n - \boldsymbol{x}^{n+1}, \boldsymbol{x}^n - \boldsymbol{x}^{n+1} \rangle_{\boldsymbol{w}^n}$$
$$= \sum_{i=1}^N w_i^n (x_i^n - x_i^{n+1})^\nu$$
$$= L^{-1}||\boldsymbol{x}^n - \boldsymbol{x}^{n+1}||_{l_\nu}^\nu;$$

therefore, we obtain that the sequence $\{\Gamma_\nu^n\}_{n=1}^\infty$ is bounded as $||\boldsymbol{x}^n||_\nu^\nu \leq \Gamma_\nu(\boldsymbol{x}^n, \boldsymbol{w}^n, \Omega_\epsilon^n)$, and $\sum_{n=1}^\infty ||\boldsymbol{x}^{n+1} - \boldsymbol{x}^n||_\nu^\nu \leq 2L^\nu$. In particular, we have

$$\lim_{n \to \infty} ||\boldsymbol{x}^{n+1} - \boldsymbol{x}^n||_\nu^\nu = 0. \tag{3.27}$$

Thus, the convergence is proved. $\qquad\square$

Theorem 2 ensures that, under certain conditions, the sequence of solutions provided by the proposed algorithm converges to a fixed point as a local minima. According to [58], such local convergence results are common for nonconvex optimization problems,

e.g., l_ν-norm minimization solving by IRLS, and are actually global solutions as shown numerically in [78].

3.2.4.2 Complexity

The computational complexity reduction of the proposed AR-IRLS algorithm comes from two parts. Firstly, the computational complexity reduction is contributed by the fewer number of iterations. In each iteration of the conventional IRLS algorithms, the complexity of matrix multiplication $\boldsymbol{\Phi W}^{(l)}\boldsymbol{\Phi}^T$ is $O(NM^2)$ since matrix $\boldsymbol{W}^{(l)}$ is diagonal, and the inverse of $(\boldsymbol{\Phi W}^{(l)}\boldsymbol{\Phi}^T + \lambda(\boldsymbol{x}^{(l)}) * \boldsymbol{I})$ takes $O(M^3)$. Therefore, the complexity of solving $(\boldsymbol{\Phi W}^{(l)}\boldsymbol{\Phi}^T + \lambda(\boldsymbol{x}^{(l)}) * \boldsymbol{I})^{-1}$ is $O(NM^2)$ due to $N > M$. Secondly, the computational complexity reduction is contributed by the fewer compressive samples required to guarantee the reconstruction performance. In the proposed AR-IRLS algorithm, the minimum number of compressive samples M is reduced, which leads to a large computational complexity reduction as the complexity of solving $(\boldsymbol{\Phi W}^{(l)}\boldsymbol{\Phi}^T + \lambda(\boldsymbol{x}^{(l)}) * \boldsymbol{I})^{-1}$ is $O(NM^2)$. The performance analyses of the reduced iterations and compressive samples are further shown in experimental results.

3.3 Low-complexity IRLS-based Compressive Spectrum Sensing Algorithm

Each iteration of IRLS algorithms requires solving a weighted least squares problem that can be expressed in the matrix form (4.5). For the illustration simplification purpose, we drop the interval number p as:

$$\boldsymbol{x}^{(l)} = \left(\boldsymbol{\Phi}^T\boldsymbol{\Phi} + \lambda(\boldsymbol{x}^{(l-1)}) * \boldsymbol{W}^{(l-1)}\right)^{-1}\boldsymbol{\Phi}^T\boldsymbol{y}. \tag{3.28}$$

Therefore, the efficiency of the IRLS-based algorithm is mainly constrained by the inverse of the matrix $\boldsymbol{H} = \boldsymbol{\Phi}^T\boldsymbol{\Phi} + \lambda(\boldsymbol{x}^{(l-1)}) * \boldsymbol{W}^{(l-1)}$, which takes $O(N^3)$ time. It is difficult

(a). Outdoor sensor node setup at
Queen Mary University of London

(b). Rfeye portable sensing node

Figure 3.3: (a) Outdoor fixed sensor node deployed in Queen Mary University of London and (b) the portable sensor node for mobile spectrum surveillance.

and costly to solve $\boldsymbol{H}^{-1}$ for many cases especially when the dimension of the original wideband signal is large. The conventional way to approximate the matrix inverse is conjugate gradient (CG) descent method. According to the observation that the matrix $\boldsymbol{H}$ is usually diagonal dominance due to the square of measurement matrix $\boldsymbol{\Phi}^T\boldsymbol{\Phi}$ is diagonal dominance, we proposed to utilize the preconditioned conjugate gradient (PCG) method which has better performance than CG [93]. To find the best approximation of $\boldsymbol{H}$, the preconditioner can be given by

$$\boldsymbol{P} := \underset{\boldsymbol{Z} \in D}{\arg\min} \ ||\boldsymbol{H} - \boldsymbol{Z}||_2^2, \tag{3.29}$$

where $\boldsymbol{D}$ is a set of diagonal or pseudo-diagonal matrices. Since $\lambda(\boldsymbol{x}^{(l-1)}) * \boldsymbol{W}^{(l-1)}$ is a diagonal matrix and $\boldsymbol{\Phi}^T\boldsymbol{\Phi}$ is diagonal dominance for the measurement matrix utilized in compressive spectrum sensing, e.g., random projection matrix for analog-to-information

---

Algorithm 2 Low-Complexity IRLS-based Compressive Spectrum Sensing Algorithm

---

Require: samples vector $\boldsymbol{y} \in \mathbb{R}^N$, measurement matrix $\boldsymbol{\Phi} \in \mathbb{R}^{M \times N}$, initial value $\Omega_\epsilon^{(0)}$, $\boldsymbol{W}^{(0)}$ and $\lambda(\boldsymbol{x}^{(0)})$.

Ensure: Practical solution $\boldsymbol{x}^*$

1: **for** $l = 1, \cdots, l_{\max}$ **do**
2:    Update: $\boldsymbol{H} = \boldsymbol{\Phi}^T \boldsymbol{\Phi} + \lambda(\boldsymbol{x}^{(l-1)}) * \boldsymbol{W}^{(l-1)}$
3:    Update: $\boldsymbol{P}^{-1} = (\overline{\boldsymbol{\Phi}^T \boldsymbol{\Phi}} * \boldsymbol{I} + \lambda(\boldsymbol{x}^{(l-1)}) * \boldsymbol{W}^{(l-1)})^{-1}$
4:    Update $\boldsymbol{x}^{(l)}$ with the inverse of preconditioner $\boldsymbol{P}^{-1}$
5:    Regularizer update:
6:    **if** $||\Delta \boldsymbol{x}^{(l)}|| \leq \frac{\epsilon^\nu}{100}$: $\Omega_\epsilon^{(l)} = \left(1 + \frac{e^{-2l}}{h(\boldsymbol{x}^{(l)})_{k+1}}\right) h(\boldsymbol{x}^{(l)})_{k+1}$
7:    **else**: $\Omega_\epsilon^{(l)} = \Omega_\epsilon^{(l-1)}$
8:    Weights update: $\boldsymbol{w}^{(l)} = \left((x_i^{(l)})^2 + \Omega_\epsilon^{(l)}\right)^{\frac{\nu}{2}-1}$
9:    Penalty parameter update:
        $\lambda(\boldsymbol{x}^{(l)}) = \frac{1}{2}||\boldsymbol{\Phi}\boldsymbol{x}^{(l)} - \boldsymbol{y}||_2^2 / [\varrho - \sum_{i=1}^N w_i^{(l)}(x_i^{(l)})^2]$
10: **end for**
11: **return** $\boldsymbol{x}^* = \boldsymbol{x}^{(l+1)}$.

---

converter (AIC), partial Fourier matrix for multi-coset sampling and etc., $\boldsymbol{H}$ is diagonal dominance which could be approximated by a diagonal or pseudo-diagonal matrix $\boldsymbol{P}$. According to the diagonal dominance feature, the exact solution of (3.29) is given as

$$\boldsymbol{P} = (\overline{\boldsymbol{\Phi}^T \boldsymbol{\Phi}} * \boldsymbol{I} + \lambda(\boldsymbol{x}^{(l-1)}) * \boldsymbol{W}^{(l-1)}), \tag{3.30}$$

where $\overline{\boldsymbol{\Phi}^T \boldsymbol{\Phi}}$ denotes the average of all diagonal values of the matrix $\boldsymbol{\Phi}^T \boldsymbol{\Phi}$, which can be pre-calculated since $\boldsymbol{\Phi}$ is preset before the sensing. Therefore, compared with the inverse of the original matrix $\boldsymbol{H}$ which takes $O(N^3)$ time, $\boldsymbol{P}^{-1} = (\overline{\boldsymbol{\Phi}^T \boldsymbol{\Phi}} * \boldsymbol{I} + \lambda(\boldsymbol{x}^{(l-1)}) * \boldsymbol{W}^{(l-1)})^{-1}$ only require linear time $O(N)$. The Low-complexity IRLS reconstruction algorithm is summarized in Algorithm 2.

3.4 Real-time Compressive Spectrum Sensing Testbed over TV White Space

The proposed testbed consists of a sensor node and a real-time spectral information processing platform based on National Instruments (NI) LabVIEW software [94] to pro-
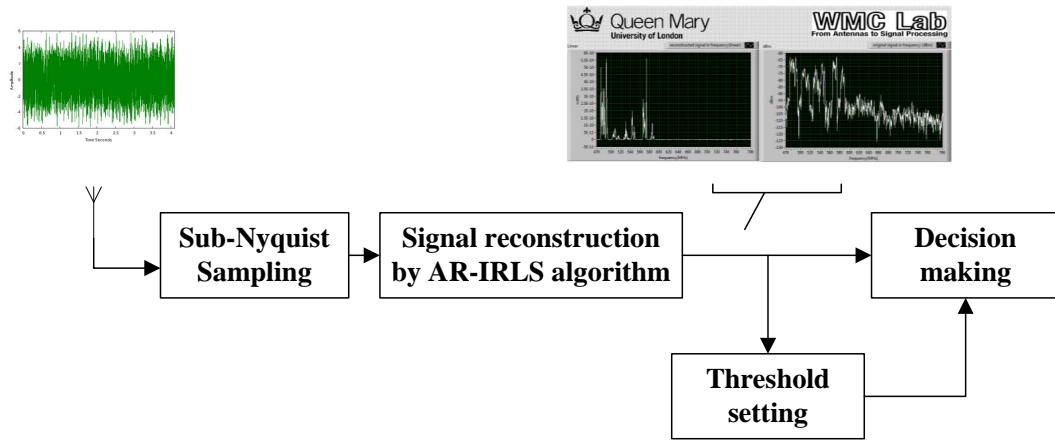
Figure 3.4: Block diagram of the compressive spectrum sensing measurement for real-world signal on TVWS.

cess the data and control the hardware. Different to the simulation or small controlled laboratory experiments, the proposed testbed offers a realistic environment for verifying the reconstruction algorithms with the practical and varying channel environment.

3.4.1 Sensor Node System

The sensor node applied in the proposed real-time compressive spectrum sensing testbed is a RFeye node, which is an intelligent spectrum monitoring system. According to the working type of sensor node, the testbed has two sensing modes: fixed sensing mode and portable sensing mode. As shown in Fig. 3.3, the fixed outdoor RFeye node is located at Queen Mary University of London (51.523021°N 0.041592°W), and the antenna height is about 20 meters above ground. The portable sensor node is for mobile spectrum surveillance in urban/rural areas and demonstration purpose. When the fixed outdoor sensing node is applied in the proposed testbed, the collected data is transmitted through the Internet or local area network (LAN), which is encrypted as javascript object notation (JSON) message. If the portable sensing node is utilized to form the testbed, the sensor node is directly connected with PC which runs the spectral information processing platform via Ethernet cable.
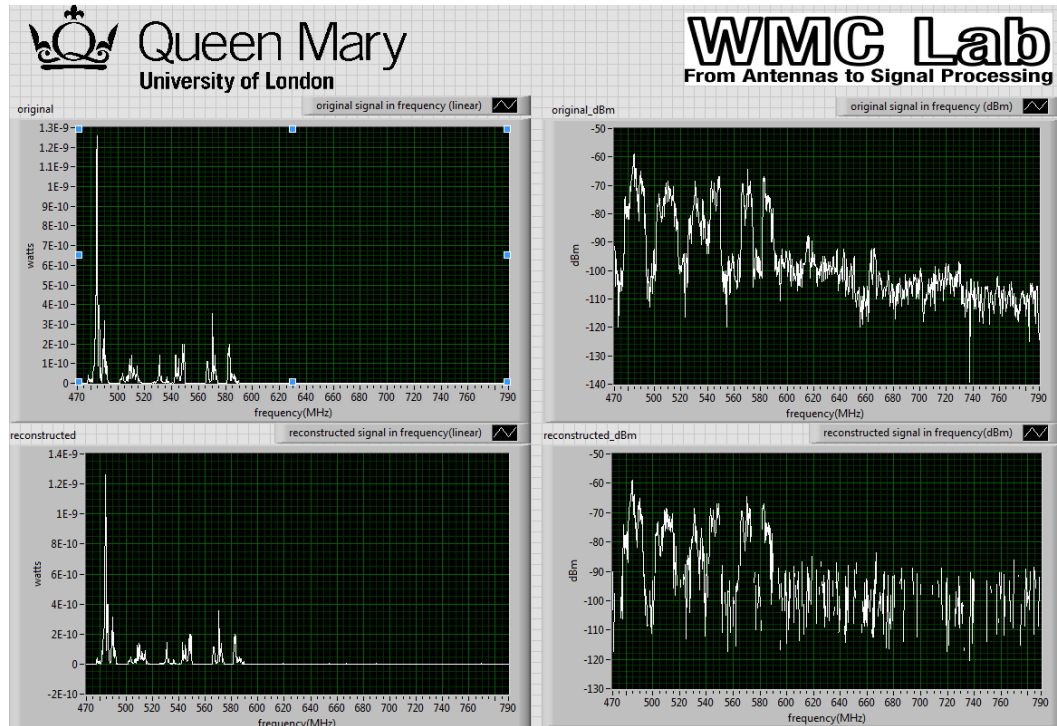
Figure 3.5: The front panel of the proposed testbed.

3.4.2   Real-time Spectral Information Processing Platform

Based on the NI LabVIEW software, as the second part of the proposed testbed, the real-time spectral information processing platform is developed for processing the information collected by the sensor node and displaying the reconstructed results. As shown in Fig. 3.4, the proposed platform is mainly composed of four parts: sub-Nyquist samples collection, signal reconstruction by proposed AR-IRLS algorithm, threshold setting and decision making. As the reconstruction performance of CS-based spectrum sensing scheme has significant impact on the detection capabilities [73], one targets of the propose testbed is to implement the reconstruction algorithms and verify their performance in the real-world scenario. As shown in Fig. 3.5, the front panel of the proposed testbed displays both original signals and reconstructed signals in order to demonstrate the reconstruction performance. The power spectrum of signals shown in the left two diagrams is in linear form and the other two diagrams show the signals in dBm form. The signals at the top are the original signals collected in real-time and the signals at the
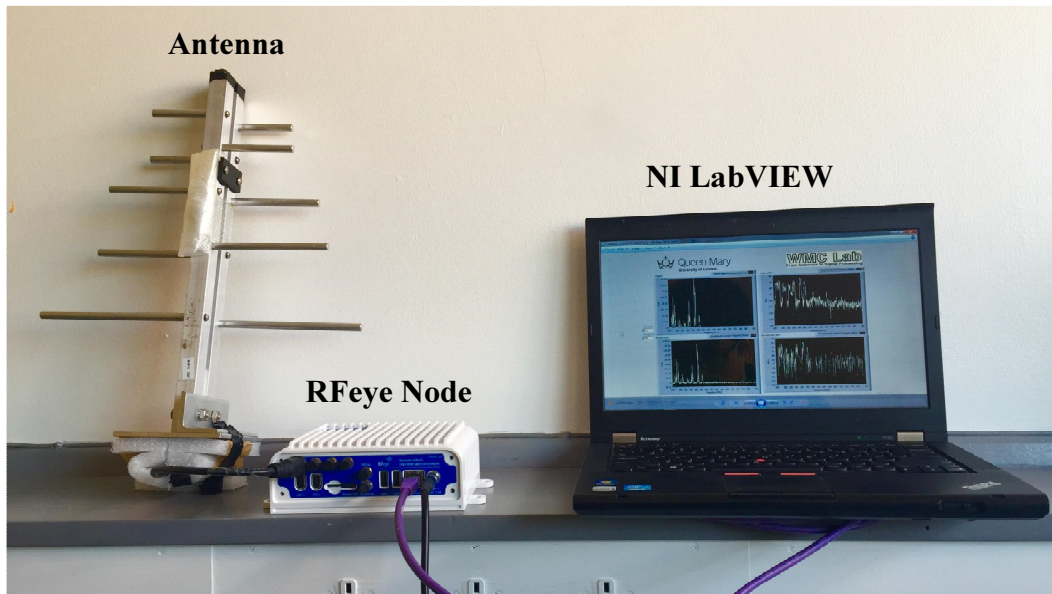
Figure 3.6: Experimental setup for real-time processing and live compressive spectrum sensing testbed on TVWS.

bottom are the corresponding reconstructed signals. Therefore, the differences between original signals and reconstructed signals could be visualized and easily to be identified by audiences.

As shown in Fig. 3.6, the proposed testbed consists of the commercial nondirectional UHF antenna, the portable sensor node, and a laptop installed our real-time spectral information processing platform.

3.5 Numerical Analysis

As a proof of concept for the proposed scheme, we discuss a series of experiments to test them using both simulated signals and real-world signals in this section.

3.5.1 Experiment Setups and Performance Measures

To verify the recovery accuracy of the proposed AR-IRLS algorithm that works with varying bandwidths and power levels in the primary signals, the simulated signals $\boldsymbol{x}_0^{\text{sim}}$ are generated by choosing k nonzero components uniformly at random out of $N = 1024$ and drawing the amplitude of each nonzero component from a uniform distribution of $U([-1,1])$, where the sparsity level is $\mu = k/N$. The entries of the sensing matrix $\boldsymbol{\Phi} \in \mathbb{R}^{M \times N}$ are generated by an i.i.d. Gaussian process with zero mean and variance $1/M$, where M/N is the corresponding compressive ratio ρ.

The real-world TVWS signals $\boldsymbol{x}_0^{\text{real}}$ are received by the proposed real-time compressive spectrum sensing testbed. The frequency of the received real-world TVWS signal ranges from 470 to 790 MHz and the channel bandwidth is 8 MHz in Europe. The setting is consistent with the current bandwidth used in TV broadcasting. Therefore, the total bandwidth of the real-world signals is 320MHz.

To quantify the reconstruction accuracy of the proposed algorithm, we calculate the conventional relative mean square error (r-MSE):

$$\text{r-MSE} = \frac{||\boldsymbol{x}^* - \boldsymbol{x}_0||}{||\boldsymbol{x}_0||}, \tag{3.31}$$

where $\boldsymbol{x}_0 = \boldsymbol{x}_0^{\text{sim}}$ in the simulation mode and $\boldsymbol{x}_0 = \boldsymbol{x}_0^{\text{real}}$ in the real-time mode. We also calculate the acceptable reconstruction frequencies, which is the fraction of successful reconstructions, defined as the case with r-MSE $\leq 10^{-2}$. The convergence speed of the proposed AR-IRLS algorithm is also compared with the traditional regularized IRLS [78] (termed Reg-IRLS), unregularized IRLS (termed Unreg-IRLS), and the IRL1 approach [61] (termed IRL1). The comparison among these three conventional IRLS algorithms and the proposed algorithm is shown in Table 3-A. The first two algorithms and the proposed AR-IRLS algorithm utilize the l_ν-norm minimization, where ν is set as 0.5, and the last one utilizes the l_1-norm minimization.
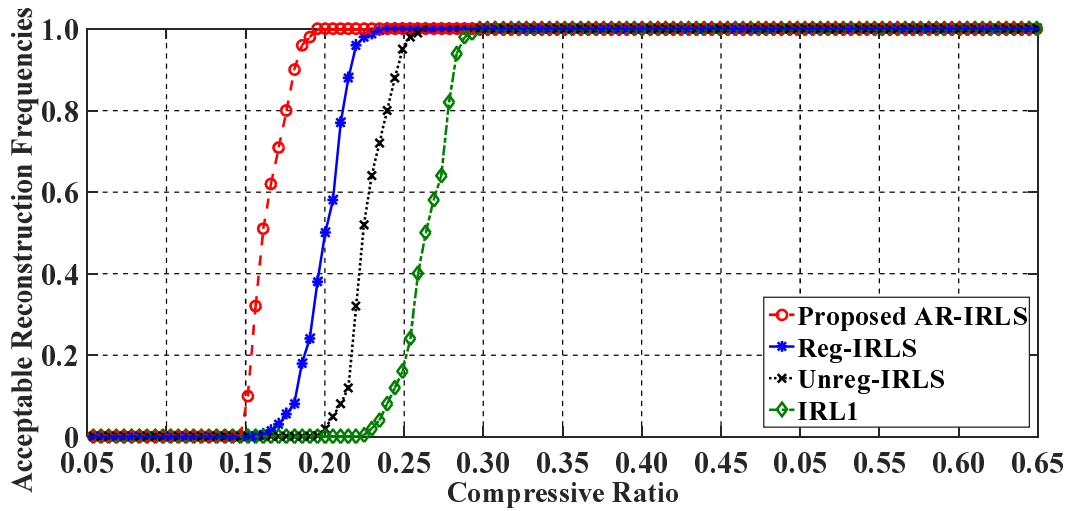
Figure 3.7: Acceptable reconstruction frequencies vs. compressive ratio ρ between the proposed AR-IRLS algorithm and other conventional IRLS algorithms when sparsity level $\mu = 0.05$.
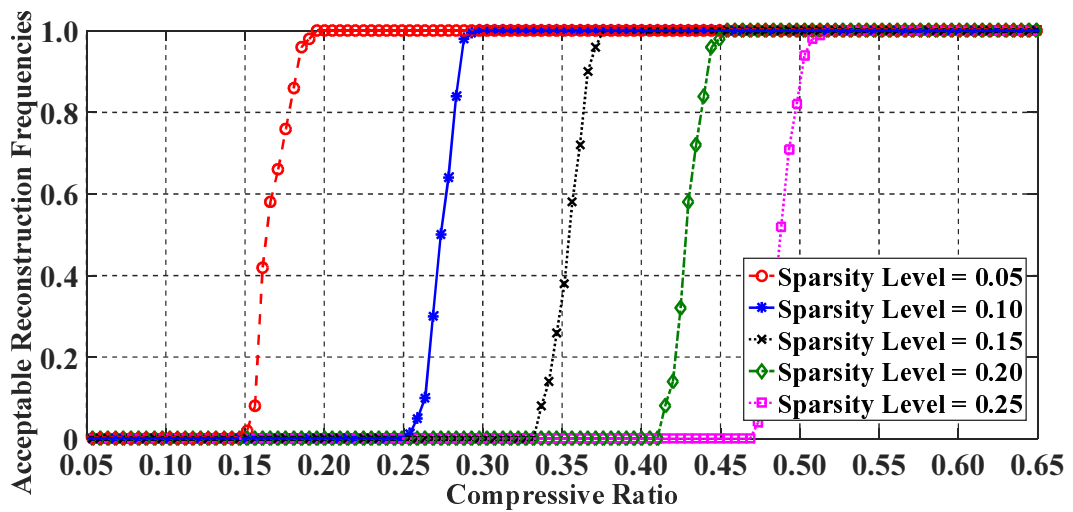
Figure 3.8: Acceptable reconstruction frequencies vs. compressive ratio ρ for the proposed AR-IRLS algorithm under different sparsity levels $\mu = 0.05, 0.10, 0.15, 0.20, 0.25$.

3.5.2 Results over simulated signals

In this section, the acceptable reconstruction frequency performance of the proposed AR-IRLS algorithm is compared with the conventional IRLS algorithms including Reg-IRLS, Unreg-IRLS and IRL1. The impacts of system parameters such as the compression ratio and sparsity level are also investigated.

Table 3-A: Comparison Among Conventional IRLS Algorithms and the proposed AR-IRLS algorithm

Algorithm	Compression Capability	Sparsity Tolerance	Computational Complexity
Reg-IRLS	high	high	high
Unreg-IRLS	medium	medium	medium
IRL1	low	low	low
AR-IRLS	high	high	low

3.5.2.1 Reconstruction Performance versus Compressive Ratio

Fig. 3.7 shows the reconstruction performance against the compressive ratio ρ of the proposed AR-IRLS algorithm. For evaluation, we compare it with the other three IRLS algorithms. The sparsity level μ of the received signal is fixed to 0.05. It can be seen that the reconstruction performance of the proposed AR-IRLS algorithm is superior over that with the conventional IRLS algorithms under the same compression ratio. Therefore, a lower compressive ratio is enabled by the proposed AR-IRLS algorithm to achieve the same reconstruction accuracy, which decreases the required sampling rate in practical implementation.

As the PUs and SUs are frequently switching between the modes of offline and online, the sparsity levels of the received wideband signals in practice would fluctuate. A real-time wideband spectrum sensing scheme, therefore, should be robust against different signal sparsity levels. To validate that the proposed algorithm can work with different sparsity levels, Fig. 3.8 shows the reconstruction performance of the proposed scheme, which is improved with an increasing compressive ratio under different sparsity levels. Under the same sparsity level μ, the lower compressive ratio achieved by proposed sensing scheme in comparison with that of the conventional algorithms, could reduce the required sampling rate and lead to power savings. It is shown in Fig. 3.8 that the gap between adjacent curves gets smaller as the compressive ratio ρ increases, which matches the theoretical results regarding the formula $\rho = M/N \geq Ck \log(N/k)$ to calculate the minimum compressive ratio ρ for a Gaussian measurement matrix, where C denotes a
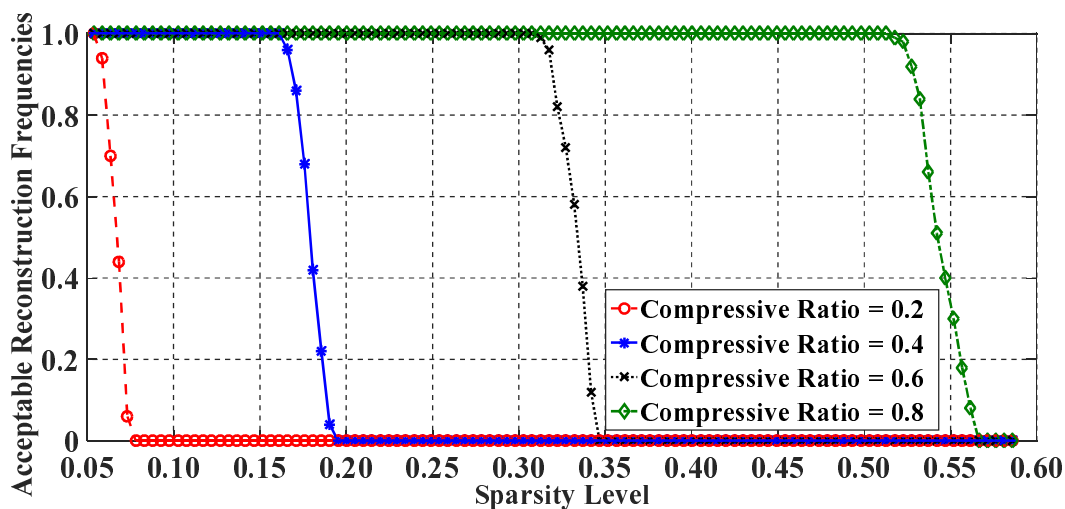
Figure 3.9: Acceptable reconstruction frequencies vs. sparsity level μ under different compressive ratios $\rho = 0.2, 0.4, 0.6, 0.8$ for the proposed AR-IRLS algorithm.
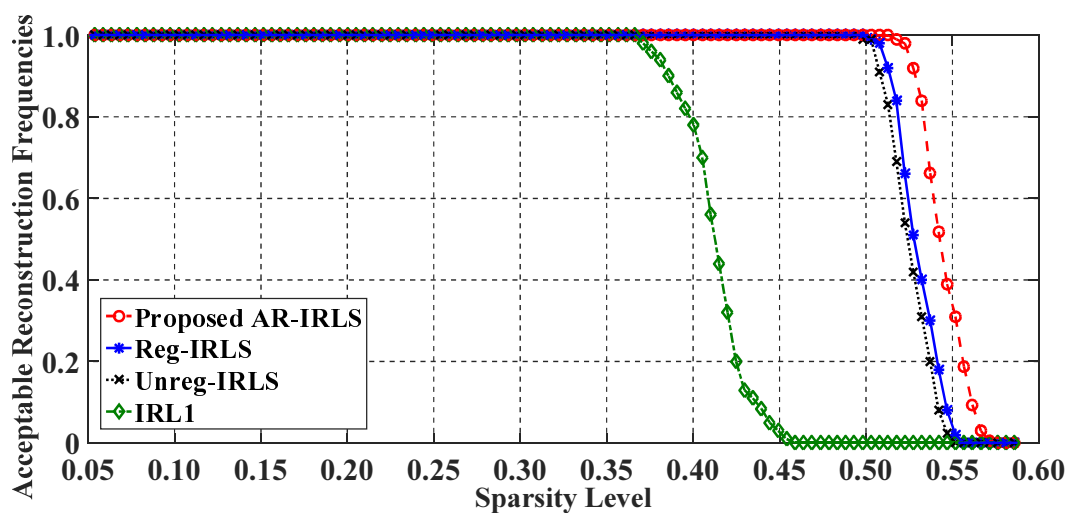

Figure 3.10: Acceptable reconstruction frequencies vs. sparsity level μ between proposed AR-IRLS algorithm and other conventional IRLS algorithms when compressive ratio $\rho = 0.8$.

constant and $k = \mu \cdot N$ [11].

3.5.2.2 Reconstruction Performance versus Sparsity Level

To show the relationship between the reconstruction performance of the proposed algorithm and the sparsity level μ, we plot the acceptable reconstruction frequencies against

the sparsity level μ ranging from 0.05 to 0.60 under compressive ratios $\rho = 0.2, 0.4, 0.6, 0.8$ in Fig. 3.9. It can be observed that the reconstruction performance degrades as the sparsity level increases, which indicates that more samples should be collected for signal reconstruction to ensure that the reconstruction performance is not degraded as μ increases. As Fig. 3.9 shows, although the signals with high sparsity levels require high compressive ratios, our algorithm can recover the signal with a sparsity level μ as high as 50%. By taking the advantage of robustness against different sparsity levels, our proposed scheme can deal with more SU on/off switchings over the spectrum of interest.

Fig. 3.10 shows the acceptable reconstruction frequency against the signal sparsity level μ under a compressive ratio $\rho = 0.8$ and the performance over a large sparsity level range could be observed in this setting. Although IRL1 has the minimum computational complexity, its reconstruction performance is the worst. The proposed one has the best reconstruction performance than the other three conventional IRLS algorithms, which recovers the largest sparsity range under the same ρ. This ensures that the proposed sensing scheme could cope with highly occupied channels.

To demonstrate that the reconstruction performance is not degraded with the reduced computational complexity of the proposed low-complexity-IRLS (termed as LC-IRLS) based reconstruction algorithm, we plot the acceptable reconstruction frequencies against the sparsity level ranging from 0.05 to 0.60 under compressive ratios = 0.2, 0.4, 0.6 for both the proposed LC-IRLS and AR-IRLS in Fig. 3.11. It can be seen that the signal reconstruction of the proposed LC-IRLS algorithm has high fidelity guarantee as same as the AR-IRLS algorithm under different compression ratios.

3.5.3 Analysis on Real-World Signals

After the performance of the proposed scheme has been validated with the simulated signals, we further test it over real-world signals. The sparsity level of the received real-world signal is 0.2.
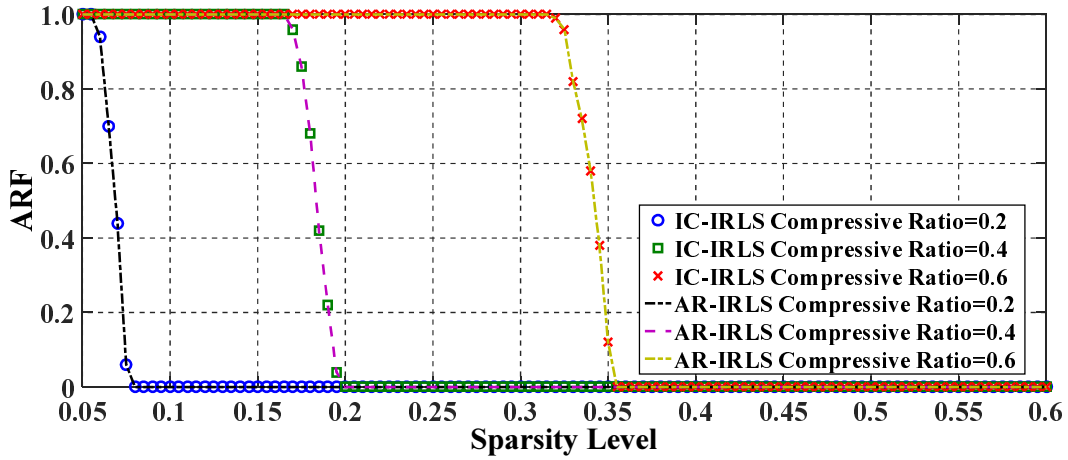
Figure 3.11: ARF vs. sparsity level between the proposed LC-IRLS algorithm and AR-IRLS algorithm with simulated signals under different compressive ratios = 0.2, 0.4, 0.6.
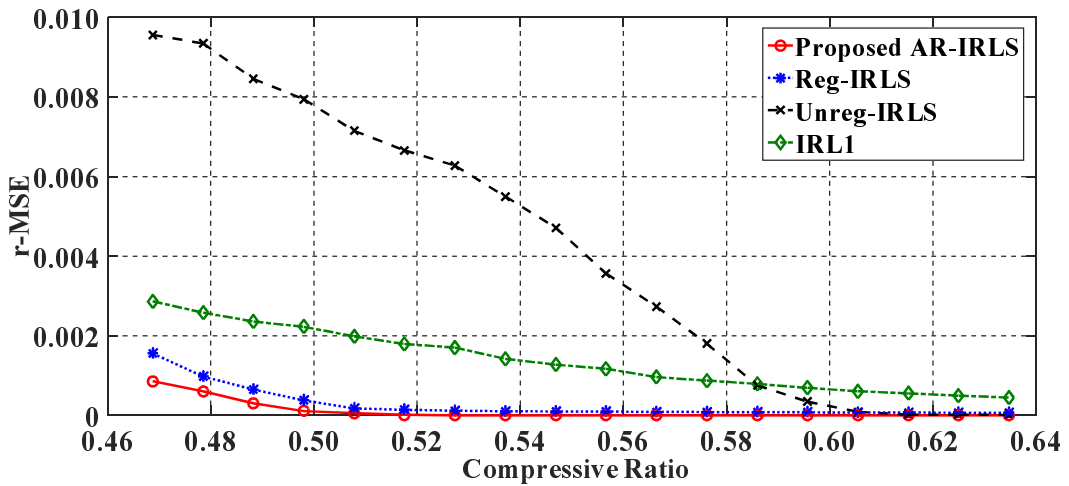
Figure 3.12: r-MSE vs. compressive ratio ρ between proposed AR-IRLS algorithm and other conventional IRLS algorithms after 50 iterations.

3.5.3.1   Reconstruction Performance versus Compressive Ratio

To analyze the reconstruction performance of the proposed scheme with real-world signals over the compressive ratio ρ, we compare the r-MSE of the proposed algorithm against the conventional algorithms under different compressive ratios. Fig. 3.12 shows that the reconstruction performance gets better with a higher compressive ratio at the receiver. More precisely, the relative reconstruction error, obtained after all algorithms converge, and averaged over enough repeats (e.g., 1000 runs), is depicted as a function of the
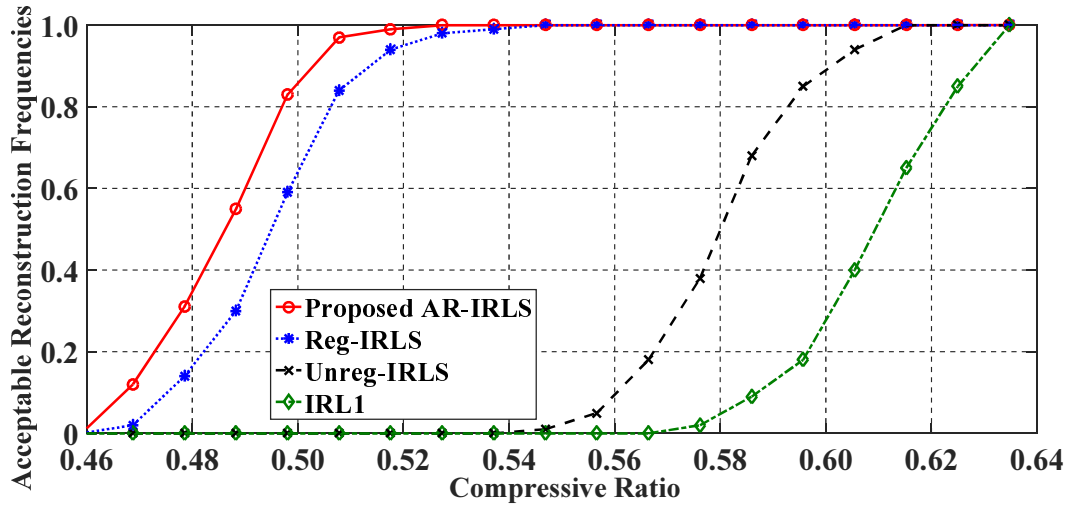
Figure 3.13: Acceptable reconstruction frequencies vs. compressive ratio ρ between proposed AR-IRLS algorithm and other conventional IRLS algorithms after 50 iterations.

compressive ratio ρ in Fig. 3.12. As shown in Fig. 3.12, we see that the proposed AR-IRLS algorithm only requires a few iterations to reach a satisfactory degree of accuracy and it outperforms the conventional algorithms. Fig. 3.13 indicates that as the compressive ratio ρ increases, better reconstruction performance is achieved. It is observed that the curve of Reg-IRLS is close to that of the proposed AR-IRLS since a small regularizer $\epsilon > 0$ is also added to the iteration process different from the other two. Fig. 3.13 also shows that the performance of the proposed IRLS-based spectrum sensing is better than that of the conventional IRLS-based spectrum sensing without regularization when the compression ratio is between 46% and 53%.

3.5.3.2 Reconstruction Performance versus Iterations

Table 3-B shows the least number of iterations required by the proposed AR-IRLS algorithm and by the conventional Reg-IRLS algorithm to achieve a successful reconstruction, and their r-MSEs after the convergence under different sparsity levels μ. As seen from Table 3-B, compared with the Reg-IRLS algorithm, the proposed AR-IRLS algorithm achieves faster convergence as it significantly reduces the number of required iterations for accurate reconstruction. For instance, the least number of iterations for successful
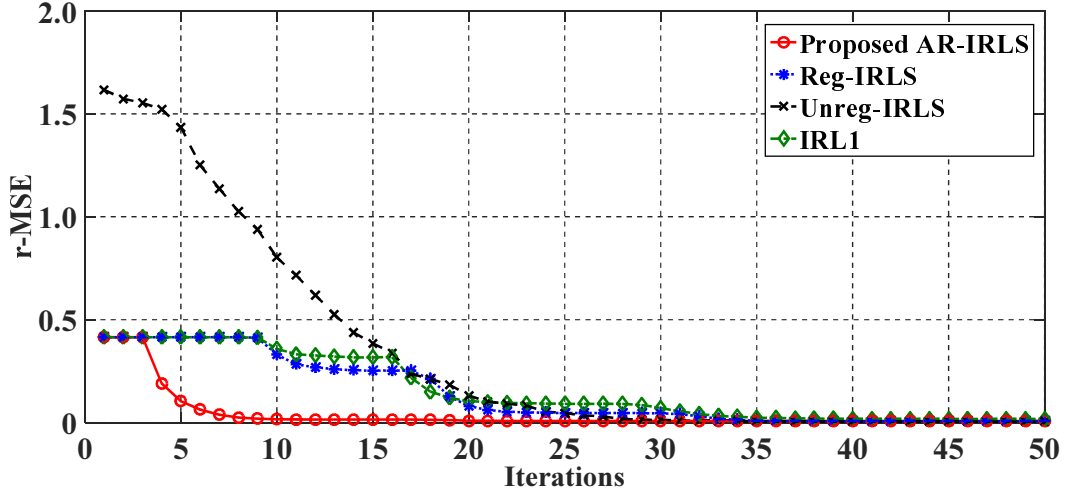
Figure 3.14: r-MSE vs. Iterations between proposed AR-IRLS algorithm and other conventional IRLS algorithms when compressive ratio $\rho = 0.52$.

Table 3-B: Comparison of the convergence speed and reconstruction accuracy under different sparsity levels.

k/N	Iterations		r-MSE after Convergence		Iterations
	Reg-IRLS	**AR-IRLS**	Reg-IRLS	**AR-IRLS**	Reduction
0.1	40	**12**	$7.8 \cdot 10^{-3}$	$\mathbf{6.1 \cdot 10^{-5}}$	70.0%
0.2	40	**14**	$7.2 \cdot 10^{-3}$	$\mathbf{4.3 \cdot 10^{-5}}$	65.0%
0.3	41	**17**	$8.7 \cdot 10^{-3}$	$\mathbf{8.8 \cdot 10^{-5}}$	58.6%
0.4	42	**20**	$9.6 \cdot 10^{-3}$	$\mathbf{6.3 \cdot 10^{-5}}$	52.4%
0.5	44	**26**	$1.1 \cdot 10^{-2}$	$\mathbf{8.6 \cdot 10^{-5}}$	41.0%

reconstruction of the proposed AR-IRLS algorithm is reduced by up to 70% when the sparsity level $\mu = 0.1$, and 41% when the sparsity level $\mu = 0.5$. Furthermore, it shows that the proposed AR-IRLS algorithm achieves higher reconstruction accuracy than that of the Reg-IRLS algorithm under the same number of iterations. When the algorithms reach convergence, the r-MSE of the proposed algorithm is of order 10^{-5}, smaller than that of the proposed algorithm of order 10^{-3}. Therefore, the proposed AR-IRLS algorithm can achieve faster recovery with higher reconstruction resolution compared with the conventional IRLS algorithms.

Under a compression ratio of 0.64, we then compute the r-MSE of the proposed AR-IRLS algorithm against the number of iterations to evaluate its convergence speed and compare it with the conventional IRLS algorithms, to illustrate its reduction of required
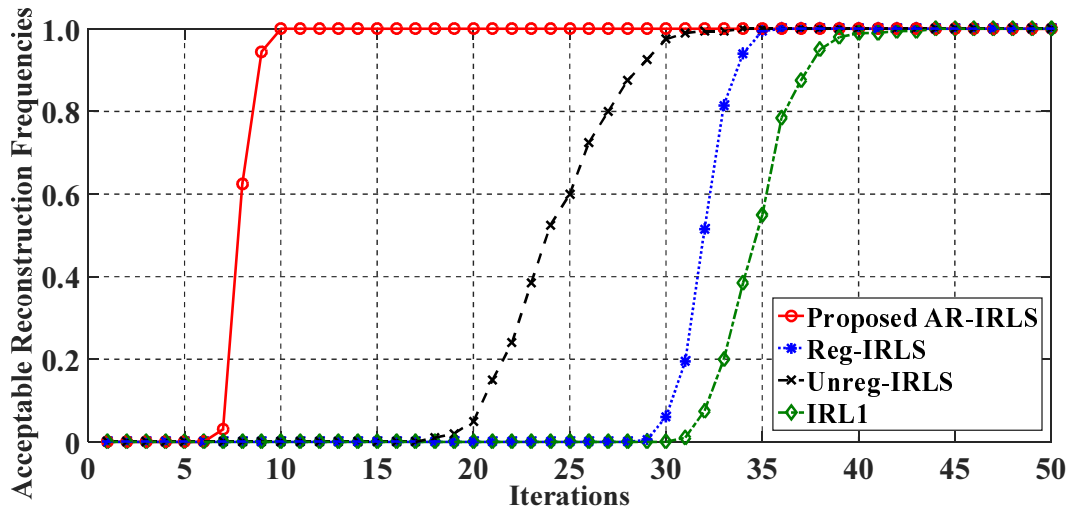
Figure 3.15: Acceptable reconstruction frequencies vs. iterations between proposed AR-IRLS algorithm and conventional IRLS algorithms when compressive ratio $\rho = 0.52$.

iterations under the same reconstruction accuracy, which is presented in Fig. 3.14. As the proposed algorithm directly converges to the actual global minimum shown in Theorem 2, it accomplishes the convergence with a faster speed, while other IRLS algorithms get into several wrong local solutions in the middle of the iteration processes. Moreover, since the proposed algorithm can converge to the actual global minimum without being stuck in wrong local solutions, the reconstruction accuracy of proposed algorithm is monotonically improving with the number of iterations.

Fig. 3.15 shows that the proposed algorithm achieves a 100% successful reconstruction frequency when the number of iterations increases to 9. In contrast, the conventional IRLS algorithms require at least 34 iterations to achieve the same performance. Therefore, the number of iterations is reduced by 70% in the proposed AR-IRLS algorithm without degrading the reconstruction accuracy. This gained benefits can significantly speed up the reconstruction process and reduce the computational burden in comparison with the conventional IRLS algorithms.

To validate the effectiveness of the proposed IC-IRLS algorithm with real-world signals as well as to prove that the reduced computational complexity in the proposed algorithm from cubic time to linear is not achieved at the cost of more iterations, we compare
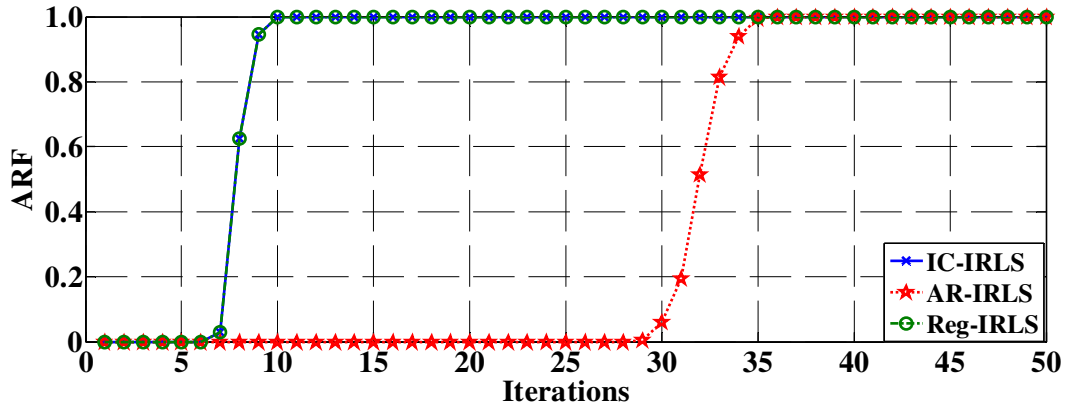
Figure 3.16: ARF vs. iterations between the proposed IC-IRLS algorithm and conventional IRLS algorithms with real-world signals, where the sparsity level of the received real-world signal is about 0.2 and compressive ratio = 0.52.

the number of iterations of the proposed algorithm with the AR-IRLS algorithm and the regularized IRLS algorithm under the compressive ratio = 0.52 in Fig. 3.16, where the sparsity level of the received real-world signal is about 0.2. It can be observed that the proposed algorithm holds fast convergence rate, which achieves the 100% successful reconstruction of the real-world signals when the number of iterations is 9 without introducing any prior information, where the conventional IRLS algorithms require at least 34 iterations to achieve the same performance. Therefore, the proposed algorithm keeps the fast convergence speed with significantly reduced computational complexity.

3.6 Summary

A real-time wideband spectrum sensing scheme with sub-Nyquist sampling was developed. To achieve fast reconstruction from the compressive samples, an AR-IRLS algorithm has been proposed to implement the CS-based wideband spectrum sensing with a high fidelity guarantee, which could cope with varying bandwidths and power levels in real-world signals. The proposed algorithm was tested over the real-world measurements after having been validated by the simulated signals with random supports and amplitudes. Numerical results showed that the convergence speed of the proposed recon-

struction algorithm has been increased by up to 70% in comparison with the conventional IRLS algorithms. Due to the optimization-based algorithm nature, the proposed AR-IRLS algorithm does have higher computational complexity than those greedy methods, e.g., OMP and CoSaMP even though the proposed algorithm has reduced the number of iterations by up to 70% in comparison with the conventional IRLS algorithms. Moreover, a descent-based algorithm has been proposed to distinguish the primary signals from the mixture of reconstruction errors and unknown noises, by dynamically setting the threshold without any prior knowledge of the noise power. These benefits enable the proposed algorithm to be implementable for in real-time processing in new wireless services such as machine-to-machine communications. Consequently, the proposed algorithm would be a strong candidate to sense over a much wider spectrum spanning the cellular and industrial scientific medical (ISM) bands.

Chapter 4

Blind Compressive Sensing Augmented Spectrum Sensing

This chapter proposes a new spectrum sensing technique, referred to as blind compressive sensing (CS) augmented spectrum sensing, which aims to address the varying sparsity levels and the number of cooperating IoT devices issues in cognitive IoT environment. In the proposed scheme, the compressive samples are collected block-by-block in time while the spectral is gradually reconstructed until the stopping criterion is reached. After the number of minimum sensing time intervals is chosen without knowledge of spectral sparsity or channel characteristics, the adaptive sampling rates or sensing time can be reduced/increased with the varying sparsity levels afterwards. Moreover, to select the suitable number of cooperating IoT devices for spectrum sensing, a CS-based blind cooperating user selection algorithm is proposed via indirectly measuring the degeneration of SNR experienced by different SUs. Numerical and real-world test results demonstrate that the proposed algorithms achieve high detection performance with reduced sensing time and number of cooperating SUs in comparison with the conventional compressive spectrum sensing algorithms. Specifically, the related work and main contributions are firstly introduced in Section 4.1. Section 4.2 describes the system model. Based on it,

66

Section 4.3 develops the proposed blind compressive sensing augmented spectrum sensing scheme. Section 4.4 analyses and validates the proposed schemes. Finally, Section 4.5 concludes this chapter.

4.1 Introduction

4.1.1 Related Work

Recently, there are some works employing CS into spectrum sensing. In [95] and [96], novel frequency-domain cyclic prefix (CP) autocorrelation based compressive spectrum sensing algorithms were proposed to detect PUs in the presence of noise uncertainty and frequency selectivity. By making use of sparsity in the spectral domain, CS was utilized to construct the autocorrelation of the received signal from its subband sample sequences. In [14] and [97], hybrid frameworks are proposed to incorporate the advantages of both geolocation database and CS-based spectrum sensing. However, the aforementioned works require the prior knowledge such as instant sparsity level of the wideband spectrum for signal reconstruction. Since the instant sparsity level is often unknown in practice, most of CS approaches such as the above mentioned works have to assume a large sparsity level and choose the excess number of compressive samples to guarantee the quality of reconstruction. It turns out that these approaches require more sensing time or higher sampling rates to collect compressive samples, which causes larger sensing latency and therefore loses the advantage of using CS technologies. Therefore, to eliminate the prior knowledge of instant spectral sparsity level in CS-based spectrum sensing. Authors in [98] proposed a sparsity order estimation method to obtain the minimum sampling rate. To further improve the sparsity order estimation performance, a dynamic sparsity upper bound adjustment scheme was proposed in [99] for obtaining a proper sparsity upper bound. Compared with these algorithm, The idea that autonomously choose the number of compressive measurements without sparsity estimation efforts could be utilized to address this challenge [100].

To solving the cooperating SUs selection problem in spectrum sharing framework, with the knowledge of the SUs' locations, the authors in [101] addressed the user selection problem by selecting a set of SUs which experience uncorrelated shadow fading. The knowledge of the distance between SUs and base station is required by those algorithms which also need the central coordination, i.e., the sensing results should be sent to the fusion center for selection. In [102], without the prior knowledge of the SUs' locations, three methods for selecting the SUs based on hard local decisions were proposed, which outperform the purely random selection method of SUs. Moreover, a correlation-aware user selection scheme was proposed in [103], which was developed by adaptively selecting the SUs based on the evaluation of the correlation experienced by the SUs. However, the aforementioned algorithms are under the circumstance of narrowband sensing rather than wideband one and therefore are not suitable for wideband CSS. In [104], a hybrid double threshold based CSS scheme was proposed, which could improve the detection performance at SUs by exploiting both local decisions and global decisions feedback from the fusion center. Based on order statistic information of the reporting links between SUs and fusion center, a multi-selective sensing scheme was proposed in [105]. The links with high SNRs are selected and the number of selected links is decided centrally. Although the two schemes could be applied in wideband CSS, the selection process would be inefficient since the schemes introduce large latency due to the sequential manner of sensing. Our proposed blind user selection algorithm in this paper could capture the whole wide spectrum at the same time based on CS but utilizes a few compressive samples to select the SUs with high detection capabilities.

4.1.2 Contributions

Motivated by the above challenges, the contribution of this paper is two-fold.

1. Firstly, in order to reduce both the sensing time and data processing burden, and provide the exact signal reconstruction without any extra channel assumption including prior knowledge of sparsity, we propose an blind CS-based sensing

algorithm that enables the local SUs to choose the number of compressive samples automatically. More specifically, instead of assuming the upper limit of sparsity level, which would not take the full advantage of CS due to redundant samples collection, the proposed algorithm can blindly terminate the samples acquisition when the proposed Euclidean distance D_p is smaller than a given threshold. The proposed algorithm could therefore achieve the minimum sensing time under the given sampling rate. Moreover, based on the achieved minimum sensing time according to the current signal sparsity, the adaptive sampling rates or sensing time can be reduced/increased with the varying sparsity levels afterwards.

2. Secondly, we propose a CS-based blind cooperating user selection algorithm over wide spectrum without any prior knowledge of the primary signals, sensor locations. More specifically, by observing the reconstruction error of CS is degraded with the SNR experienced by SUs, i.e., lower SNR leading to larger reconstruction error under given sampling rate and sensing time, the proposed algorithm employ the same mathematical mechanism as the proposed blind CS-based sensing algorithm to indirectly compare the degenerating of SNRs according to the approximated reconstruction errors.

4.2 System Model

4.2.1 System Architecture

Apart from the TV white space (TVWS), the 3550-3700 MHz (referred to as 3.5 GHz band) Citizens Broadband Radio Service (CBRS), is considered for the spectrum sharing by Federal Communications Commission (FCC) in the US. Meanwhile, UK Office of Communications (Ofcom) has published the call for input [25] which considers the 3.8 GHz to 4.2 GHz as the first band where they apply the spectrum sharing framework. Those shared spectrum could be utilized for the communications in IoT. In order to share

the spectrum efficiently and limit the interference among users, three-tiered spectrum access framework was introduced in the above-mentioned shared spectrums [26, 27], where the incumbent users as the PUs operate at the top tier, while the CBRS users as the SUs operate at the second or third tiers holding priority access license (PAL) or generalized authorized access (GAA), respectively. Each tier accepts interference from tiers above and is protected from tiers below. In the conventional three-tiered spectrum access framework, the responsibility of spectrum access system (SAS) is to manage all the incumbent and secondary operations based on the information obtained from the incumbent database and the incumbent detection, i.e., environmental sensing capability (ESC). The incumbent database provides all the necessary spectrum usage and operational information of the incumbent users. ESC detects the presence of shipborne incumbent users with a group of RF sensors and the interference from the unregistered users. As shown in Fig. 4.1, the proposed scheme adopt the CBSD sensing network that consists of the CBRS access points and the CBRS users, e.g., IoT devices, with sensing capability to identify spectrum opportunities and the unregistered users operating on the target spectrum. Moreover, due to the centralized nature of SAS and the availability of the multiple SUs, the proposed scheme can utilize the CSS scheme over the SUs within the same secondary access network to deal with the issues such as multi-path and shadowing, which also can increase the spatial diversity and reduce the probability of deep fading across all the SUs.

4.2.2 Signal Model

Since the sensing in the three-tiered spectrum access framework aims to find the spectrum holes which could be used for secondary access and identify the unwanted interference event over the whole shared spectrum as well, without loss of generality and content repetition, we shall use the same signal model presented in the Chapter 3.
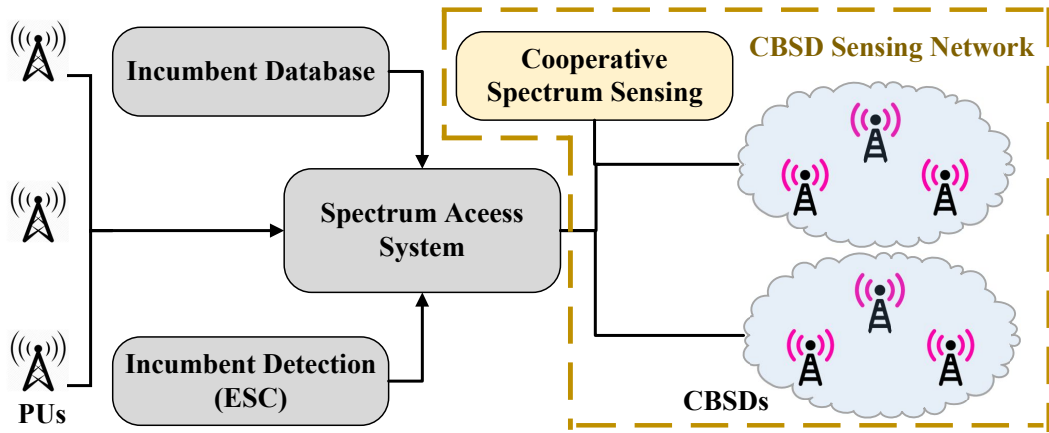
Figure 4.1: The proposed sensing-augmented spectrum sharing architecture

4.3 Blind Compressive Sensing Augmented Spectrum Sensing Scheme

4.3.1 Blind CS-based Sensing Algorithm

Due to the shorter propagation distance as the result of higher central frequencies (3.5GHz or above) used in three-tiered spectrum access framework, most spectrum occupancy status varies with users accessing or releasing the spectrum randomly. Therefore, the sparsity of the wideband signals is also varying and unknown [106]. In CS theory, the number of compressive samples M is chosen regarding the sparsity level k of the signal in order to guarantee the quality of reconstruction, e.g., $M \geq Ck \log(N/k)$ for a Gaussian measurement matrix, where C denotes a constant [11]. The sparsity level k of the spectrum is assumed to be known in most of the CS-based spectrum sensing approach. These approaches intend to assume a maximum sparsity level $k_{\max}$ to ensure a high successful recovery rate since the sparsity level is often unknown and fluctuates in practice. Therefore, the required number of compressive samples is larger than the necessary amount, which causes unnecessary sensing latency or higher sampling rate for collecting extra samples.

In contrast, our blind CS-based sensing algorithm is adaptive to actual sparsity level.

Firstly, the sensing time T_s is divided into several time intervals and the wideband signal is acquired block-by-block in time until the stopping criterion regarding reconstruction accuracy is reached. Based on the achieved minimum sensing time according to the current signal sparsity, the adaptive sampling rates or sensing time can be reduced/increased with the varying sparsity levels afterwards. Therefore, the waste of samples can be averted and the sensing latency or sampling rate could be further reduced.

Specifically, under the assumption of stationary signals, the proposed algorithm divides the total sensing time T_s into P time intervals where p ($p \in [1, P]$) refers to the index of each time intervals. Let $\boldsymbol{y}_p$ represents a vector contains all the samples which are collected until the end of the p-th time interval, and M_p denotes the number of elements in vector $\boldsymbol{y}_p$, where $0 < M_1 < \cdots < M_p$. $\boldsymbol{\Delta y}_p$ and ΔM represent a vector contain the samples collected during the p-th time interval and the number of samples collected in each time interval, respectively, i.e., $\Delta M = M_p - M_{p-1}$. The iterative estimates $\{\boldsymbol{x}_p^{(l)}\}_{l=1}^{\infty}$ of $\boldsymbol{x}_p$ is given by

$$
\begin{aligned}
\boldsymbol{x}_p^{(l)} &:= \underset{\boldsymbol{x}_p \in \mathbb{R}^N}{\arg\min} ||\boldsymbol{\Phi}_p \boldsymbol{x}_p - \boldsymbol{y}_p||_2^2 + \lambda ||\boldsymbol{x}_p||_2^{2(\boldsymbol{w}_p^{(l)})}, \\
\boldsymbol{w}_p^{(l)} &:= (w_{p(1)}^{(l)}, ..., w_{p(N)}^{(l)}),
\end{aligned}
\tag{4.1}
$$

where $||\boldsymbol{x}||_2^{2(\boldsymbol{w})}$ denotes $\sum_{i=1}^N w_i x_i^2$ and $w_{p(j)}^{(l)}$ is defined as

$$
w_{p(j)}^{(l)} = \left(\left(x_{p(j)}^{(l-1)} \right)^2 + \epsilon \right)^{\frac{\nu}{2}-1} \qquad 0 < \nu < 1.
\tag{4.2}
$$

After convergence, $\boldsymbol{x}_p^{(l-1)}$ will be sufficiently close to $\boldsymbol{x}_p^{(l-1)}$, so that $||\boldsymbol{x}_p||_2^{2(\boldsymbol{w}_p^{(l)})} = \sum_{j=1}^N w_{p(j)}^{(l)} x_{p(j)}^2 = \sum_{j=1}^N ((x_{p(j)}^{(l-1)})^2 + \epsilon)^{\frac{\nu}{2}-1} \cdot x_{p(j)}^2$ would be close to $||\boldsymbol{x}_p||_v^v$. To simplify the illustration of the proposed algorithm, we define a function F_ν as

$$
F_\nu(\boldsymbol{x}, \boldsymbol{\Phi}, \boldsymbol{w}) := \left[\frac{1}{2} ||\boldsymbol{\Phi}\boldsymbol{x} - \boldsymbol{y}||_2^2 + \lambda \sum_{i=1}^N w_{(i)} x_{(i)}^2 \right],
\tag{4.3}
$$

Therefore, the estimate in each iteration is equal to

$$\boldsymbol{x}_p^{(l)} := \arg\min \ F_\nu(\boldsymbol{x}_p, \boldsymbol{\Phi}_p, \boldsymbol{w}^{(l)}), \tag{4.4}$$

which requires solving a least squares problem that can be expressed in this matrix form:

$$\boldsymbol{x}_p^{(l)} = \boldsymbol{W}_p^{(l)} \boldsymbol{\Phi}_p^T \left(\boldsymbol{\Phi}_p \boldsymbol{W}_p^{(l)} \boldsymbol{\Phi}_p^T + \lambda \boldsymbol{I} \right)^{-1} \boldsymbol{y}_p, \tag{4.5}$$

where $\boldsymbol{W}_p^{(l)}$ is the $N \times N$ diagonal matrix with $1/w_{p(i)}^{(l)}$ as the i-th diagonal element and $\boldsymbol{\Phi}_p^T$ refers to the transpose of the sensing matrix $\boldsymbol{\Phi}_p$. Once $\boldsymbol{x}_p^{(l)}$ is obtained, we then update the weights accordingly. Repeating the whole procedure of signal acquisition and reconstruction, a sequence of spectrum reconstruction by increasing the number of time intervals, i.e., $\boldsymbol{x}_1, \boldsymbol{x}_2, \ldots, \boldsymbol{x}_p$, would be obtained. We now analyze the stopping criterion of signal acquisition. After each signal reconstruction process, the proposed algorithm decides whether the reconstruction of the original signal is accurate enough or not. If the reconstructed signal does not satisfy certain accuracy requirement of spectral detection, the algorithm should require more time intervals until the accuracy requirement is met. However, since the original signal $\boldsymbol{x}$ is unknown before the reconstruction in real-world, the exact reconstruction error $e = ||\boldsymbol{x} - \boldsymbol{x}_p||_2^2$, could not be obtained to determine how accuracy the reconstructed signal is. Therefore, we measure the reconstruction error e indirectly and set stopping criterion in such a practical way. As the compressive samples vector $\boldsymbol{y}_p$ could be treated as the linear projection of the original signal $\boldsymbol{x}$ during the sampling process, the Euclidean distance D_p between the sampling result obtained by applying the same linear function, i.e., sensing matrix, to the reconstructed signal, and the actual compressive samples should not be too far, otherwise we shall tell the reconstructed signal $\boldsymbol{x}_p$ is quite different from the original signal $\boldsymbol{x}$ with high probability. Specifically, the proposed Euclidean distance D_p is defined as

$$D_p = ||\boldsymbol{\Phi}_{\Delta M} \boldsymbol{x}_p - \boldsymbol{\Delta} \boldsymbol{y}_{p+1}||_2^2, \tag{4.6}$$

Algorithm 3 Blind CS-based sensing algorithm

Require: Equally divide the total spectrum sensing time T_s into P time intervals and set the start time interval index $p = 1$. Sampling rate f_s, number of samples ΔM collected in each time interval and the reconstruction error threshold κ.

Ensure: The reconstructed signal $\boldsymbol{x}^*$

 1: **for** $p = 1, \ldots, P$ **do**

 2:     Sampling the wideband signal using f_s till the time interval $p + 1$ so as to obtain the compressive samples vector $\boldsymbol{y}_p$ and the samples $\Delta\boldsymbol{y}_{p+1}$ collected in time interval $p + 1$.

 3:       Reconstruct the spectral from $\boldsymbol{y}_p$ by utilizing Algorithm 2 to solve the l_ν-norm minimization problem

$$\arg\min_{\boldsymbol{x}_p \in \mathbb{R}^N} ||\boldsymbol{\Phi}_p\boldsymbol{x}_p - \boldsymbol{y}_p||_2^2 + \lambda||\boldsymbol{x}_p||_\nu^\nu,$$

   which leads to a spectral reconstruction $\boldsymbol{x}_p$.

 4:     Calculate the proposed Euclidean distance

$$D_p = ||\boldsymbol{\Phi}_{\Delta M}\boldsymbol{x}_p - \Delta\boldsymbol{y}_{p+1}||_2^2$$

 5:     **if** D_p smaller than threshold κ is true

 6:         Terminate the signal acquisition process.

 7:     **else**

 8:          $p = p + 1$

 9:     **end if**

10: **end for**

---

and $\boldsymbol{\Delta y}_{p+1}$ is obtained by

$$\boldsymbol{\Delta} y_{p+1} = \boldsymbol{\Phi}_{\Delta M}\boldsymbol{x} + \boldsymbol{\xi}, \tag{4.7}$$

where $\boldsymbol{\Phi}_{\Delta M}$ denotes a $\Delta M \times N$ matrix. The Johnson-Lindenstrauss Lemma presented in [107] asserts that a high-dimensional space can be projected into a low-dimensional signal, where the dimension is equal or larger than $O(\zeta^{-2}\log N)$ so that all distances are preserved up to a multiplicative factor between $1 - \zeta$ and $1 + \zeta$ with $0 < \zeta \leq 1/2$. Therefore, we demonstrate the rigorous relationship between the proposed Euclidean distance D_p and the actual reconstruction error e by proving the point that $e = ||\boldsymbol{x} - \boldsymbol{x}_p||_2^2$ calculated in high-dimensional, i.e., dimension of $\boldsymbol{x}_p$, could be projected into D_p calculated in low-dimensional, i.e., dimension of $\boldsymbol{\Delta y}_{p+1}$, within the boundary factor of $1 \pm \zeta$ in Theorem 3. If the proposed Euclidean distance D_p is larger than the given threshold, the algorithm would continue the signal acquisition, otherwise the acquisition is ter-

minated. For a given threshold κ which is predefined according to the reconstruction accuracy requirement, the minimum sensing time of the wideband signals would adapt to the actual sparsity levels of the spectrum. After the initial sensing period, the next sensing period could increase/reduce the number of time intervals based on the sensing time adopted in the previous period. Or adjusting the sampling rates while keeping the sensing time fixed. It would be useful when the time window of transmission need to be stable. The rate switching can be conveniently integrated in practical hardware implementations. For example, a serial random sampler such as the analog-to-information converter (AIC) [43], can flexibly adjust its sampling rate at the last ADC block to yield the different effective sampling rates. The outline of the proposed algorithm is summarized in Algorithm 3.

In theorem 3, we prove that the actual reconstruction error e could be estimated by the proposed Euclidean distance D_p within the boundary factor of $1 \pm \zeta$.

Theorem 3. *Given multiplicative factor $\zeta \in (0, 1/2]$, $\gamma \in (0, 1)$ and $\Delta M \leq C\zeta^{-2}log(1/2\gamma)$, we have*

$$Prob\left[\frac{D_p}{(1+\zeta)} \leq e \leq \frac{D_p}{(1-\zeta)}\right] \geq 1 - \gamma, \tag{4.8}$$

where the parameter C depends on the concentration property of random variables in measurement matrix $\mathbf{\Phi}_{\Delta M}$ [107]. D_p and e are defined as before.

Proof. With the aid of Johnson-Lindenstrauss Lemma, if the number of row r in $\mathbf{\Phi}_{\Delta M}$ is equal or larger than $C\zeta^{-2}\log(1/2\gamma)$, we have

$$(1 - \zeta)||\mathbf{X}||_2^2 \leq ||\mathbf{\Phi}_{\Delta M}\mathbf{X}||_2^2 \leq (1 + \zeta)||\mathbf{X}||_2^2, \tag{4.9}$$

where $\zeta \in (0, 1/2]$ and $\gamma \in (0, 1)$. Then we replace $\mathbf{X}$ in (4.9) by $\mathbf{x} - \mathbf{x}_p$ and obtain

$$(1 - \zeta)||\mathbf{x} - \mathbf{x}_p||_2^2 \leq ||\mathbf{\Phi}_{\Delta M}(\mathbf{x} - \mathbf{x}_p)||_2^2$$
$$\leq (1 + \zeta)||\mathbf{x} - \mathbf{x}_p||_2^2. \tag{4.10}$$

Since measurement matrix $\boldsymbol{\Phi}_{\Delta M}$ could be seen as a linear projection from $\mathbb{R}^N$ to $\mathbb{R}^{\Delta M}$, we can transform (4.10) into

$$(1 - \zeta)||\boldsymbol{x} - \boldsymbol{x}_p||_2^2 \leq ||\boldsymbol{\Phi}_{\Delta M}\boldsymbol{x_p} - \Delta\boldsymbol{y}_{p+1}||_2^2$$
$$\leq (1 + \zeta)||\boldsymbol{x} - \boldsymbol{x}_p||_2^2. \tag{4.11}$$

Finally, to obtain the observation that $e = ||\boldsymbol{x} - \boldsymbol{x}_p||_2^2$ could be bounded and estimated by $D_p = ||\boldsymbol{\Phi}_{\Delta M}\boldsymbol{x}_p - \Delta\boldsymbol{y}_{p+1}||_2^2$, we change the (4.11) to another form (4.12) and simplify it to (4.13):

$$\frac{1}{(1 + \zeta)}||\boldsymbol{\Phi}_{\Delta M}\boldsymbol{x}_p - \Delta\boldsymbol{y}_{p+1}||_2^2 \leq ||\boldsymbol{x} - \boldsymbol{x}||_2^2$$
$$\leq \frac{1}{(1 - \zeta)}||\boldsymbol{\Phi}_{\Delta M}\boldsymbol{x}_p - \Delta\boldsymbol{y}_{p+1}||_2^2, \tag{4.12}$$

$$\frac{D_p}{(1 + \zeta)} \leq e \leq \frac{D_p}{(1 - \zeta)}. \tag{4.13}$$

Therefore, when the row number ΔM in $\boldsymbol{\Phi}_{\Delta M}$ is equal or larger than $C\zeta^{-2}\log(1/2\gamma)$, the distance between D_p and e could be bounded up to a multiplicative factor between $1 - \zeta$ and $1 + \zeta$. Hence, we could state that the actual reconstruction error e could be estimated by the proposed Euclidean distance D_p when ΔM is larger than a lower bound and D_p could be utilized as the stopping criterion of the algorithm. See Theorem 4 for The proof of that (4.12) is satisfied with probability larger than $1 - \gamma$. $\square$

Theorem 4. *Given that:*

$$\frac{1}{(1 + \zeta)}||\boldsymbol{\Phi}_{\Delta M}\boldsymbol{x}_p - \Delta\boldsymbol{y}_{p+1}||_2^2 \leq ||\boldsymbol{x} - \boldsymbol{x}||_2^2 \leq \frac{1}{(1 - \zeta)}||\boldsymbol{\Phi}_{\Delta M}\boldsymbol{x}_p - \Delta\boldsymbol{y}_{p+1}||_2^2, \tag{4.14}$$

where the symbols are defined as above, we shall have (4.14) is satisfied with probability larger than $1 - \gamma$.

Proof. Let $\boldsymbol{X} \in \mathbb{R}^n$ be an arbitrary fixed unit vector, i.e., $||\boldsymbol{X}||_2^2 = 1$ for simplicity, and

the linear projection $\boldsymbol{X} \to \boldsymbol{Y}$ is defined by

$$Y_{(i)} = \sum_{j=1}^{n} A_{(ij)} X_{(j)}, \qquad i = 1, 2, \ldots, r, \tag{4.15}$$

where $A_{(ij)}$ are independent random variables with $\mathrm{E}[A_{(ij)}] = 0$ and $\mathrm{Var}[A_{(ij)}] = 1$, which has an uniform sub-Gaussian tail. Since $\boldsymbol{Y}$ could be seen as a linear combination of the $\boldsymbol{A}_{(i)}$ which is the i-th row of $\boldsymbol{A}$, $Y_{(i)}$ has an uniform sub-Gaussian tail as well. Therefore, according to the Proposition 3.2 in [107], we could define a random variable as

$$Z = \frac{1}{\sqrt{r}}(Y_{(1)}^2 + \cdots + Y_{(r)}^2 - r), \tag{4.16}$$

where Z has a sub-Gaussian tail up to $\sqrt{r}$. Therefore, $||\boldsymbol{Y}||_2^2 - 1$ is distributed as $Z/\sqrt{r}$ and we can get

$$\begin{aligned}
\mathrm{Prob}[||\boldsymbol{Y}||_2 \geq 1 + \zeta] &= \mathrm{Prob}[||\boldsymbol{Y}||_2^2 \geq 1 + \zeta^2 + 2\zeta] \\
&\leq \mathrm{Prob}[||\boldsymbol{Y}||_2^2 \geq 1 + 2\zeta] \\
&= \mathrm{Prob}[Z \geq 2\zeta\sqrt{r}].
\end{aligned} \tag{4.17}$$

As $\zeta \in (0, 1/2]$, by utilizing the Chernoff-type inequality, we have

$$\mathrm{Prob}[Z \geq 2\zeta\sqrt{r}] \leq \exp^{-a(2\zeta\sqrt{r})^2} = \exp^{-4a\zeta^2 C\zeta^{-2}\log(2/\gamma)} \leq \frac{\gamma}{2} \tag{4.18}$$

for $C \geq 1/2a$. Applying the same principle and the similar calculation as above, $\mathrm{Prob}[||\boldsymbol{Y}||_2 \leq 1 - \zeta] \leq \gamma/2$ could be demonstrated as well. Therefore, we can get the conclusion that

$$\mathrm{Prob}\left[(1 - \zeta)||\boldsymbol{X}||_2^2 \leq ||\boldsymbol{A}\boldsymbol{X}||_2^2 \leq (1 + \zeta)||\boldsymbol{X}||_2^2\right] \geq 1 - \gamma. \tag{4.19}$$

Then we replace $\boldsymbol{X}$ in (4.19) by $\boldsymbol{x} - \boldsymbol{x}_p$ to obtain (4.20). As $\boldsymbol{A}$ refer to the linear

projection $\boldsymbol{X} \to \boldsymbol{Y}$, we could get (4.21) and its another form (4.22), shown below:

$$\text{Prob}\big[(1-\zeta)||\boldsymbol{x}-\boldsymbol{x}_p||_2^2 \leq ||\boldsymbol{\Phi}_{\Delta M}(\boldsymbol{x}-\boldsymbol{x}_p)||_2^2$$
$$\leq (1+\zeta)||\boldsymbol{x}-\boldsymbol{x}_p||_2^2\big] \geq 1-\gamma, \tag{4.20}$$

$$\text{Prob}\big[(1-\zeta)||\boldsymbol{x}-\boldsymbol{x}_p||_2^2 \leq ||\boldsymbol{\Phi}_{\Delta M}\boldsymbol{x}_p - \Delta\boldsymbol{y}_{p+1}||_2^2$$
$$\leq (1+\zeta)||\boldsymbol{x}-\boldsymbol{x}_p||_2^2\big] \geq 1-\gamma, \tag{4.21}$$

$$\text{Prob}\left[\frac{1}{(1+\zeta)}||\boldsymbol{\Phi}_{\Delta M}\boldsymbol{x}_p - \Delta\boldsymbol{y_{p+1}}||_2^2 \leq ||\boldsymbol{x}-\boldsymbol{x}^*||_2^2 \right.$$
$$\left. \leq \frac{1}{(1-\zeta)}||\boldsymbol{\Phi}_{\Delta M}\boldsymbol{x}_p - \Delta\boldsymbol{y}_{p+1}||_2^2\right] \geq 1-\gamma. \tag{4.22}$$

Finally, we shall simplify (4.22) to the result

$$\text{Prob}\left[\frac{D_p}{(1+\zeta)} \leq e \leq \frac{D_p}{(1-\zeta)}\right] \geq 1-\gamma. \tag{4.23}$$

□

4.3.2 CS-based Blind Cooperating User Selection Algorithm

In this section, we present a CS-based blind cooperating user selection algorithm applied in the CBSD sensing network for selecting the SUs with high SNR in the proposed scheme without the degradation of the detection performance by utilizing fewer SUs. In a CBRS sensing network, not every SU could produce informative spectrum sensing results due to the different deployment scenarios of the SUs. Moreover, as the number of cooperating SUs grows, the energy efficiency of the network decreases [108] and the sensing performance of the network only marginally increases once the number of cooperating SUs is sufficiently large [109]. Therefore, it is not an optimal choice to cooperate all SUs no matter whether they have high detection capability or not. The optimal performance could be achieved by selectively cooperating among SUs with high sensing performance of the transmission signals [110] where the sensing performances of SUs are fundamen-
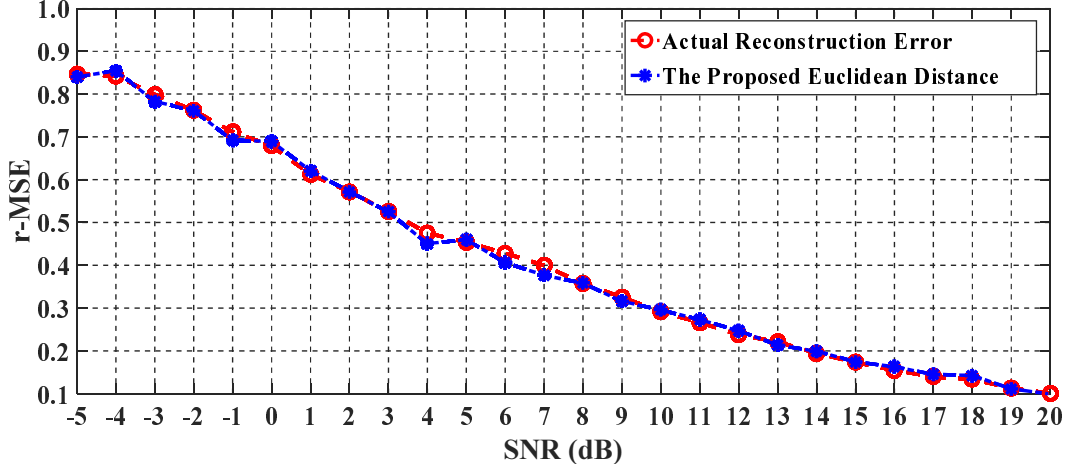
Figure 4.2: r-MSE vs. average SNR between the actual reconstruction error and the estimated reconstruction error.

tally limited by the signal transmission channels since the reconstruction accuracy would be effected by the SNR of received signals.

As shown in Fig. 4.2, if the sampling rate is fixed and sufficient for signal reconstruction, reconstruction performance would be affected by the SNR of the transmission signal, which is likely caused by the channel fading, i.e., shadowing and multi-path. Therefore, CS could be utilized for cooperating user selection and the proposed blind CS-based spectrum sensing scheme could perform user selection without extra SNR estimation algorithms. The SUs with high SNR, could be selected by utilizing the proposed D_p to approximate the unknown reconstruction error. From the perspective of topological geo-positioning, the distance between cooperating IoT devices is assumed sufficient close in the proposed scheme, which means the true status of spectrum occupancy is same. Specifically, the compressed samples vector $\boldsymbol{y}$ is divided into two vectors $\boldsymbol{y}_r$ ($\boldsymbol{y}_r \in \mathbb{R}^{r \times 1}$) and $\boldsymbol{y}_v$ ($\boldsymbol{y_v} \in \mathbb{R}^{v \times 1}$) for estimating the reconstruction error. These two vectors can be expressed as $\boldsymbol{y}_r = \boldsymbol{\Phi}_r \boldsymbol{x} + \boldsymbol{\xi}$ and $\boldsymbol{y}_v = \boldsymbol{\Phi}_v \boldsymbol{x} + \boldsymbol{\xi}$, respectively, where $\boldsymbol{x} \in \mathbb{R}^{N \times 1}$, $\boldsymbol{\Phi}_r \in \mathbb{R}^{r \times N}$ and $\boldsymbol{\Phi}_v \in \mathbb{R}^{v \times N}$. Parameter r as the number of compressed measurements in $\boldsymbol{y}_r$, is determined to ensure the successful reconstruction, and v is set to guarantee the sufficient accuracy of reconstruction error estimation as illustrated in Theorem 1. To select the suitable cooperating SUs, one can compare the estimated reconstruction error

e^* with a predefined threshold which could be determined according to the detection capability requirement of SUs. Moreover, without the effort of signal reconstruction, only the locally collected samples should be sent to the fusion center for SUs selection under the centralized manner or be passed to other SUs under the distributed manner of the distributed CSS network.

4.4 Experimental Results

As a proof of concept for the proposed scheme, we verify the effectiveness of the proposed algorithms using both simulated signals and real-world signals in this section.

4.4.1 Results over Simulated Signals

Consider the simulated wideband signal $x(t) \in \mathcal{F} = [0, 500]$ MHz, whose DFT is denoted as $\boldsymbol{x_0^{\mathrm{sim}}}$ which contains up to k active channels:

$$x(t) = \sum_{i=1}^{k} \sqrt{E_i B_i} \mathrm{sinc}(B_i(t - t_i)) e^{j2\pi f_i t} + n(t), \tag{4.24}$$

where $\mathrm{sinc}(x) = \sin(\pi x)/(\pi x)$, E_i, t_i and f_i represent the energy, the time offset, and the central frequency of the i-th sub-band and $n(t)$ denotes the noise. The i-th sub-band covers the frequency range $[f_i - \frac{B_i}{2}, f_i + \frac{B_i}{2}]$. Typically, the critical influences of a signal transmission channel consist of path loss, small-scale fading, e.g., multi-path, and large-scale fading, e.g., shadowing [101]. In each CBSD sensing network, the path loss could be approximately the same for all SUs since the maximum distance among SUs are assumed to be much smaller than the distance between the PUs and the SUs. For the fading effects, the multi-path effect exhibits a Rayleigh distribution, which could cause random variations in the SNR at the SUs, while the shadowing effect could be viewed as extra losses via a series of obstacles which is notoriously hard to model accurately and its statistics can vary widely with the deployment environments [109]. Therefore,

we assume the SNR is varying in some channels for the different SUs in order to model both the large-scale and the small-scale fading effects.

To demonstrate the effectiveness of the proposed scheme over the wideband spectrum with the varying bandwidths and power levels of primary signals, the bandwidths B_i of i-th primary signal is varying from 5 to 20 MHz and the corresponding central frequency f_i is randomly located in $[\frac{B_i}{2}, W - \frac{B_i}{2}]$. The total sensing time is assumed as $T = 10\mu s$, and thus the number of samples collected by the Nyquist sampling rate could be calculated as $N = T \cdot f_{NYQ}$. Rather than using the Nyquist sampling rate $f_{NYQ} \geq 2W = 1000$ MHz, we adopt the sub-Nyquist sampling rate $f_s < 2W$ which is depended on the maximum sparsity level $k_{\max}$ that can be estimated by long-term spectral observations. In the conventional CS approaches, the number of compressive samples $M = T \cdot f_s = K_0 s_{\max} \log(N/s_{\max})$ [11] should be determined by the worst case of sparsity level $k_{\max}$ to guarantee a very high acceptable reconstruction frequencies over the total sensing time T since the actual sparsity level is unknown in the real-world. In the proposed scheme, the total sensing time T is divided into $P = T \cdot f_s/\Delta M$ time intervals, where $P \in \mathbb{Z}^+$. The signal acquisition process would be terminated once the stopping criterion is reached. Therefore, the actual sensing time of the proposed scheme is equal or lower than T. The rest of sensing time could be utilized for data transmission besides, the shorter sensing time would prevent the further interference to the PUs.

4.4.1.1 r-MSE versus Number of Time Intervals

To prove the effectiveness of the proposed scheme and verify the theoretical results in Theorem 3, we compare the actual reconstruction error and the proposed Euclidean distance D_p which is referred as stopping criterion with the different number of time intervals in Fig. 4.3. It shows that the original signal is successfully reconstructed and the signal acquisition could be terminated at the time interval $p = 10$, rather than $p = 50$ (total sensing time) by the conventional CS-based algorithms. Since the proposed Euclidean distance D_p become very close to the actual reconstruction error when the actual recon-
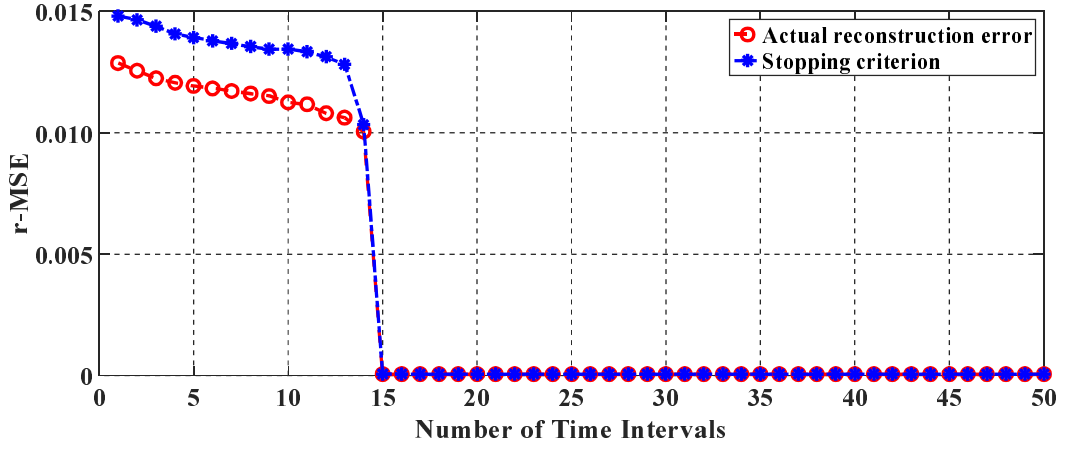
Figure 4.3: r-MSE vs. number of time intervals between the actual reconstruction error and the stopping criterion D_p when sparsity level is fixed as $k = 0.1N$ for the proposed scheme.

struction error becomes sufficiently small, D_p could be utilized as the stopping criterion to terminate the signal acquisition process as presented in Theorem 3. Moreover, Fig. 4.3 shows that the reconstruction accuracy could not be significantly improved by collecting additional samples. Therefore, the proposed scheme utilizes less sensing time than that of conventional CS approaches with the same sub-Nyquist sampling rate. The remaining sensing time can be utilized for future data transmission, besides, the shorter sensing time would prevent the further interference to the PUs.

Since the PUs and the SUs could randomly enter or leave the shared spectrum, the sparsity levels of the received wideband signals in practice are unknown and fluctuant. A practical CS-based sensing algorithm should be robust against different signal sparsity levels. Therefore, in Fig. 4.4, we demonstrate the performance of the proposed scheme under the different sparsity levels with a fix sampling rate $f_s = 0.5f_{NYQ}$. From Fig. 4.4, it can be observe that the proposed scheme could successfully reconstruct the signals and terminate the sensing process at the time interval $p = 8, 15, 20$ under the sparsity levels $k = 0.05N, 0.10N, 0.15N$, where the higher sparsity levels of the signals would lead to the more time intervals needed for guaranteeing the reconstruction accuracy. Therefore, without the prior knowledge of the actual spectral sparsity, the proposed scheme can blindly adopt a proper number of time intervals for signal reconstruction.
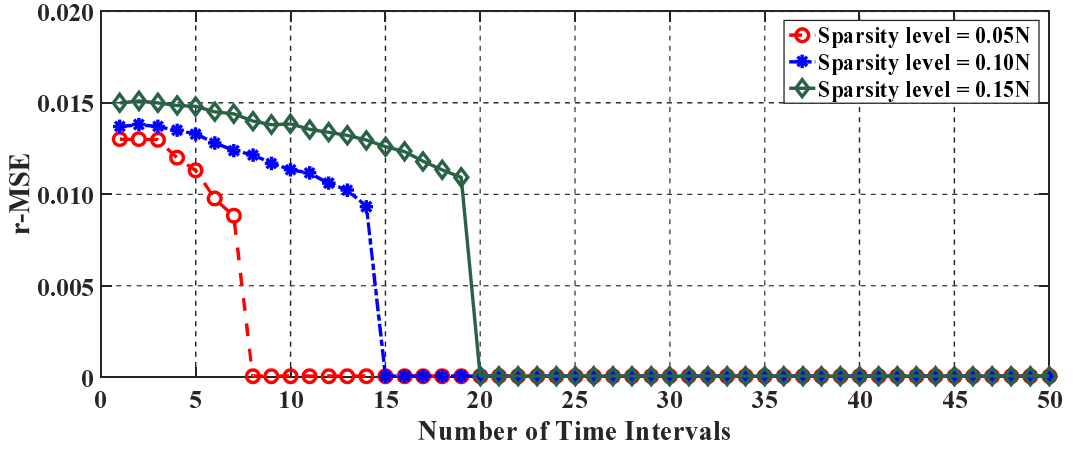
Figure 4.4: r-MSE vs. number of time intervals under different sparsity levels $k = 0.05N, 0.10N, 0.15N$ for the proposed scheme.
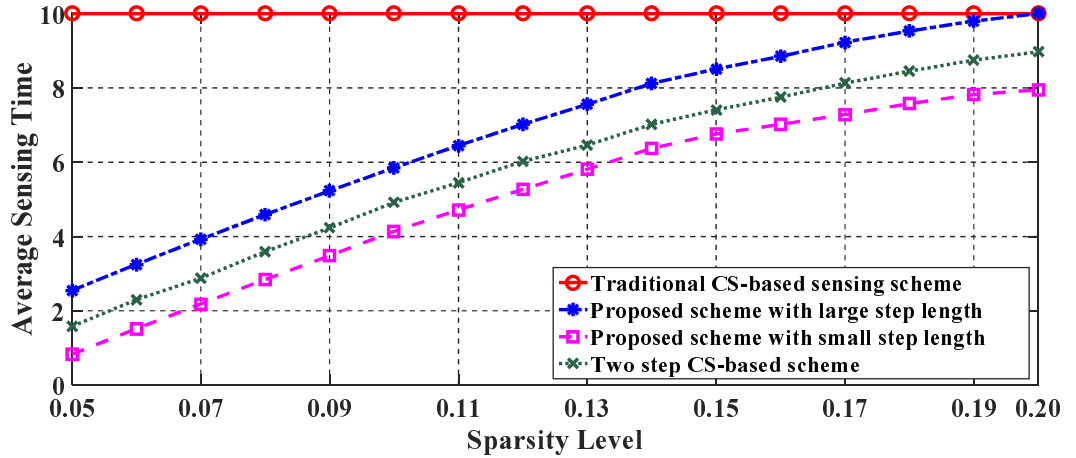
Figure 4.5: Average sensing time (μs) vs. the sparsity level (N) between the proposed scheme and other CS-based spectrum sensing algorithms.

4.4.1.2 Average sensing time versus Sparsity level

In Fig. 4.5, we present the comparison among the two-step CS-based spectrum sensing scheme [98] (termed two-step CS-based scheme), the conventional compressive spectrum sensing scheme [30] (termed traditional CS-based scheme) and the proposed scheme. We use the average sensing time in μs instead of the number of time intervals to measure the reduction of the sensing cost, since only the proposed scheme needs to divide the total sensing time into multiple small time intervals. Without loss of generality, we test different schemes with a fixed sampling rate $f_s = 0.5f_{NYQ}$. To illustrate the impact of

adopting different step lengths ΔM, the proposed scheme is tested with both the large step length and with the small step length, which adopts $\Delta M = 500$ and $\Delta M = 50$, respectively. It is shown in Fig. 4.5 that the performance of the proposed scheme is influenced by the step length ΔM. If the ΔM is too large, the proposed scheme will lose its advantage and be worse than the two-step CS-based scheme. To understand this, we consider an extreme setting: the total number of time intervals is set to 1 and thus the step length become $\Delta M = M = T \cdot f_s$, where the proposed scheme is degraded to the conventional compressive spectrum sensing scheme which could not work with unknown sparsity levels efficiently. Therefore, ΔM should not be too large in order to keep the effectiveness of the proposed scheme. However, if ΔM is too small, it will require many steps, e.g., maximum 250 time intervals are required if $\Delta M = 20$ in this simulation, although it is more likely to reach the minimum sensing time. Therefore, there is a trade-off need to be balanced between computational complexity and the effectiveness of the proposed scheme.

4.4.1.3 Detection probability versus Sparsity level

To illustrate the functionality of the proposed CS-based blind cooperating user selection algorithm, we show the detection probability against the sparsity level between the proposed scheme with and without cooperating user selection under different sampling rates (200 MHz and 400MHz) in Fig. 4.6. In the proposed scheme, we select half of the SUs to perform CSS for demonstration purpose. The maximum number of the cooperating SUs could be set according to the capacity in the practical network environment. It is shown that the detection probability of the proposed scheme with user selection is always higher than or equal to that of the proposed scheme without user selection. Therefore, there is no degeneration of the detection probability when cooperating with fewer SUs. Moreover, the detection probability is improved when sparsity level of the wideband spectrum is high, i.e., higher occupancy ratio, under different sampling rates. That is because the proposed cooperating user selection scheme could take out the SUs
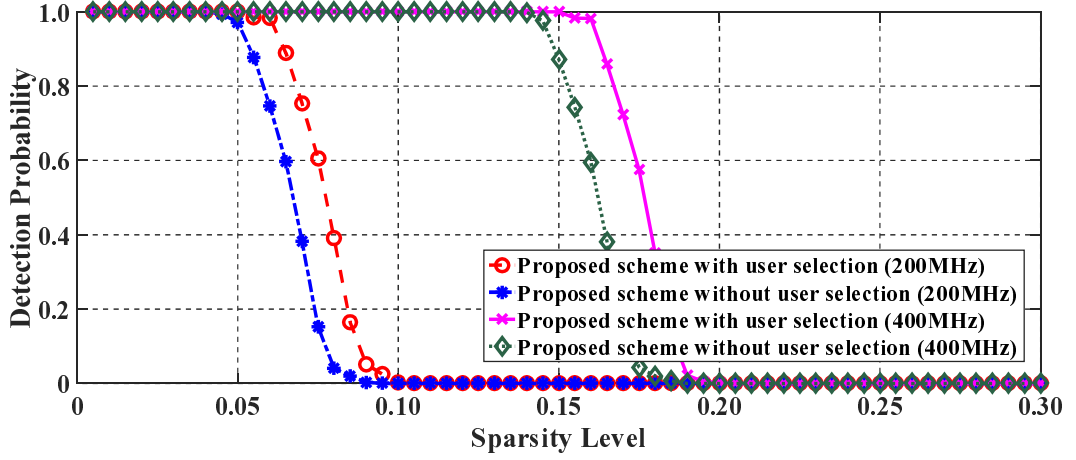
Figure 4.6: Detection probability vs. the sparsity level (N) between the proposed algorithm with and without cooperating user selection under different sampling rates = 200MHz and 400MHz.

with bad detection results, e.g., malicious users, which could affect the overall detection performance.

4.4.2   Analysis on Real-world Signals

The real-world signals $\boldsymbol{x}_0^{\text{real}}$ are received by real-time compressive spectrum sensing testbed proposed in the Chapter 3.

4.4.2.1   r-MSE versus Average sensing time

To analyze the performance of the proposed scheme with real-world signals over the different spectrums, e.g., TVWS spectrum and 3.5GHz spectrum in the UK, we compare the r-MSE of the proposed scheme against the two-step CS-based spectrum sensing scheme with the same sampling rate in Fig. 4.7. It is shown that the proposed scheme not only can work properly in the 3.5GHz shared spectrum, but also can deal with the TVWS spectrum. Particularly, as the real-world 3.5GHz spectrum is much sparser than the TVWS spectrum in the UK, the required sensing time of the 3.5GHz spectrum is less than that of the TVWS spectrum. The proposed method outperforms the two-step CS in
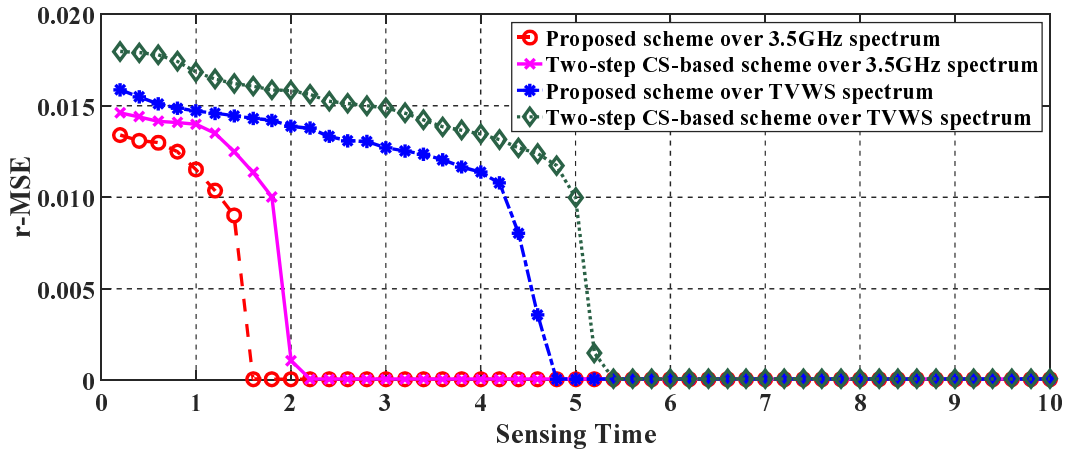
Figure 4.7: r-MSE vs. the sensing time (μs) over different real-world spectrum signals.

terms of sensing time under give sampling rate since the adopted AR-IRLS reconstruction algorithm requires fewer compressive samples to achieve the same reconstruction accuracy compared with the basis pursuit denoising (BPDN) reconstruction algorithm adopted in two-step CS [111]. The proposed scheme is suitable for the practical measurements and can be extended to other shared spectrums like TVWS and the bands with the higher central frequencies.

4.5 Summary

We have proposed an blind CS augmented spectrum sharing scheme to provide more efficient spectrum opportunities identification within the CBSD sensing network. In order to tackle the challenges of realizing the CBSD sensing network, firstly we proposed an blind CS-based sensing algorithm which enables the local SUs to automatically choose the minimum sensing time while guaranteeing the exact wideband signal reconstruction. Secondly, to enhance the detection performance and use fewer SUs in each CBSD sensing network, a CS-based blind cooperating user selection algorithm is proposed to select the SUs which could produce informative spectrum sensing results according to the detection SNR of the transmission signals. The robust performance of the proposed CS-based blind sensing scheme has also been validated over both simulated signals and

real-world signals. Numerical analysis and experimental results have shown that the proposed scheme could not only adaptively select an appropriate number of time intervals without the estimation of sparsity level but also offer exact signal reconstruction for varying bandwidth of channels and power levels under different unknown sparsity levels. In comparison with conventional compressive spectrum sensing schemes and two-step CS-based spectrum sensing schemes, it is shown that the proposed scheme can achieve the better detection performance as well as the shorter sensing time and fewer number of cooperating SUs. Additionally, the remaining sensing time can be utilized for data transmission and avoiding the further interference to the ongoing primary transmissions. These benefits enable the proposed scheme to be implementable for spectrum sharing, especially over the 3.5GHz spectrum and the higher frequencies. Moreover, we shall extend the proposed scheme with advanced detector such as frequency domain autocorrelation [96] and maximum-minimum energy detection sensing algorithm [112] to further enhance the ability against the noise uncertainty and frequency selective channel in future work.

Chapter 5

Distributed Compressive Sensing Augmented Wideband Spectrum Sharing for Cognitive IoT

The increasing number of Internet of things (IoT) objects has been a growing challenge of the current spectrum supply. To handle this issue, the IoT devices should have cognitive capabilities to access the unoccupied portion of the wideband spectrum. In this paper, we propose a blind joint sub-Nyquist sensing scheme by utilizing the surround IoT devices to jointly sample the spectrum based on the multi-coset sampling theory. Thus, only the low-rate analog-to-digital converters (ADCs) on the IoT devices are required to form coset samplers and only the minimum number of coset samplers are adopted without the prior knowledge of the number of occupied channels and signal-to-noise ratios. Moreover, to further reduce the number of coset samplers and transfer part of the computational burden from the IoT devices to the core network, we adopt the PU's spectrum access information from geo-location database when applicable. Specifically, the related work and main contributions are firstly introduced in Section 5.1. Section 5.2 presents the problem formulation of the proposed hybrid scheme. Section 5.3 and Sec-

tion 5.4 describe the proposed blind joint sub-Nyquist sensing scheme and the joint iterative reweighted sparse recovery with geo-location database. Section 5.5 analyses and validates the proposed schemes. Finally, Section 5.6 concludes this chapter.

5.1 Introduction

5.1.1 Related work

The precondition for implementing the dynamic spectrum access in IoT paradigm over TVWS or other shared spectrum is the real-time observation of spectrum occupancy status. One of the current operational mechanism to attain this information is using the geo-location databases. However, it only protects registered primary systems and those databases are only available in certain locations and spectrum, e.g., TVWS in U.K. and U.S. [97]. For the concern of limited access to database and the database update speed, spectrum sensing, as one of the vital important technologies in cognitive radio (CR), was proposed to efficiently explore the underutilized spectrum [10].

However, it is unrealistic to directly acquiring the wideband signals by conventional Nyquist sampling scheme, especially in the energy-constrained IoT devices, since that requires high sampling rates (double or more than the bandwidth of the signal in frequency domain) and high power consumption in the ADC. In [113, 114], sequential sensing approaches were proposed to individually sense the channels by using the tunable narrowband bandpass filter with low-rate ADC. Due to the sequential nature of those schemes, the large sensing latency would be introduced, which may lead to missed opportunities or interferences [83]. Therefore, compressive sensing (CS) [11] was applied to to realize wideband spectrum sensing without the high rate signal sampling and processing. It enables the fast and accurate spectrum detection with sub-Nyquist sampling rates by exploiting the sparse nature of the underutilized wideband spectrum in practice [12]. However, the specialized sampling schemes for CS are difficult to be implemented in most

of compact IoT devices with limited energy supply and cost constraints. For example, the random demodulation sampling [43] which employs the high rate pseudorandom sequence to modulate the input signal, and the conventional multi-coset sampling [6, 73, 74] which have to assemble numerous ADCs into a single sensing equipment due to the unknown number of occupied channels in practice.

Therefore, the wideband spectrum sensing scheme without employing either high-rate ADCs or specialized sampling schemes is urgently needed for low-power IoT scenario. On the other hand, as the rapid growth of low-power IoT market, large number of IoT devices would be deployed closely in order to achieve multiple environment sensing and machine control functions, which are equipped with commercial low-rate ADCs for data transmission [115].

5.1.2 Contributions

Motivated by the above challenges, the contribution of this paper is threefold.

Firstly, we propose a distributed sub-Nyquist sampling scheme by utilizing adjacent IoT devices which have cognitive capabilities with wide-range radio frequency (RF) front-end, to jointly sample the spectrum based on the multi-coset sampling theory. It means that only the low-rate ADC on each IoT device is required for sampling and formed as the coset sampler. Secondly, we consider the situation in which the number of occupied channels is unknown. As the multi-coset sampling theory indicates that the number of cosets should be at least more than two times of the number of occupied channels [6], in the conventional multi-coset sampling scheme [6, 73, 74], the prior knowledge of occupied channel number is required to adopt the minimum number of cosets, which is difficult to know in practice. Furthermore, even the number of occupied channels is known, the least number of coset to achieve the same detection performance is varying under different signal-to-noise ratios (SNRs) [73]. Therefore, the aforementioned schemes tend to further increase the amount of cosets in order to keep stable detection performance. In the pro-
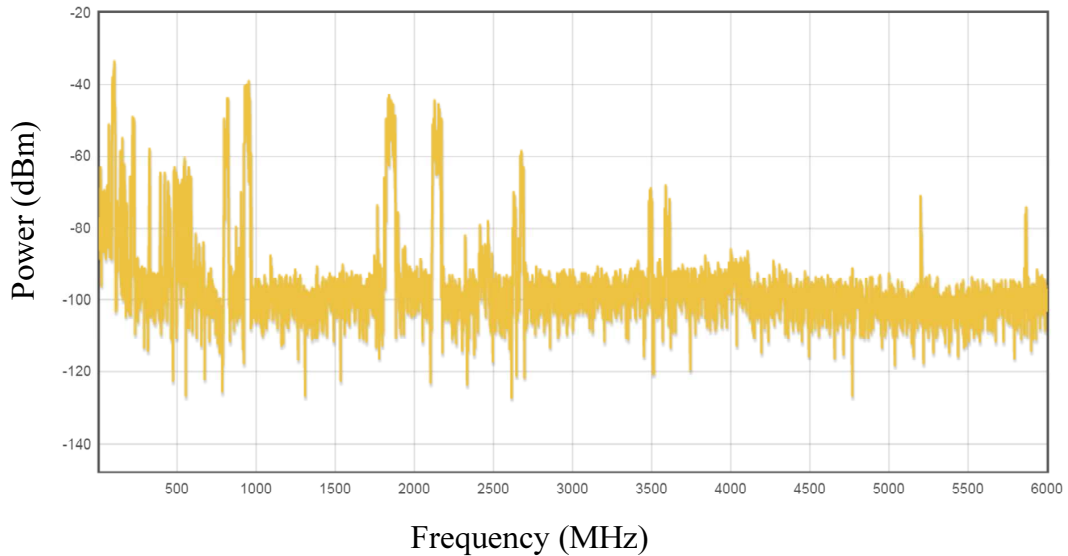
Figure 5.1: The real-time spectrum occupancy recorded at Queen Mary University of London (51.523021°N 0.041592°W). The figure shows that the spectrum is sparsely occupied below 6 GHz.

posed scheme, only the minimum number of coset samplers are adopted without the prior knowledge of occupied channel number by gradually increasing the number of involved coset samplers and indirectly estimating the reconstruction errors until the spectrum recovery is satisfactory. Thirdly, we propose to incorporate the channel occupancy information from geo-location database when it is applicable. In [14], a database-assisted CS algorithm employs the channel historical power information from geo-location database to reduce the iterations of weights updating in the iteratively reweighted least square (IRLS) algorithm. However, the dynamic change of channel power information from geo-location database could severely degrade the reconstruction accuracy, i.e., newly added PUs and the errors in the prior information from geo-location database. Therefore, we proposed a hybrid reconstruction scheme with the awareness that the prior information from geo-location is not perfectly reliable. Moreover, the proposed can track the changes of spectrum occupancy state in real-time, i.e., newly added users. With the assists from geo-location database, part of the complexity of local wideband sensing is transferred to the core network, thus further decreasing the processing complexity and energy consumption required on the IoT devices.

5.2   Problem Formulation

In this chapter, we consider that the same signal model as the one adopted in Chapter 3 and 5. The corresponding discrete Fourier transform (DFT) of the signal $x[\frac{n}{f_N}]$ could be obtained as

$$X[k] = \sum_{n=0}^{N-1} x\left[\frac{n}{f_N}\right] e^{-2\sqrt{-1}\pi kn/N}, \quad k = 0, 1, \ldots, N-1, \tag{5.1}$$

where $N = f_N \cdot T_o$ and $X[k]$ typically bears a near sparse property due to the under-utilization of wideband spectrum as shown in Fig. 5.1. Without loss of generality, the wideband spectrum is evenly segmented into H channels. Since the probabilities that PUs present in any channel are assumed to be unknown, we model the multiband sensing on each channel as a binary hypothesis test [2]. The general compressive spectrum sensing framework utilized in the proposed scheme is illustrated in Fig. 5.2. The aim of compressive spectrum sensing is to reconstruct signal $x[\frac{n}{f_N}]$ or its spectrum $X[k]$ from the sub-Nyquist samples and then perform the spectrum sensing techniques, e.g., energy detection and feature detection, on the reconstructed signal in order to decide the occupancy status. Compared with other conventional spectrum detection technologies [3], the energy detection does not require any prior knowledge of the PUs, i.e., modulation type, with lower implementation and computational complexity [108], therefore, we adopt the energy detection method [32] in this paper.

In the context of wideband spectrum sensing in shared spectrum, some of the frequency bands are heavily used by the primary users such as local radio stations, local TV stations, etc., so the related information at the geo-location database will be stable due to TV broadcasting arrangement in the long run (e.g., years). Therefore, although the side-information from geo-location database is possibly with some errors due to the dynamic changes of the spectrum state, such information can be incorporated at the sensing terminals to reduce the sensing costs.
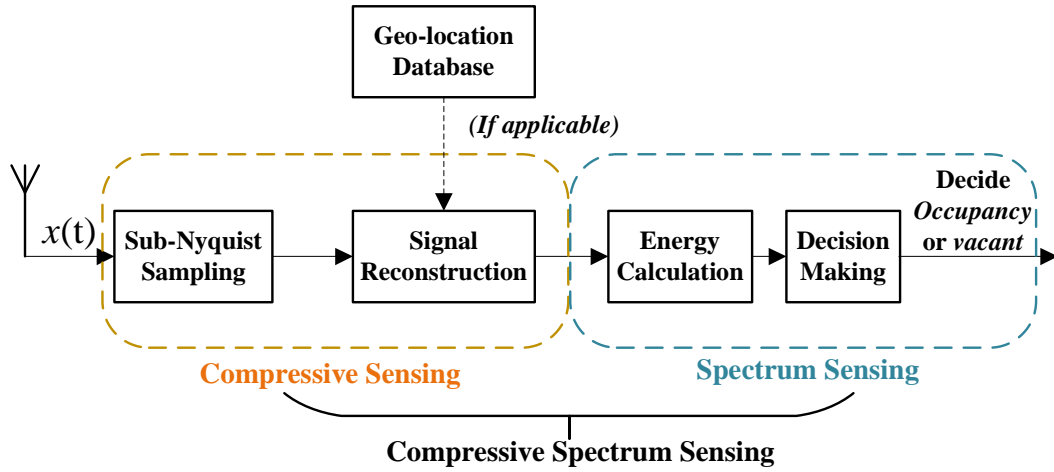
Figure 5.2: Block diagram of compressive spectrum sensing framework.

According to the general CS-based spectrum sensing framework shown in Fig. 5.2, we know that the spectrum recovery performance would have direct impact on the sensing results. For the compressive multi-coset sampling theory, the reconstruction performance mainly depends on three factors: the number of cosets, the reconstruction algorithm and the occupancy ratio, i.e., bandwidth of transmission signals/total bandwidth. As the occupancy ratio is determined by transmission activities within the desired wideband spectrum. In this paper, we focus on discussing how to choose the minimum number of cosets samplers without the prior knowledge of the occupied channel number and how to optimize the reconstruction stage in terms of number of required measurements and computational burden with the coexistence of dynamic incumbent systems over TVWS.

As illustrated in the chapter 3 and 4, the compressive signal reconstruction can be expressed as

$$\boldsymbol{x}^* := \arg\min_{\boldsymbol{x} \in \mathbb{R}^N} \frac{1}{2} ||\boldsymbol{\Phi}\boldsymbol{x} - \boldsymbol{y}||_2^2 + \lambda ||\boldsymbol{x}||_1. \tag{5.2}$$

Recent works [116] show that additional prior knowledge on the original signal can be utilized to enhance the reconstruction capabilities of CS algorithms. For example, the signal reconstruction stage could adapt to the incomplete or complete prior information on the support of original signal in sparse domain, e.g., frequency spectrum, which aims to obtain a result that explains the samples, whose support contains the smallest

number of new additions to the known support $\mathcal{T}$ and subject to the target sparsity, so the solution is given by

$$\boldsymbol{x}^* := \underset{\boldsymbol{x} \in \mathbb{R}^N}{\arg\min} \frac{1}{2} ||\boldsymbol{\Phi}(\boldsymbol{x})_{\mathcal{T}^c} - \boldsymbol{y}||_2^2 + \lambda ||(\boldsymbol{x})_{\mathcal{T}^c}||_1. \tag{5.3}$$

Suppose that the support set of $\boldsymbol{x}$ is denoted as $\mathcal{S} = \mathrm{supp}(\boldsymbol{x})$, where the known part of the support set is $\mathcal{T}$, the unknown support set is $\mathcal{U}$ and the error in the known part set is $\mathcal{U}_e := \mathcal{T} \backslash \mathcal{S}$. The size of these sets are denoted as $s := |\mathcal{S}|$, $u := |\mathcal{U}|$ and $e := |\mathcal{U}_e|$, so that $s = t + u - e$. The theoretical lower bound for exact reconstruction based on the l_0-norm minimization can be expressed with the restricted orthogonality constant δ as [117]

$$\delta_{t+2u} < 1, \tag{5.4}$$

which is much weaker than that of the original sparse recovery $\delta_{2s} < 1$ [31] as the restricted orthogonality constant δ is nondecreasing, and $s \gg u$; $s \gg e$. Sufficient condition for exact reconstruction in terms of δ measures the theoretical minimum number of samples needed. Therefore incorporating the prior known part of the signal support can reduce the number of samples to guarantee the successful reconstruction, so that the sampling rate and computational burden will be further reduced for the power-constrained IoT devices.

5.3 The Blind Joint Sub-Nyquist Sensing Scheme

In this section, the proposed blind joint sub-Nyquist sensing scheme is presented, which utilizes adjacent IoT devices to jointly sense the wideband spectrum. Compared with the conventional multi-coset sampling scheme, the adaptive number of cosets samplers are adopted without the prior knowledge of the occupied channel number.

As shown in Fig. 5.3, the joint sub-Nyquist sensing system is realized by utilizing multiple IoT devices which are served as low-rate coset samplers, and the edge computing

unit which could be either the IoT device or independent computing unit if the IoT device with sufficient power supply and computing capability is not available in surrounding area. The power-constrained IoT devices could benefit from transferring the computing task to the edge computing unit, especially for those IoT devices with sensing capability but sufficient computing resource. Given the number of channels H and corresponding Nyquist sampling rate $f_N = 1/T_N \geq 2W$, each of the coset samplers takes uniform samples by a significantly decreased sampling rate $f_s = \frac{1}{HT_N} = f_N/H$ with a time offset of $\{c_i T_N\}$, $i = 1, ..., p$, where $p < H$ is the number of coset samplers and the set $\mathcal{C} = \{c_i\}_{i=1}^p$ consists of p distinct integers randomly selected from $[0, H-1]$. Thus the average compressive ratio could be given as $\alpha = (f_N/H)T_N \cdot p/(f_N \cdot T_N) = p/H$. For the i-th coset sampler, the uniform sampling sequence is defined as

$$
x_{c_i}[n] = \begin{cases} x(nT_N), & n = mH + c_i, \ m \in \mathbb{Z} \\ 0, & \text{otherwise.} \end{cases}
\tag{5.5}
$$

Furthermore, by applying Fourier transform to $x_{c_i}[n]$, the relationship between its spectrum $X_{c_i}(e^{2\sqrt{-1}\pi k T_N})$ and the unknown Fourier spectrum $X(k)$ of $x(t)$ is presented as [75]

$$
\begin{aligned}
X_{c_i}(e^{2\sqrt{-1}\pi k T_N}) &= \sum_{n=-\infty}^{+\infty} x_{c_i}[n]e^{-\sqrt{-1}2\pi f n T} \\
&= \frac{1}{HT_N}\sum_{h=0}^{H-1} \underbrace{X(k + \frac{m}{MT})}_{X_h(k)} e^{\sqrt{-1}\frac{2\pi}{H}c_i h} \\
&= \frac{1}{HT_N}\sum_{h=0}^{H-1} X_h(k)e^{\sqrt{-1}\frac{2\pi}{H}c_i h}, \qquad \forall f \in [0, W],
\end{aligned}
\tag{5.6}
$$

for every $1 \leq i \leq p$, where $X_h(k) = X(k + \frac{h}{HT_N})$ corresponds to the pieces of the original spectrum $X(k)$ in the h-th channel, which is shifted to the left by $\frac{h}{HT_N}$ units. Therefore, (5.6) could be simplified into the matrix form as

$$
\boldsymbol{Y}(k) = \boldsymbol{A}\boldsymbol{X}(k), \ \forall k \in [0, W],
\tag{5.7}
$$

$$
\underbrace{\begin{bmatrix} X_{c_1}(e^{2\sqrt{-1}\pi kT_N}) \\ X_{c_2}(e^{2\sqrt{-1}\pi kT_N}) \\ \vdots \\ X_{c_p}(e^{2\sqrt{-1}\pi kT_N}) \end{bmatrix}}_{\boldsymbol{Y}(f)}
$$

$$
= \frac{1}{HT_N} \underbrace{\begin{bmatrix} e^{\frac{2\sqrt{-1}\pi c_1 0}{M}} & e^{\frac{2\sqrt{-1}\pi c_1 1}{M}} & \cdots & e^{\frac{2\sqrt{-1}\pi c_1 (M-1)}{M}} \\ e^{\frac{2\sqrt{-1}\pi c_2 0}{M}} & e^{\frac{2\sqrt{-1}\pi c_2 1}{M}} & \cdots & e^{\frac{2\sqrt{-1}\pi c_2 (M-1)}{M}} \\ \vdots & \vdots & \vdots & \vdots \\ e^{\frac{2\sqrt{-1}\pi c_p 0}{M}} & e^{\frac{2\sqrt{-1}\pi c_p 1}{M}} & \cdots & e^{\frac{2\sqrt{-1}\pi c_p (M-1)}{M}} \end{bmatrix}}_{\mathbf{A}} \tag{5.8}
$$

$$
\times \underbrace{\begin{bmatrix} X_0(f) \\ X_1(f) \\ \vdots \\ X_{M-1}(f) \end{bmatrix}}_{\boldsymbol{X}(k)} = \mathbf{A}\boldsymbol{X}(k), \ \forall k \in [0, W],
$$

where $\boldsymbol{Y}(k) \in \mathbb{C}^{p \times L}$ is a matrix whose i-th row is $X_{c_i}(e^{2\sqrt{-1}\pi kT_N})$, $\boldsymbol{X}(k) = [X_0(k), X_1(k), ..., X_{H-1}(k)]^T$ is the unknown spectrum vectors of $x(t)$ in the H channels, and $\boldsymbol{A} \in \mathbb{C}^{p \times H}$ is a matrix with (i, j)-th element given by

$$
\boldsymbol{A}_{i,j} = \frac{1}{HT_N} e^{\sqrt{-1}\frac{2\pi}{H} c_i (j-1)}. \tag{5.9}
$$

The multi-coset sampling theory indicates that the number of cosets p should be at least more than two times of the number of occupied channels [6]. Therefore, in the conventional multi-coset sampling scheme [6, 73], the number of occupied channels κ is assumed as the prior knowledge to decide the number of coset p needed in integrated sampling hardware. However, as the number of occupied channels is unknown in practice, p could be set unnecessary large when it is determined by κ. Moreover, even if the exact number of occupied channels is known or estimated, the least number of cosets to achieve the same detection performance are still varying under different SNRs [73]. Therefore,
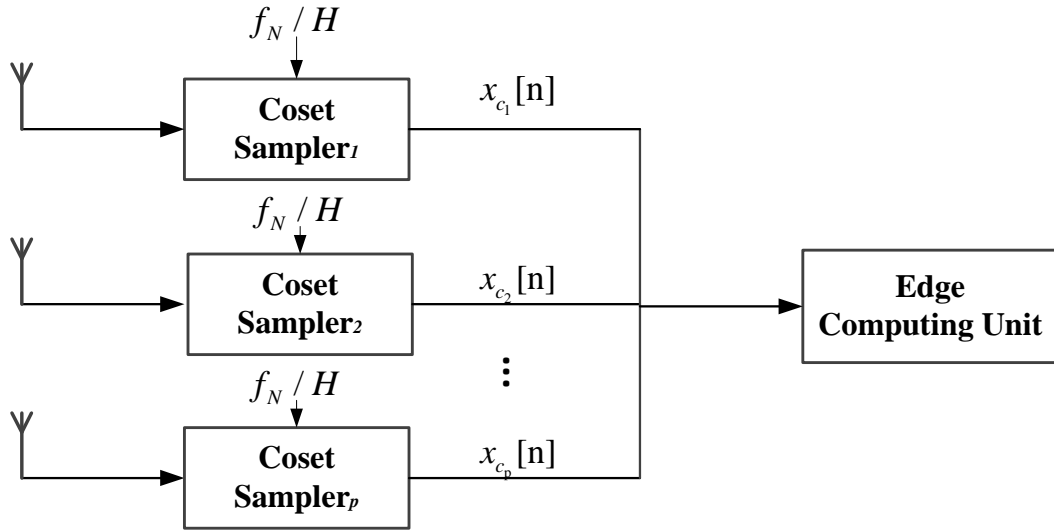
Figure 5.3: Block diagram of the proposed joint sub-Nyquist sensing system.

fixing the number of coset when produce the sampling hardware could cause either performance degeneration or the waste of sampling resources.

In the proposed scheme, only the minimum coset samplers are adopted without the prior knowledge of the number of occupied channels or its upper bound value κ. Specifically, through repeating the procedure of signal acquisition by gradually increasing the number of involved coset samplers and performing signal reconstruction, we could obtain a sequence of reconstructed signal, i.e., $\hat{x}_1, \hat{x}_2, \cdots, \hat{x}_p$, where $\hat{x} = \text{vec}(\hat{X}(k))$. After each time of signal reconstruction, the proposed scheme should decide whether the reconstruction of the original signal is accurate enough or not. If the reconstructed signal does not satisfy certain accuracy requirement of spectral detection, the scheme should require more coset samplers until the accuracy of the signal reconstruction is good enough. However, the actual reconstruction error $e = ||x - \hat{x}||_2^2$ is inaccessible since the original signal $x = \text{vec}(X(k))$ is unknown. In this paper, we propose to estimate the reconstruction error e indirectly and set stopping criterion.

Before proposing the scheme to approximate reconstruction error, we give the vectorization of (5.7) in the following lemma.

Lemma 5. *Given the matrix form $Y(k) = AX(k)$, we could obtain the vector form as*

vec($\boldsymbol{Y}(k)$) = $\boldsymbol{\Phi}$vec($\boldsymbol{X}(k)$), where the matrix $\boldsymbol{\Phi} = \boldsymbol{I_L} \otimes \boldsymbol{A}$ and the operator $\otimes$ represents

the Kronecker product.

Proof. Let $\boldsymbol{X}(k) = [\boldsymbol{X}_{(1)}(k), \boldsymbol{X}_{(2)}(k), \cdots, \boldsymbol{X}_{(L)}(k)]$ and $\boldsymbol{u_1}, \boldsymbol{u_2}, \cdots, \boldsymbol{u_L}$ denote the unit

vectors. We could obtain

$$
\begin{aligned}
\text{vec}(\boldsymbol{Y}(k)) = \text{vec}(\boldsymbol{AX}(k)) &= \text{vec}(\boldsymbol{AX}(k)\boldsymbol{I_L}) \\
&= \text{vec}\Big(\sum_{i=1}^{L} \boldsymbol{AX_i}(k)\boldsymbol{u_i}^T \boldsymbol{I_L}\Big) \\
&= \sum_{i=1}^{L} \text{vec}\big((\boldsymbol{AX_i}(k))(\boldsymbol{I_L}\boldsymbol{u_i})^T\big) \\
&= \sum_{i=1}^{L} \big(\boldsymbol{I_L}\boldsymbol{u_i} \otimes \boldsymbol{AX_i}(k)\big) \\
&= (\boldsymbol{I_L} \otimes \boldsymbol{A}) \sum_{i=1}^{L} \big(\boldsymbol{u_i} \otimes \boldsymbol{X_i}(k)\big) \\
&= (\boldsymbol{I_L} \otimes \boldsymbol{A}) \sum_{i=1}^{L} \text{vec}\big(\boldsymbol{X_i}(k)\boldsymbol{u_i}^T\big) = \boldsymbol{\Phi}\text{vec}(\boldsymbol{X}(k))
\end{aligned}
\tag{5.10}
$$

Thus vec($\boldsymbol{Y}(k)$) = vec($\boldsymbol{AX}(k)$) = $\boldsymbol{\Phi}$vec($\boldsymbol{X}(k)$) is obtained. $\square$

In the following of this section, we denote vec($\boldsymbol{Y}(k)$) as $\boldsymbol{y}$. Specifically, the samples

vector $\boldsymbol{y}$ in each step is divided into two vectors $\boldsymbol{y_r}$ ($\boldsymbol{y_r} \in \mathbb{R}^{r \times 1}$) and $\boldsymbol{y_v}$ ($\boldsymbol{y_v} \in \mathbb{R}^{v \times 1}$).

According to Lemma 5, these two vectors therefore can be expressed as $\boldsymbol{y_r} = \boldsymbol{\Phi_r}\boldsymbol{x}$ and

$\boldsymbol{y_v} = \boldsymbol{\Phi_v}\boldsymbol{x}$ respectively, where $\boldsymbol{\Phi_r}$ is a $r \times HL$ matrix and $\boldsymbol{\Phi_v}$ is a $v \times HL$ matrix.

Parameter r represents the number of samples in $\boldsymbol{y_r}$ for signal recovery and v is the

number is set to guarantee the sufficient accuracy of reconstruction error estimation as

illustrated later.

As mentioned before, the exact reconstruction error $e = ||\boldsymbol{x} - \hat{\boldsymbol{x}}||_2^2$ could not be

obtained to determine how accuracy the reconstructed signal is. Therefore, we propose

to estimate the actual reconstruction error e indirectly by using the verification vector

y_v and the proposed stopping criterion is defined as

$$S_p = ||\boldsymbol{\Phi_v}\hat{\boldsymbol{x}} - \boldsymbol{y_v}||_2^2. \tag{5.11}$$

The Johnson-Lindenstrauss Lemma presented in [107] asserts that a high-dimensional space can be projected into a low-dimensional one whose dimension is equal or larger than $O(\zeta^{-2}\log HL)$ so that all distances are preserved up to a multiplicative factor between $1 - \zeta$ and $1 + \zeta$ with the factor $\zeta \in [0, \leq 1/2]$. To demonstrate the rigorous relationship between the actual reconstruction error e and the proposed stopping parameter S_p, we prove the point that the actual reconstruction error $e = ||\boldsymbol{x} - \hat{\boldsymbol{x}}||_2^2$ could be approximated by S_p within the boundary factor of $1 \pm \zeta$ in Theorem 6. Therefore, in order to terminate the signal acquisition process, i.e., determine whether the number of coset samplers are sufficient or not, one can compare the proposed stopping parameter S_p with a predefined threshold which could be determined according to the certain reconstruction accuracy requirement.

Theorem 6. *Given $\zeta \in (0, 1/2]$, and $\gamma \in (0, 1)$ and $v \leq C\zeta^{-2}log(1/2\gamma)$, we have*

$$\frac{S_p}{(1 + \zeta)} \leq e \leq \frac{S_p}{(1 - \zeta)} \tag{5.12}$$

with confidence $1 - \gamma$, where the parameter C is a constant number. $\hat{e}$ and e are defined as before.

Proof. With the aid of Johnson-Lindenstrauss Lemma, if the number of row v in $\boldsymbol{\Phi_v}$ is equal or larger than $C\zeta^{-2}\log(1/2\gamma)$, we have

$$(1 - \zeta)||\boldsymbol{x} - \hat{\boldsymbol{x}}||_2^2 \leq ||\boldsymbol{\Phi_v}(\boldsymbol{x} - \hat{\boldsymbol{x}})||_2^2 \leq (1 + \zeta)||\boldsymbol{x} - \hat{\boldsymbol{x}}||_2^2 \tag{5.13}$$

with confidence $1 - \gamma$, where $\zeta \in (0, 1/2]$ and $\gamma \in (0, 1)$. As matrix $\boldsymbol{\Phi_v}$ could be seen as

---

Algorithm 4 The proposed blind joint sub-Nyquist sensing scheme

---

Require: Sampling rate f_s, the maximum number of available coset samplers $p_{\max}$, the stopping parameter threshold δ, $\boldsymbol{A}$.

Ensure: The reconstructed signal $\hat{\boldsymbol{x}}$

1: **while** $p = 0, \cdots, p_{\max}$ **do**
2:     Sampling the wideband signal using f_s with p coset samplers so as to obtain the compressive measurement matrix $\boldsymbol{Y}(k)$ and the corresponding covariance matrix $\boldsymbol{R}$.
3:     Reconstruct the support and spectral from $\boldsymbol{R}$ by utilizing SOMP algorithm according to (5.18), leading to a spectral reconstruction $\hat{\boldsymbol{x}}_{\boldsymbol{p}}$.
4:     Calculate the stopping parameter

$$S_p = ||\boldsymbol{\Phi_v}\hat{\boldsymbol{x}} - \boldsymbol{y_v}||_2^2$$

5:     **if** S_p smaller than predefined threshold is true
6:         Terminate the signal acquisition process.
7:     **else**
8:         $p = p + 1$
9: **end if**
10: **end while**

---

a linear projection from $\mathbb{R}^{HL}$ to $\mathbb{R}^v$, we can get

$$(1 - \zeta)||\boldsymbol{x} - \hat{\boldsymbol{x}}||_2^2 \leq ||\boldsymbol{\Phi_v}\hat{\boldsymbol{x}} - \boldsymbol{y_v}||_2^2$$
$$\leq (1 + \zeta)||\boldsymbol{x} - \hat{\boldsymbol{x}}||_2^2. \tag{5.14}$$

To obtain the observation that $e = ||\boldsymbol{x} - \hat{\boldsymbol{x}}||_2^2$ could be bounded and estimated by $S_p = ||\boldsymbol{\Phi_v}\hat{\boldsymbol{x}} - \boldsymbol{y_v}||_2^2$, we change the (5.14) to another form (5.15) and simplify it to (5.16):

$$\frac{1}{(1 + \zeta)}||\boldsymbol{\Phi_v}\hat{\boldsymbol{x}} - \boldsymbol{y_v}||_2^2 \leq ||\boldsymbol{x} - \hat{\boldsymbol{x}}||_2^2$$
$$\leq \frac{1}{(1 - \zeta)}||\boldsymbol{\Phi_v}\hat{\boldsymbol{x}} - \boldsymbol{y_v}||_2^2, \tag{5.15}$$

$$\frac{S_p}{(1 + \zeta)} \leq e \leq \frac{S_p}{(1 - \zeta)}. \tag{5.16}$$

$\square$

Therefore, when the row number v in $\boldsymbol{\Phi_v}$ is equal or larger than $C\zeta^{-2}\log(1/2\gamma)$, the distance between S_p and e could be bounded up to a multiplicative factor between $1 - \zeta$ and $1 + \zeta$ with the confidence $1 - \gamma$.

To further reduce the computation complexity of the signal reconstruction of (5.7), we compute the covariance matrix of the sample sequences as [118]

$$\boldsymbol{R} = \mathbb{E}[\boldsymbol{Y}(k)\boldsymbol{Y}^H(k)] = \boldsymbol{A}\boldsymbol{R}_X\boldsymbol{A}^H, \tag{5.17}$$

where $\boldsymbol{R}_X = \mathbb{E}[\boldsymbol{X}(k)\boldsymbol{X}^H(k)]$ is the $H \times H$ primary signal correlation matrix and σ_n^2 is the noise variance. According to the eigenvalue decomposition (EVD) method [73], the covariance matrix $\boldsymbol{R}$ could be decomposed as $\boldsymbol{R} = \boldsymbol{U}\boldsymbol{\Lambda}\boldsymbol{U}^H$. Utilizing eigenvalues $\boldsymbol{\Lambda}$ and the corresponding eigenvectors $\boldsymbol{U}$, the measurement matrix could be constructed as $\boldsymbol{\chi} = \boldsymbol{U}\sqrt{\boldsymbol{\Lambda}}$, and we can define the following linear system

$$\boldsymbol{\chi} = \boldsymbol{A}\boldsymbol{\nu}, \tag{5.18}$$

where the support of the sparest solution to (5.18) converges to the original spectrum in matrix form, i.e., $supp(\boldsymbol{\nu}) = supp(\boldsymbol{X}(k))$ [73]. Compared with original sub-Nyquist samples $\boldsymbol{Y}(k) \in \mathbb{C}^{p \times N}$, using $\boldsymbol{\chi} \in \mathbb{C}^{p \times p}$ for support recovery reduces the computation complexity required on the SUs. After the support recovery, the exact signal reconstruction could be achieved by the reconstruction algorithm. In CS, the original signal could be recovered from sub-Nyquist samples by solving the l_1-norm minimization. Since the reconstruction of the unknown matrix $\boldsymbol{\nu}$ with jointly sparse columns in (5.18) is referred to as the joint sparse problem [119], we extend greedy-type algorithm such as simultaneous orthogonal matching pursuit (SOMP) [120] to solve this joint sparse problem, because of its lower complexity compared with the l_1-norm minimization [54]. Besides, the related exact recovery criterion for the conventional orthogonal matching pursuit (OMP) remains valid for its extension to SOMP [121].

5.4   Joint Iterative Reweighted Sparse Recovery with Geo-location Database

In this section, firstly we extend the single measurement vector (SMV) problem to the multiple measurement vectors (MMV) problem in (5.7), where $\boldsymbol{X}(k)$ is row-sparse, i.e., having nonzero entries in only a few rows. Then the l_ν-norm ($0 < \nu < 1$) minimization problem solving by the iteratively reweighted least square (IRLS)-type algorithm is modified to incorporate the information from geo-location database for enhancing the recovery performance with fewer measurements. Based on the white space channel information from the geo-location database, the sensor node can get a response with details of available channels in the vicinity. For simplifying the notation, $\boldsymbol{X}(k)$ and $\boldsymbol{Y}(k)$ are denoted as $\boldsymbol{X}$ and $\boldsymbol{Y}$ respectively.

Since the parameter H is set based on the number of channels in the spectrum of interest, the positions of nonzero rows in (5.7) is equivalent to the active channel index set $\mathcal{S}$. Therefore, the channel status information from geo-location database could be incorporated on the indices of the corresponding rows with large norm in the recovery process. To that end, the single measurement vector (SMV) is extended to the MMV problem, where the objective is to minimize the number of rows containing nonzero entries while satisfying the measurement constraint in (5.7). The problem can be formulated as [119]

$$\arg\min_{\boldsymbol{X}} \frac{1}{2}||\boldsymbol{AX} - \boldsymbol{Y}||_2^2 + \lambda||\mathcal{R}_{l_\nu}(\boldsymbol{X})||_1. \tag{5.19}$$

$\mathcal{R}_{l_\nu}(\boldsymbol{X})$ is a vector in $\mathbb{R}^H$ whose i-th entry is the l_ν norm of the i-th row of $\boldsymbol{X}$:

$$\mathcal{R}_{l_\nu}(\boldsymbol{X}) = [v_1, v_2, ..., v_H]^T, \tag{5.20}$$

where $v_i = ||\boldsymbol{X}_{[i]}||_q = (\sum_{j=1}^N |x_{i,j}|^q)^{1/q}$.

Compared with the l_1-norm minimization in (5.2), the l_ν-norm minimization with

---

Algorithm 5 Iterative Reweighted Sparse Recovery with Prior Information

---

Require: matrix of p samples sequence $\boldsymbol{Y} \in \mathbb{C}^{p \times N}$, measurement matrix $\boldsymbol{A} = [\boldsymbol{a}_1, ..., \boldsymbol{a}_M] \in \mathbb{C}^{p \times M}$, information from geo-location database $\mathcal{T}$, $\hat{\kappa}$ from EFT, $\boldsymbol{W}^{(0)}$ and $\lambda(\boldsymbol{X}^{(0)})$.

Ensure: $\mathcal{S}$

 1: **for** $l = 1, \cdots, l_{\max}$ **do**
 2:   Compute
 3:     $\boldsymbol{X}^{(l)} = \boldsymbol{W}^{(l-1)}\boldsymbol{A}^T(\boldsymbol{A}\boldsymbol{W}^{(l-1)}\boldsymbol{A}^T + \lambda(\boldsymbol{X}^{(l-1)})\boldsymbol{I})^{-1}\boldsymbol{Y}$
 4:   if $||\Delta\boldsymbol{X}^{(l+1)}|| \leq \delta$ break;
 5:   Update
 6:   Weights: $w_i^{(l)} = (||\boldsymbol{X}^{(l-1)}[i]||_2)^{v-2}$
 7:   Penalty parameter:
 8:   $\lambda(\boldsymbol{X}^{(l)}) = \frac{1}{2}||\boldsymbol{A}\boldsymbol{X}^{(l)} - \boldsymbol{Y}||_2^2 / [\varrho - \sum w_i^{(l)}(||\boldsymbol{X}_{[i]}^{(l)}||_2)^2]$
 9:   $l = l + 1$
10: **end for**
11: Estimate support $\mathcal{S}$ by selecting the position of the first $\hat{\kappa}$ smallest components in $\boldsymbol{W}^{(l+1)}$
12: **return** $\mathcal{S}=\mathcal{S}$-1

$0 < \nu < 1$ leads to the better sparsity approximation performance with the fewer samples since it is an intermediate problem in the sense of norm minimization between (2.9) and (5.2) [57]. Therefore the l_1-norm minimization is replaced with the l_ν-norm minimization for signal reconstruction in this section. It can be given as

$$\underset{\boldsymbol{X}}{\arg\min} \frac{1}{2}||\boldsymbol{A}\boldsymbol{X} - \boldsymbol{Y}||_2^2 + \lambda||\mathcal{R}_{l_\nu}(\boldsymbol{X})||_v^v. \tag{5.21}$$

where the penalty parameter $\lambda > 0$ is introduced to balance the reconstruction accuracy and the sparsity of minimization result as discussed in Section II. Since the choice of λ greatly influences the behavior of the spectrum reconstruction [111], in this work, λ is defined as a function of the target signal to optimize λ along with the signal reconstruction process, such that the problem in (5.21) can be transformed into the following form:

$$\underset{\boldsymbol{X}}{\arg\min} F(\boldsymbol{X}) = \frac{1}{2}||\boldsymbol{A}\boldsymbol{X} - \boldsymbol{Y}||_2^2 + \lambda(\boldsymbol{X})||\mathcal{R}_{l_\nu}(\boldsymbol{X})||_v^v. \tag{5.22}$$

Without losing the numerical property of (5.21), we define the linear function of the form: $F(\boldsymbol{X}) = \varrho\lambda(\boldsymbol{X})$ [89] to preserve the convexity in each iteration and exhibits only a

global minimizer regardless of the value of $\lambda(\boldsymbol{X})$, where ϱ is the coefficient representing the slope of the line and also controls convexity. We substitute $F(X) = \varrho\lambda(\boldsymbol{X})$ to (5.22) and therefore $\lambda(\boldsymbol{X})$ can be expressed as

$$\lambda(\boldsymbol{X}) = \frac{\frac{1}{2}||\boldsymbol{AX} - \boldsymbol{Y}||_2^2}{\varrho - ||\mathcal{R}_{l_\nu}(\boldsymbol{X})||_v^v} \quad 0 < \nu < 1. \tag{5.23}$$

However, it is general computationally hard and not guaranteed to obtain its global minimum due to the nonconvexity of the l_ν-norm minimization. It is shown in [57] that under certain assumptions such as the null space property (NSP) on measurement matrix $\boldsymbol{A}$, the solution sequence generated by the IRLS algorithm converges to the local minimum as the sparsest solution that is also the actual global l_ν-norm minimizer. With $q = 2$, each iteration of the IRLS algorithm corresponds to a convex weighted least squares subproblem that can be formulated as

$$\arg\min_{\boldsymbol{X}} \frac{1}{2}||\boldsymbol{AX} - \boldsymbol{Y}||_2^2 + \lambda(\boldsymbol{X})\sum_{i=1}^{H} w_i(||\boldsymbol{X}_{[i]}||_2)^2, \tag{5.24}$$

The problem in (5.24) will be repeatedly solved by updating the weight w_i at each iteration using the solution from previous iteration: at each iteration, w_i will be set as

$$w_i^{(l)} = (||\boldsymbol{X}_{[i]}^{(l-1)}||_2)^{v-2}. \tag{5.25}$$

where $w_i^{(l)}$, $i = 1, ..., H$ is the value of the weighting vector to be used at the l-th iteration and $\boldsymbol{X}^{(l-1)}$ is the $(l-1)$-th iterate. After convergence, $\boldsymbol{X}^{(l-1)}$ will be sufficiently close to $\boldsymbol{X}^{(l)}$. The weighting parameter $\boldsymbol{w}^{(l)}$ are computed from the row norms of the solution obtained in the previous iteration, so the corresponding rows with smaller norm are likely to be de-emphasised as they are irrelevant in fitting the data and vice versa. In (5.25), as $0 < v < 1$, the weights will be chosen inversely proportional to the l_2-norm of the rows. Since it gives a large weight to the small component, it will encourage a sparse solution in the minimization problem of (5.24). Assuming that $\mathcal{T} \subset [0, H-1]$ is the

prior knowledge of the occupied channel indices from geo-location database, its relation to the actual occupied channel set $\mathcal{S}$ can be expressed as:

$$\mathcal{S} = \mathcal{T} \cup \triangle \setminus \triangle_e, \tag{5.26}$$

where $\triangle := \mathcal{S} \setminus \mathcal{T}$ is newly occupied channel set, and $\triangle_e := T \setminus S$ are the newly released channel indices, i.e., the occupied channel indices recorded at geo-location database but actually released as vacant at current time.

As the i-th row in $\boldsymbol{X}$ corresponds to the piece of the original spectrum in the subchannel, the occupied channel information from geo-location database indicates the indices of the corresponding rows with large norm. Similar as (5.3), the objective function in (5.24) can therefore be changed as the l_ν minimisation over the remaining positions only, $i \notin \mathcal{T}$, i.e.,

$$\underset{\boldsymbol{X}}{\arg\min} \ \frac{1}{2}||\boldsymbol{AX} - \boldsymbol{Y}||_2^2 + \lambda(\boldsymbol{X}) \sum_{i \notin \mathcal{T}} w_i(||\boldsymbol{X}_{[i]}||_2)^2. \tag{5.27}$$

By defining

$$w_i = 0, \forall i \in \mathcal{T}, \tag{5.28}$$

the minimisation in (5.24) is transformed in the form of (5.27).

Here, in order to add the prior channel occupancy information from geo-location database, the weighing strategy in the joint sparse reconstruction is modified as

$$w_i^{(l)} = \begin{cases} \varphi(||\boldsymbol{X}_{[i]}^{(l-1)}||_2)^{v-2}, & i \in \mathcal{T} \\ (||\boldsymbol{X}_{[i]}^{(l-1)}||_2)^{v-2}, & \text{otherwise}, \end{cases} \tag{5.29}$$

where φ is a specified small constant. For $\varphi = 0$, the first expression in (5.29) reduces to 0 as required by (5.28).

Given an initial guess of the signal $\boldsymbol{X}^{(0)}$ (e.g., the least-squares solution), the iterative

reweighting algorithm generates a sequence of iterations of as follows:

$$
\begin{aligned}
\boldsymbol{X}^{(l+1)} = \arg\min_{\boldsymbol{X}} \ & \frac{1}{2}||\boldsymbol{A}\boldsymbol{X}^{(l)} - \boldsymbol{Y}||_2^2 + \\
& \lambda(\boldsymbol{X}^{(l)})\sum_{i\notin\mathcal{T}} w_i^{(l)}(||\boldsymbol{X}_{[i]}^{(l)}||_2)^2.
\end{aligned}
\tag{5.30}
$$

The solution to (5.30) at the l-th iteration can be expressed as

$$
\boldsymbol{X}^{(l+1)} = \boldsymbol{W}^{(l)}\boldsymbol{A}^T(\boldsymbol{A}\boldsymbol{W}^{(l)}\boldsymbol{A}^T + \lambda(\boldsymbol{X}^{(l)})\boldsymbol{I})^{-1}\boldsymbol{Y},
\tag{5.31}
$$

where $\boldsymbol{W}^{(l)} = \mathrm{diag}\{[1/w_1^{(l)}, ..., 1/w_H^{(l)}]\}$. The initial weight is given by

$$
w_i^{(0)} = \begin{cases} \varphi, & i \in \mathcal{T} \\ 1, & \text{otherwise.} \end{cases}
\tag{5.32}
$$

The algorithm is terminated once the convergence criterion has been satisfied, i.e.,

$$
||\Delta\boldsymbol{X}^{(l+1)}|| = \frac{||\boldsymbol{X}^{(l+1)} - \boldsymbol{X}^{(l)}||_2^2}{||\boldsymbol{X}^{(l)}||_2^2} \leq \delta,
\tag{5.33}
$$

where δ is a user-selected parameter. Here, based on the sparsity guess of the support dimension $\hat{\kappa}$ from exponential fitting test (EFT), the estimated active channel set is determined by selecting the position of the first $\hat{\kappa}$ smallest components in the final weight $\boldsymbol{w}$ or comparing the components with predefined threshold. The entire procedure of the proposed scheme in this section is summarised in Algorithm 5.

5.5   Experimental Results

In this section, we test the proposed schemes using the simulated signals as well as the real-world signals as the proof of concepts in this paper.
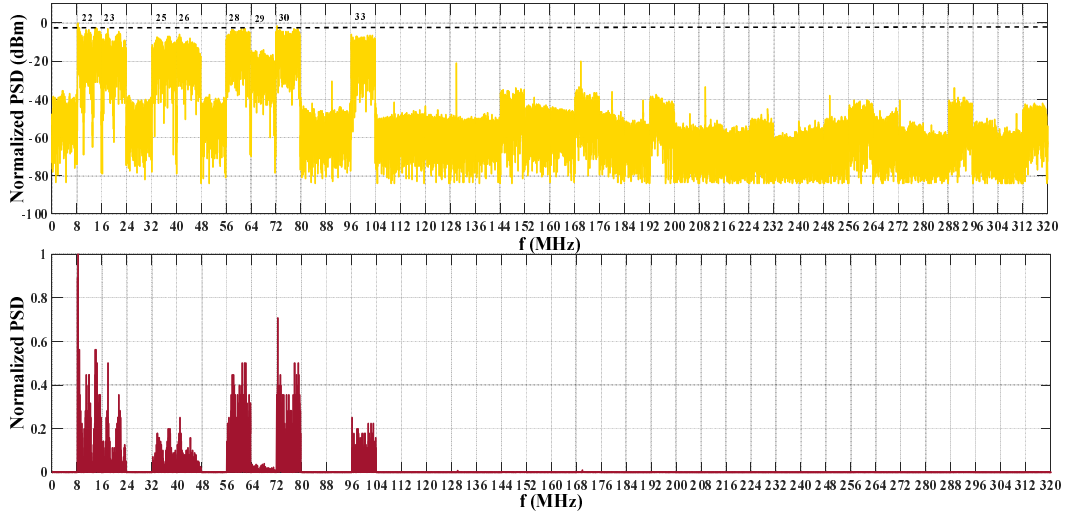
Figure 5.4: Normalized power spectrum density (PSD) of the real-time TVWS signal recorded at QMUL, $\mathcal{S} = [22, 23, 25, 26, 28, 29, 30, 33]$

5.5.1 Experiment Setups

The simulated signals are assumed as $x(t) \in \mathcal{F} = [0, 320]$ MHz, whose DFT is denoted as $\boldsymbol{x_0}^{\text{sim}}$. To keep consistency with the real TVWS setting, the spectrum is equally divided into $L = 40$ channels with bandwidth $B_0 = 8$ MHz, which contains up to J active channels:

$$x(t) = \sum_{i=1}^{J} \sqrt{E_i B_0} \text{sinc}(B_i(t - t_i))e^{j2\pi f_i t} + n(t), \tag{5.34}$$

where $\text{sinc}(x) = \sin(\pi x)/(\pi x)$, E_i, t_i and f_i represent the energy, time offset, and central frequency of the i-th channel respectively and $n(t)$ denotes the noise. The channel occupancy ratio Ω is defined as J/L. The real-world signals $\boldsymbol{x_0}^{\text{real}}$ is collected by the real-time wideband compressive spectrum sensing testbed as described in Chapter 3. There are 40 channels (indexed as Channel 21 - Channel 60) in the recorded TVWS signal, ranging from 470 to 790 MHz and each channel contains either noise only or transmitting signal with noise. Fig. 5.4 shows that the normalized downconverted real-world TVWS signal in the baseband $\mathcal{F} = [0, 320]$ MHz. Strong DVB-T signal reception at channel set $\mathcal{S} = [22, 23, 25, 26, 28, 29, 30, 33]$ can be observed in the recorded spectrum. Thus the channel occupancy ratio is $\Omega = 20\%$. To quantify the detection performance,
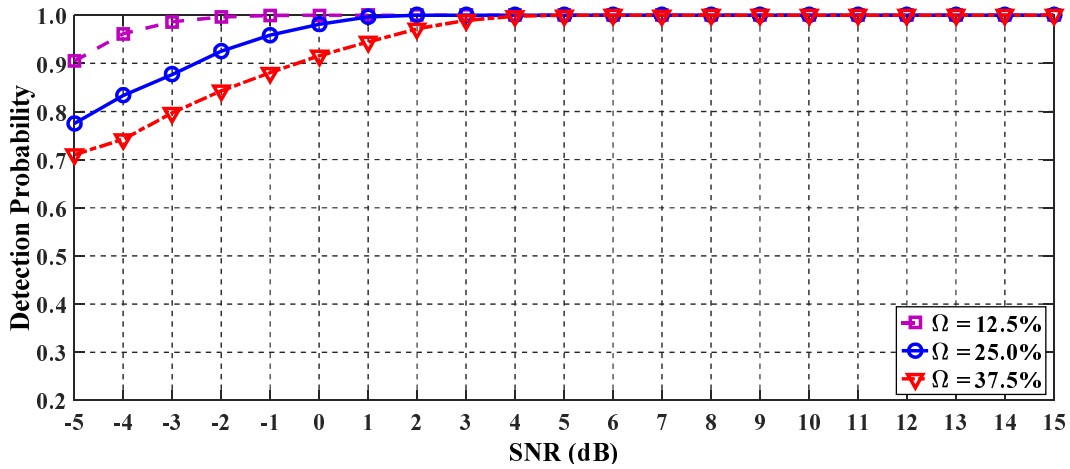
Figure 5.5: Detection Probability P_d vs. SNR (dB) with $p = 20$ under different channel occupancy ratios $\Omega = 12.5\%, 25\%, 37.5\%$.

we compute the detection probability P_d, i.e., the existing of occupied channels correctly being detected as occupied, under 1000 trials.

5.5.2 Results and Analysis

5.5.2.1 Detection Performance versus SNR and Number of Coset samplers

Firstly, we demonstrate that channel occupancy ratio Ω affects the required minimum number of coset samplers to achieve the same detection probability P_d. It shows in Fig. 5.5 that the detection performance P_d against SNR from -5 dB to 20 dB with fixed number of coset samplers $p = 20$. Moreover, it is observed that P_d improves as SNR increases under different scenarios with channel occupancy ratios $\Omega = 12.5\%, 25\%, 37.5\%$, which means the minimum number of coset samplers varying with the channel occupancy ratio Ω to achieve the same detection probability P_d. However, the information of channel occupancy ratio Ω is usually unknown in practice.

To verify the theory that the better detection performance P_d always could be achieved by evolving more coset samplers, we compare P_d against different number of coset samplers p with fixed Ω and SNR. It is shown in Fig. 5.6 that detection perfor-
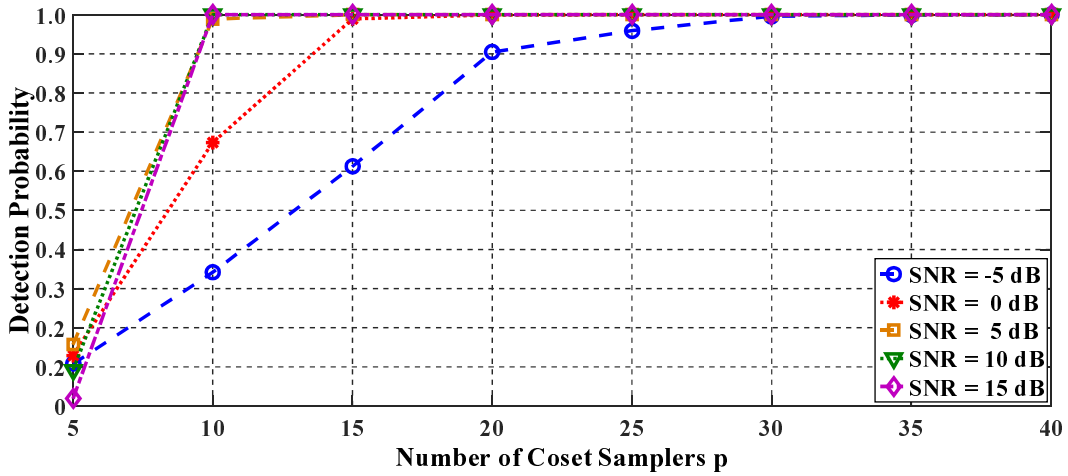
Figure 5.6: Detection Probability P_d vs. number of coset samplers p with $\Omega = 12.5\%$ under different SNRs.

mance P_d increases with the number of coset samplers but the extra coset samplers are unnecessary after the optimal detection performance is obtained by minimum number of coset samplers.

The proposed scheme could prevent the waste of sampling resources and guarantee the detection performance with sufficient number of coset samplers under different channel environments, i.e., SNRs. As demonstrated in Fig. 5.7, the proposed scheme therefore can be terminated according to the stopping criterion when the number of coset samplers reaches $p = 10$ if the received SNR is equal or greater than 5 dB. Besides, more coset samplers are required in the proposed scheme under the worse SNRs to achieve accurate detection performance. Therefore, it is shown that the proposed scheme is allowed to adaptively choose the number of coset samplers under different SNRs.

5.5.2.2 Detection Performance with the Prior Information in the Geo-location Database

As the active channel set $\mathcal{S}$ is randomly generated from $\{\mathbb{Z} \cap [1, L]\}$, among which the prior known part $\mathcal{T}$ obtained from geo-location database are randomly chosen from the elements of $\mathcal{S}$. The ratio of the prior known part $\mathcal{T}$ in the active channel set $\mathcal{S}$, referred
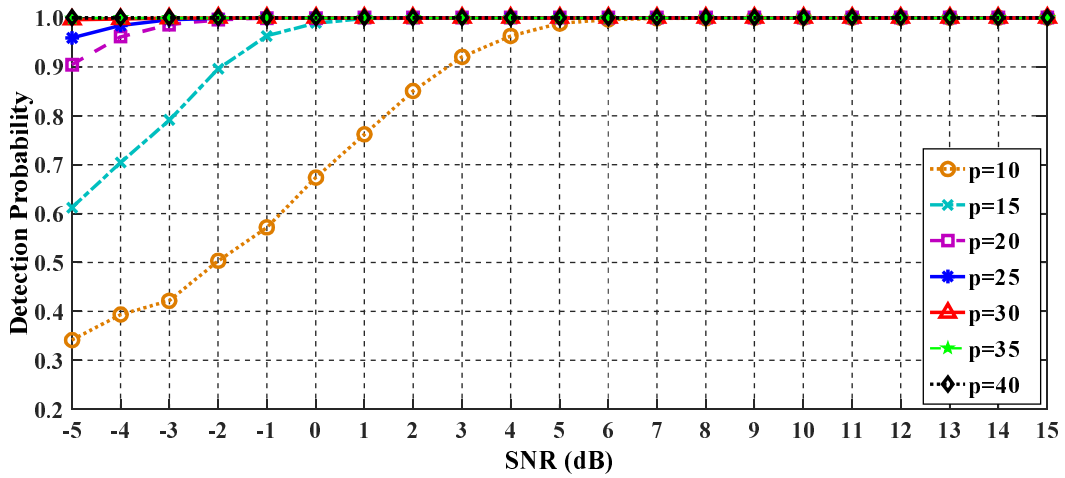
Figure 5.7: Detection Probability P_d vs. SNR (dB) with $\Omega = 12.5\%$ under different number of coset samplers.

as τ, is varied between 0 to 1. The case $\tau = 0$ and $\tau = 1$ corresponds to the sensing only case without assists from geo-location database and the case that current channel occupancy states from geo-location database are fully reliable and no change occurs on the spectrum at current time.

Firstly, the received SNR is set as -5 dB and the number of coset samplers p is varied from 15 to 35. As shown in the Fig. 5.8, the detection performance P_d generally increases with the involved number of coset samplers p, and also improves as the percentage of the known part τ increases. With the input from geo-location database, the number of coset samplers is further reduced in the the proposed joint sensing scheme to achieve the same detection probability compared with the sensing only case. For example, to achieve the desired detection probability of 0.97, sensing only method needs around $p = 20$ coset samplers, while the proposed joint sensing scheme needs only $p = 15$ coset samplers. Moreover, the proposed scheme can update the lack of channel occupancy information in the geo-location database, which helps to improve the detection performance and reduce the required number of coset samplers in the subsequent sensing activities.

Secondly, the detection performance is evaluated with varying received SNR from -5 dB to 15 dB in Fig. 5.9 with fixing the number of coset sampler as $p = 15$ to sample the
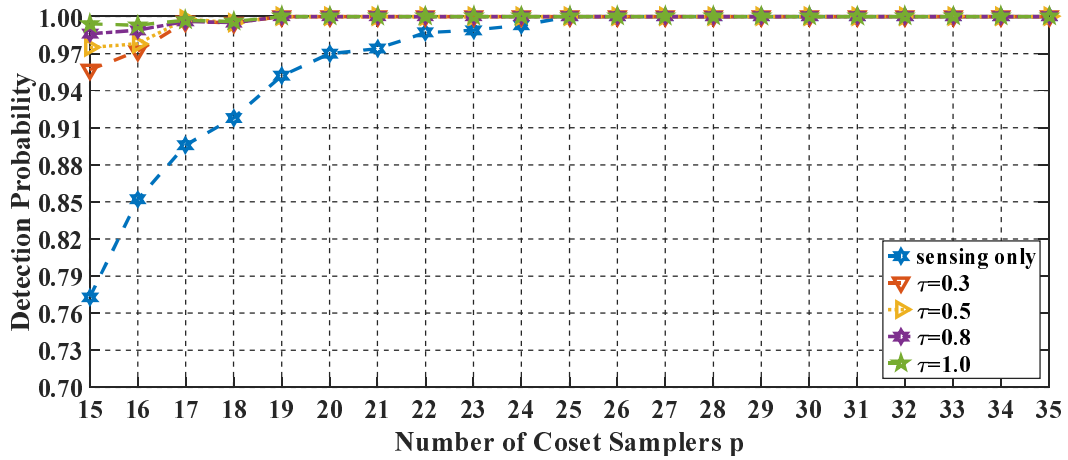
Figure 5.8: Detection Probability P_d vs. number of coset samplers p under different ratio of known part $\tau = 0.3, 0.5, 0.8, 1.0$ and sensing only.
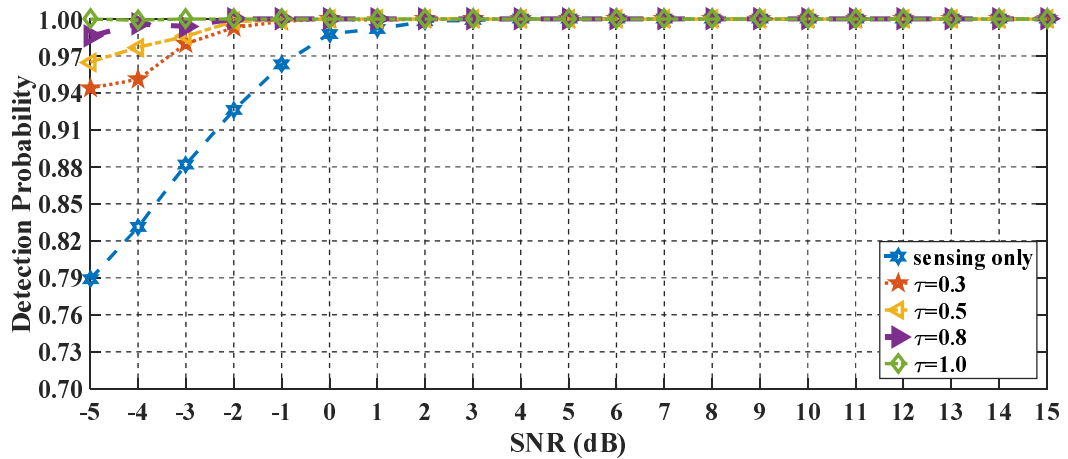
Figure 5.9: Detection Probability P_d vs. number of SNR (dB) under different ratio of known part $\tau = 0.3, 0.5, 0.8, 1.0$ and sensing only.

received signals. As shown in Fig. 5.9, the detection performance of the proposed joint sensing scheme utilizing different ratio of known part τ is always superior to that of the sensing only, especially more sensitive to the low SNR region.

5.5.2.3 Detection Performance with the Partially Incorrect Prior Information in the Geo-location Database

Both Fig. 5.8 and Fig. 5.9 follow that the prior information from geo-location database is correct for all given channels. As stated in Section IV, it may be the case that
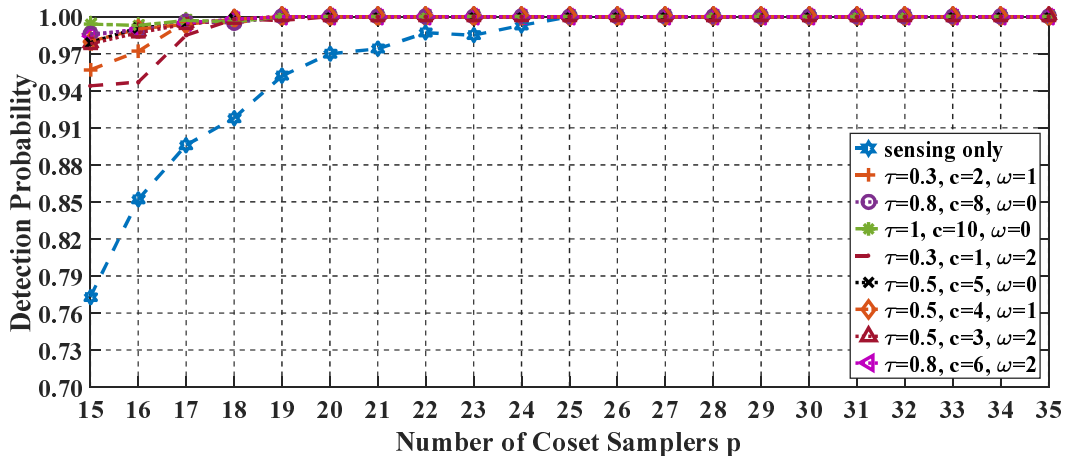
Figure 5.10: Detection Probability P_d vs. number of coset samplers p under different ratio of known part with partially incorrect prior information and sensing only.

the information from geo-location database is not fully reliable, e.g., some of the channel occupancy states are changed but the geo-location database has not been updated timely. In this situation, the proposed joint sensing scheme can still recover the actual signals since it could remove the incorrect elements in $\mathcal{T}$ from the minimization problem, but more cost samplers are adopted compared with the case when no errors are present in $\mathcal{T}$.

In Fig. 5.10, the cases in which $\mathcal{T}$ contains some incorrect prior information are simulated, which means that apart from the c channels correctly belonging to the support, there are ω out of $\tau|\mathcal{S}|$ channels in $\mathcal{T}$ that do not belong to the current signal support. The simulation setting is same as that in Fig. 5.8 and Fig. 5.9, but with different combinations of c and ω in $\mathcal{T}$. As shown in the Fig. 5.10, the proposed scheme can still reconstruct the underlying signals and shows an improvement in detection performance with respect to the case with no prior information.
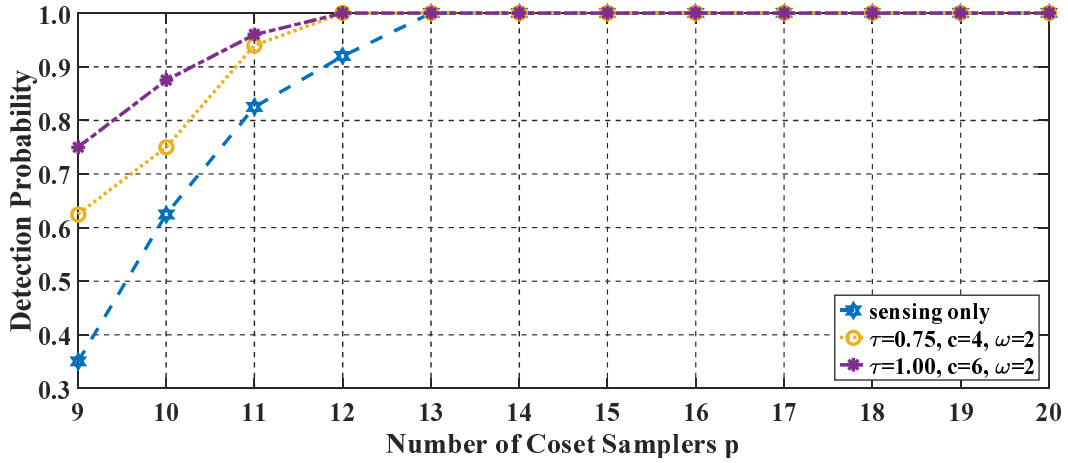
Figure 5.11: Detection Probability P_d vs. number of coset samplers p under different ratio of known part with partially incorrect prior information over real-world signals.

5.5.2.4 Detection Performance with the Partially Incorrect Prior Information in the Geo-location Database over Real-world Signal

Finally, we apply the proposed scheme on the collected real-world signal to validate the proposed scheme in the practical environment. It is shown in Fig. 5.11 that the proposed scheme could recover the spectrum even with the partially incorrect prior information from the geo-location database and the detection performance of the proposed joint sensing scheme still is superior to that of the sensing only.

5.6   Summary

In this chapter, we proposed a blind joint sub-Nyquist wideband spectrum sensing scheme for cognitive IoT, which only requires the low-rate ADCs in the wireless IoT devices which have cognitive capabilities. Without the prior knowledge of the number of occupied channels and the level of SNRs, the proposed scheme could blindly select sufficient number of coset samplers to achieve desired sensing performance. To further reduce the required number of the coset samplers, the processing complexity and the energy consumption over the evolved IoT devices, we proposed to incorporate the channel occupancy infor-

mation from the geo-location database and the wideband signal reconstruction process. Moreover, with the awareness that the information from geo-location is not fully reliable, the proposed scheme could reconstruct the signal with partially correct information and return the newly updated information to databases. Experimental results have shown that the proposed scheme could not only utilize the minimum number of coset samplers without known number of occupied channels but also guarantee the desired detection performance under wide range of SNRs. Moreover, the performance of the proposed scheme assisted with geo-location database is superior to the sensing only method even when the obtained information is partially correct, especially in low SNR region. These benefits from the proposed scheme make it be a good candidate for the large-scale deployment of the power constrained IoT devices and spectrum management.

Chapter 6

Conclusions and Future Work

6.1 Summary

With turning IoT paradigm into a reality, the amount of IoT devices are expected to grow in large numbers, which leads to difficulty in allocating sufficient spectrum resource to these devices. Therefore, it is the vision that smart IoT devices should have cognitive capabilities to enable spectrum sharing over wideband spectrum [8, 9]. With cognitive capabilities, interference among the IoT devices can be alleviated by seeking vacant channels through dynamic spectrum access [10]. Compared with conventional wideband spectrum sensing scheme, compressive sensing (CS) based sub-Nyquist wideband spectrum sensing can enable fast and accurate spectrum detection with sub-Nyquist sampling rates by exploiting the sparse nature of the underutilized wideband spectrum in practice. This thesis presents several algorithms that implement wideband spectrum sensing with CS, aiming to invoking the efficient usage of the underutilized spectrum in cognitive IoT scenarios.

In Chapter 3, to achieve fast reconstruction from the compressive samples, an adaptively-regularized iterative reweighted least squares (AR-IRLS) algorithm has been proposed to implement the CS-based wideband spectrum sensing with a high fidelity guarantee,

which could cope with varying bandwidths and power levels in real-world signals. The proposed algorithm was tested over the real-world measurements after having been validated by the simulated signals with random supports and amplitudes. Numerical results showed that the convergence speed of the proposed reconstruction algorithm has been increased by up to 70% in comparison with the conventional iterative reweighted least squares (IRLS) algorithms, which makes the proposed AR-IRLS algorithm more efficient over shared spectrums such as TV white space (TVWS). To further reduce the computational complexity of signal reconstruction, a low-complexity compressive spectrum sensing algorithm is proposed. It could keep the fast convergence speed of the previous algorithms such as [14] and AR-IRLS with reduced computational complexity by exploiting the diagonally dominant feature in the square of measurement matrix. Moreover, a descent-based algorithm has been proposed to distinguish the primary signals from the mixture of reconstruction errors and unknown noises, by dynamically setting the threshold without prior knowledge of the noise power.

In Chapter 4, a blind CS-based sensing algorithm is proposed to enable the local SUs to automatically choose the minimum sensing time without knowledge of spectral sparsity or channel characteristics. The compressive samples are collected block-by-block in time and SUs can adaptively adjust the sensing time or sampling rate afterwards. Moreover, a CS-based blind cooperating user selection algorithm is proposed to select the cooperating SUs via indirectly measuring the degeneration of signal-to-noise ratio (SNR) experienced by different SUs. Numerical and real-world test results demonstrate that the proposed algorithms achieve high detection performance with reduced sensing time and number of cooperating SUs in comparison with the conventional compressive spectrum sensing algorithms.

Finally, in Chapter 5, a distributed sub-Nyquist sensing scheme is proposed by utilizing the surround IoT devices to jointly sample the spectrum based on multi-coset sampling theory. Thus, only the low-rate ADCs are required on the IoT devices to form coset samplers. Without prior knowledge of the number of occupied channels and

the level of SNRs, the proposed scheme could blindly select sufficient number of coset samplers to achieve desired sensing performance. To further reduce the required number of the coset samplers, the processing complexity and the energy consumption over the evolved IoT devices, we proposed to incorporate the channel occupancy information from the geo-location database and the wideband signal reconstruction process. Moreover, with the awareness that the information from geo-location is not fully reliable, the proposed scheme could reconstruct the signal with partially incorrect information and return the newly updated information to databases. Experimental results have shown that the proposed scheme could not only utilize the minimum number of coset samplers without known number of occupied channels but also guarantee the desired detection performance under wide range of SNRs. Moreover, the performance of the proposed scheme assisted with geo-location database is superior to the sensing only method even when the obtained information is partially correct.

6.2 Future work

Apart from the IoT application, the machine-to-machine (M2M) communications and mobile broadband communication beyond 5G would have the demand for more available spectrum, especially for sub-1GHz which has good penetration capability. The sub-Nyquist wideband spectrum sensing can be extended to these areas to assist the spectrum access. Moreover, the sub-Nyquist enabled cognitive IoT system should have the capability to compress other sensor information for compact communication and data analysis. In this section, we also identify the following research challenges that need to be addressed in the future work.

6.2.1 Limitations of work under Practical Imperfections

Most of current compressive wideband sensing techniques including the proposed work in this thesis assume relatively ideal operating conditions in terms of noise, channel,

and hardware components. However, the performance of proposed works over practical environments should be further investigated under the compressive spectrum sensing scenario, such as fading channels, frequency selective channels, and noise uncertainty. In chapter 4, we assume that the spectrum occupancy status would not change during the sensing period. However, the time of signal reconstruction in each iteration would increase the total time for sensing, in which the wideband signal might not be static. In chapter 5, the assumption of wideband signals is that the bandwidth of each channel is equal in consistency of TVWS. However, in other shared spectrum, the bandwidth of available channels might be different and varying. Moreover, the accuracy requirement of time synchronization among cognitive IoT device is relatively high because of the requirements of multi-coset sampling. In chapter 6, the vectorization of matrix is required, which could increase the computational complexity of the proposed scheme.

6.2.2 Spectrum Data or Decision Fusion from Massive IoT devices

Since numerous IoT devices would joint the network, novel data or decision fusion techniques are necessary to reduce the transmission overhead and extract the reliable information from the massive IoT devices. Instead of scanning all channels and sending each channel's status to the fusion centre, each SU, equipped with a frequency selective filter, senses a linear combination of multiple channels. The filter coefficients are designed to be random numbers to mix different channel information. The support of the wideband signals is then recovered at the fusion centre from the incomplete samples sent by the SUs through matrix completion, which utilise the matrix's low rank property. Apart from the matrix completion techniques, cooperating device selection algorithms should be developed to select only a few number of IoT devices for spectrum sensing during a period of time by considering the channel environment, position, energy constraint, etc.

6.2.3 Channel Energy Statistics Learning in Compressive Spectrum Sensing

Most existing literature discusses Neyman-Pearson channel energy detection and threshold adaption schemes to achieve optimal performance of detection in conventional non-compressive spectrum sensing scenario. However, in the compressive spectrum sensing, it is found that the channel energy statistics and optimal threshold not only depend on noise energy but also compression ratio, sparsity of spectrum, and nature of recovery algorithms. Therefore, it is important to investigate the channel energy statistics of recovered spectrum and propose practical threshold adaption scheme.

References

[1] Z. Tian and G. B. Giannakis, "A wavelet approach to wideband spectrum sensing for cognitive radios," in *Proc. IEEE Int. conf. on Cognitive radio oriented wireless networks and communications (CROWNCOM)*, Mykonos Island, Jun. 2006, pp. 1–5.

[2] Z. Quan, S. Cui, A. H. Sayed, and H. V. Poor, "Optimal multiband joint detection for spectrum sensing in cognitive radio networks," *IEEE Trans. Signal Process.*, vol. 57, no. 3, pp. 1128–1140, Mar. 2009.

[3] T. Yucek and H. Arslan, "A survey of spectrum sensing algorithms for cognitive radio applications," *IEEE Commun. Surveys Tutorials*, vol. 11, no. 1, pp. 116–130, Jan. 2009.

[4] B. Farhang-Boroujeny, "Filter bank spectrum sensing for cognitive radios," *IEEE Trans. Signal Process.*, vol. 56, no. 5, pp. 1801–1811, May 2008.

[5] M. Mishali and Y. C. Eldar, "From theory to practice: Sub-nyquist sampling of sparse wideband analog signals," *IEEE J. Sel. Signal Process.*, vol. 4, no. 2, pp. 375–391, Apr. 2010.

[6] ——, "Blind multiband signal reconstruction: compressed sensing for analog signals," *IEEE Trans. Signal Process.*, vol. 57, no. 3, pp. 993–1009, Mar. 2009.

[7] Y. Gao, Z. Qin, Z. Feng, Q. Zhang, O. Holland, and M. Dohler, "Scalable & reliable IoT enabled by dynamic spectrum management for M2M in LTE-A," *IEEE Internet of Things Journal*, vol. 3, no. 6, pp. 1135 – 1145, May 2016.

[8] Q. Wu, G. Ding, Y. Xu, S. Feng, Z. Du, J. Wang, and K. Long, "Cognitive internet of things: a new paradigm beyond connection," *IEEE Internet of Things Journal*, vol. 1, no. 2, pp. 129–143, Mar. 2014.

[9] J. A. Stankovic, "Research directions for the internet of things," *IEEE Internet of Things Journal*, vol. 1, no. 1, pp. 3–9, Mar. 2014.

[10] J. J. Meng, W. Yin, H. Li, E. Hossain, and Z. Han, "Collaborative spectrum sensing from sparse observations in cognitive radio networks," *IEEE J. Sel. Areas Commun.*, vol. 29, no. 2, pp. 327–337, Jan. 2011.

[11] D. L. Donoho, "Compressed sensing," *IEEE Trans. Inf. Theory*, vol. 52, no. 4, pp. 1289–1306, Apr. 2006.

[12] Z. Tian and G. B. Giannakis, "Compressed sensing for wideband cognitive radios," in *Proc. IEEE Int. conf. on Acoust., Speech and Signal Process. (ICASSP)*, Honolulu, HI, Apr. 2007, pp. 1357–1360.

[13] Z. Qin, Y. Gao, M. Plumbley, and C. Parini, "Wideband spectrum sensing on real-time signals at sub-Nyquist sampling rates in single and cooperative multiple nodes," *IEEE Trans. Signal Process.*, vol. 64, no. 12, pp. 3106–3117, Jun. 2016.

[14] Z. Qin, Y. Gao, and C. G. Parini, "Data-assisted low complexity compressive spectrum sensing on real-time signals under sub-Nyquist rate," *IEEE Trans. Wireless Commun.*, vol. 15, no. 2, pp. 1174–1185, Feb. 2016.

[15] A. Aijaz and A. H. Aghvami, "Cognitive machine-to-machine communications for Internet of Things: A protocol stack perspective," *IEEE Internet of Things Journal*, vol. 2, no. 2, pp. 103–112, Jan. 2015.

[16] V. N. I. Cisco, "Global mobile data traffic forecast update, 2015–2020," Feb. 2016.

[17] P. Rawat, K. D. Singh, and J. M. Bonnin, "Cognitive radio for M2M and Internet of Things: A survey," *Comput. Commun.*, vol. 94, pp. 1–29, Nov. 2016.

[18] I. F. Akyildiz, W.-Y. Lee, M. C. Vuran, and S. Mohanty, "A Survey on Spectrum Management in Cognitive Radio Networks," *IEEE Commun. Mag.*, vol. 46, no. 4, pp. 40–48, Apr. 2008.

[19] G. Ding, J. Wang, Q. Wu, Y.-D. Yao, F. Song, and T. A. Tsiftsis, "Cellular-Base-Station-Assisted Device-to-Device Communications in TV White Space," *IEEE J. Sel. Areas Commun.*, vol. 34, no. 1, pp. 107–121, Jan. 2016.

[20] F. Yang, J. Li, T. Lei, and S. Wang, "Architecture and key technologies for internet of vehicles: a survey," *Journal of Commun. and Inf. Netw.*, vol. 2, no. 2, pp. 1–17, Jun. 2017.

[21] J. Holdren and E. Lander, "Report to the President: Realizing the Full Potential of Government-Held Spectrum to Spur Economic Growth," Presidents Council Advisors Sci. Technol., Washington, DC, USA, Tech. Rep., 2012.

[22] Office of Commun. (Jul. 2009). *Digital dividend: cognitive access.*

[Online]. Available: http://stakeholders.ofcom.org.uk/binaries/consultations/ cognitive/statement/statement.pdf

[23] Agre, Jonathan R. and Gordon, Karen D. (Sept. 2015). *Summary of Recent Federal Government Activities to Promote Spectrum Sharing.* [Online]. Available: https://www.ida.org/idamedia/Corporate/Files/Publications/STPIPubs/ 2015/p5186final.pdf

[24] M. Fitch, M. Nekovee, S. Kawade, K. Briggs, and R. MacKenzie, "Wireless service provision in TV white space with cognitive radio technology: A telecom operator's perspective and experience," *IEEE Commun. Mag.*, vol. 49, no. 3, Mar. 2011.

[25] Office of Commun., "3.8 GHz to 4.2 GHz band: Opportunities for Innovation," Office of Commun., London, UK, Final Rep., Apr. 2016.

[26] Fed. Commun. Commission, "Amendment of the Commission's Rules with Regard to Commercial Operations in the 3550-3650 MHz Band," Washington, DC, USA, Tech. Rep. GN Docket No. 12-354, Apr. 2014.

[27] Office of Commun., "A framework for spectrum sharing," Office of Commun., London, UK, Final Rep., Apr. 2016.

[28] Office of Communications. (Nov. 2010). *Implementing Geolocation.* [Online]. Available: https://www.ofcom.org.uk/__data/assets/pdf_file/0035/ 46889/statement.pdf

[29] J. Mitola and G. Maguire JR., "Cognitive Radio: Making software radios more personal," *IEEE Pers. Commun.*, vol. 6, no. 4, pp. 13–18, Aug. 1999.

[30] H. Sun, A. Nallanathan, C.-X. Wang, and Y. Chen, "Wideband spectrum sensing for cognitive radio network: a survey," *IEEE Trans. Wireless Commun.*, vol. 20, no. 2, pp. 74–81, Apr. 2013.

[31] A. F. Eduardo and R. G. G. Caballero, "Experimental evaluation of performance for spectrum sensing: Matched filter vs energy detector," in *Proc. IEEE Colombian Conf. Commun. Comput.*, Popayan, Colombia, May 2015, pp. 1–6.

[32] W. Zhang, R. K. Mallik, and K. B. Letaief, "Optimization of cooperative spectrum sensing with energy detection in cognitive radio networks," *IEEE Trans. Wireless Commun.*, vol. 8, no. 12, pp. 5761–5766, Dec. 2009.

[33] Y. Zeng and Y.-C. Liang, "Eigenvalue-based spectrum sensing algorithms for cognitive radio," *IEEE Trans. Commun.*, vol. 57, no. 6, Jun.

[34] K. Kim, I. A. Akbar, K. K. Bae, J.-S. Um, C. M. Spooner, and J. H. Reed, "Cyclostationary Approaches to Signal Detection and Classification in Cognitive Radio," in *Proc. IEEE Int. Symp. on Dynamic Spectrum Access Networks (DySPAN)*, Dublin, Ireland, Apr. 2007, pp. 212–215.

[35] A. Ali and W. Hamouda, "Advances on spectrum sensing for cognitive radio networks: Theory and applications," *IEEE Commun. Surveys & Tutorials*, vol. 19, no. 2, pp. 1277–1304, Jun. 2017.

[36] B. Farhang-Boroujeny, "Filter Bank Spectrum Sensing for Cognitive Radios," *IEEE Trans. Signal Process.*, vol. 56, no. 5, pp. 1801–1811, May 2008.

[37] H. J. Landau, "Necessary density conditions for sampling and interpolation of certain entire functions," *Acta Mathematica*, vol. 117, no. 1, pp. 37-52, Jul. 1967.

[38] Z. Zhang, Y. Xu, J. Yang, X. Li, and D. Zhang, "A survey of sparse representation: algorithms and applications," *IEEE Access*, vol. 3, no. 7, pp. 490–530, May 2015.

[39] E. J. Candes and T. Tao, "Decoding by linear programming," *IEEE Trans. Inf. Theory*, vol. 51, no. 12, pp. 4203–4215, Dec. 2005.

[40] E. J. Candès, J. Romberg, and T. Tao, "Robust uncertainty principles: Exact signal reconstruction from highly incomplete frequency information," *IEEE Trans. Inf. Theory*, vol. 52, no. 2, pp. 489–509, Feb. 2006.

[41] E. J. Candes, J. K. Romberg, and T. Tao, "Stable signal recovery from incomplete and inaccurate measurements," *Communications on pure and applied mathematics*, vol. 59, no. 8, pp. 1207–1223, 2006.

[42] E. J. Candes and J. Romberg, "Sparsity and Incoherence in Compressive Sampling," *Inverse Problems*, vol. 23, no. 3, pp. 969–985, Apr. 2007.

[43] J. A. Tropp, J. N. Laska, M. F. Duarte, J. K. Romberg, and R. G. Baraniuk, "Beyond nyquist: Efficient sampling of sparse bandlimited signals," *IEEE Trans. Inf. Theory*, vol. 56, no. 1, pp. 520–544, Jan. 2010.

[44] P. Feng and Y. Bresler, "Spectrum-blind minimum-rate sampling and reconstruction of multiband signals," in *Proc. IEEE Int. conf. on Acoust., Speech and Signal*

Process. (ICASSP), vol. 3, Atlanta, GA, May 1996, pp. 1688–1691.

[45] R. Venkataramani and Y. Bresler, "Optimal Sub-Nyquist Nonuniform Sampling and Reconstruction for Multiband Signals," *IEEE Trans. Signal Process.*, vol. 49, no. 10, pp. 2301–2313, Oct. 2001.

[46] A. Rosenthal, A. Linden, and M. Horowitz, "Multirate asynchronous sampling of sparse multiband signals," *JOSA A*, vol. 25, no. 9, pp. 2320–2330, 2008.

[47] M. Fleyer, A. Linden, M. Horowitz, and A. Rosenthal, "Multirate synchronous sampling of sparse multiband signals," *IEEE Trans. Signal Process.*, vol. 58, no. 3, pp. 1144–1156, 2010.

[48] H. Sun, W.-Y. Chiu, J. Jiang, A. Nallanathan, and H. V. Poor, "Wideband spectrum sensing with sub-Nyquist sampling in cognitive radios," *IEEE Trans. Signal Process.*, vol. 60, no. 11, pp. 6068–6073, Aug. 2012.

[49] J. A. Tropp and S. J. Wright, "Computational methods for sparse solution of linear inverse problems," *Proc. IEEE*, vol. 98, no. 6, pp. 948–958, Apr. 2010.

[50] D. L. Donoho, "For most large underdetermined systems of linear equations the minimal l_1-norm solution is also the sparsest solution," *Commun. Pure Appl. Math.*, vol. 59, no. 6, pp. 797–829, Mar. 2006.

[51] E. J. Candes and T. Tao, "Near-optimal signal recovery from random projections: Universal encoding strategies?" *IEEE Trans. Inf. Theory*, vol. 52, no. 12, pp. 5406–5425, Mar. 2006.

[52] R. Tibshirani, "Regression Shrinkage and Selection via the Lasso," *J. of the Roy. Stat. Soc. Series B (Methodological)*, vol. 58, no. 1, pp. 267–288, 1996.

[53] Z. Lu, "Iterative reweighted minimization methods for l_p regularized unconstrained nonlinear programming," *Math. Programm.*, vol. 147, no. 1-2, pp. 277–307, Aug. 2014.

[54] J. A. Tropp and A. C. Gilbert, "Signal Recovery From Random Measurements Via Orthogonal Matching Pursuit," *IEEE Trans. Inf. Theory*, vol. 53, no. 12, pp. 4655–4666, Dec. 2007.

[55] D. L. Donoho, Y. Tsaig, I. Drori, and J. L. Starck, "Sparse Solution of Underdetermined Systems of Linear Equations by Stagewise Orthogonal Matching Pursuit,"

IEEE Trans. Inf. Theory, vol. 58, no. 2, pp. 1094–1121, Feb. 2012.

[56] D. Needell and J. A. Tropp, "Cosamp: Iterative Signal Recovery From Incomplete and Inaccurate Samples," *Appl. and Comput. Harmonic Anal.*, vol. 26, no. 3, pp. 301–321, May 2009.

[57] M. Wang, W. Xu, and A. Tang, "On the performance of sparse recovery via l_p-minimization," *IEEE Trans. Inf. Theory*, vol. 57, no. 11, pp. 7255–7278, Nov. 2011.

[58] I. Daubechies, R. DeVore, and M. Fornasier, "Iteratively reweighted least squares minimization for sparse recovery," *Commun. Pure Appl. Math.*, vol. 63, no. 1, pp. 1–38, Jan. 2010.

[59] D. P. Wipf and B. D. Rao, "Sparse Bayesian learning for basis selection," *IEEE Trans. Signal Process.*, vol. 52, no. 8, pp. 2153–2164, Aug. 2004.

[60] D. P. Wipf, B. D. Rao, and S. Nagarajan, "Latent Variable Bayesian Models for Promoting Sparsity," *IEEE Trans. Inf. Theory*, vol. 57, no. 9, pp. 6236–6255, Sep. 2011.

[61] E. J. Candes, M. B. Wakin, and S. P. Boyd, "Enhancing sparsity by reweighted l_1 minimization," *J. Fourier Anal. Appl.*, vol. 14, no. 5-6, pp. 877–905, Oct. 2008.

[62] W. Chen, D. Wipf, Y. Wang, Y. Liu, and I. J. Wassell, "Simultaneous Bayesian sparse approximation with structured sparse models," *IEEE Trans. Signal Process.*, vol. 64, no. 23, pp. 6145–6159, Dec. 2016.

[63] Q. Ling, Z. Wen, and W. Yin, "Decentralized Jointly Sparse Optimization by Reweighted ℓ_q Minimization," *IEEE Trans. Signal Process.*, vol. 61, no. 5, pp. 1165–1170, Mar. 2013.

[64] J. Chen and X. Huo, "Theoretical Results on Sparse Representations of Multiple-Measurement Vectors," *IEEE Trans. Signal Process.*, vol. 54, no. 12, pp. 4634–4643, Dec. 2006.

[65] M. Fornasier and H. Rauhut, "Recovery Algorithms for Vector-valued Data with Joint Sparsity Constraints," *Society for Industrial and Appl. Math. J. on Numerical Analysis*, vol. 46, no. 2, pp. 577–613, Feb. 2008.

[66] Y. C. Eldar and M. Mishali, "Robust Recovery of Signals From a Structured Union

of Subspaces," *IEEE Trans. Inf. Theory*, vol. 55, no. 11, pp. 5302–5316, Nov. 2009.

[67] J. A. Tropp, A. C. Gilbert, and M. J. Strauss, "Simultaneous Sparse Approximation via Greedy Pursuit," in *Proc. IEEE Int. conf. on Acoust., Speech and Signal Process. (ICASSP)*, vol. 5, Philadelphia, PA, Mar. 2005, pp. v/721–v/724.

[68] D. Cohen, A. Akiva, B. Avraham, and Y. C. Eldar, "Centralized Cooperative Spectrum Sensing from Sub-Nyquist Samples for Cognitive Radios," in *Proc. IEEE Int. Conf. on Commun. (ICC)*, London, UK, Jun. 2015, pp. 7486–7491.

[69] Y. L. Polo, Y. Wang, A. Pandharipande, and G. Leus, "Compressive wide-band spectrum sensing," in *Proc. IEEE Int. conf. on Acoust., Speech and Signal Process. (ICASSP)*, Taipei, Apr. 2009, pp. 2337–2340.

[70] D. D. Ariananda and G. Leus, "Compressive wideband power spectrum estimation," *IEEE Trans. Signal Process.*, vol. 60, no. 9, pp. 4775–4789, Sept. 2012.

[71] G. Leus and D. D. Ariananda, "Power spectrum blind sampling," *IEEE Signal Process. Lett.*, vol. 18, no. 8, pp. 443–446, Aug. 2011.

[72] M. Mishali and Y. C. Eldar, "Blind multiband signal reconstruction: compressed sensing for analog signals," *IEEE Trans. Signal Process.*, vol. 57, no. 3, pp. 993–1009, Mar. 2009.

[73] Y. Ma, Y. Gao, Y.-C. Liang, and S. Cui, "Reliable and efficient sub-Nyquist wideband spectrum sensing in cooperative cognitive radio networks," *IEEE J. Sel. Areas Commun.*, vol. 34, no. 10, pp. 2750–2762, Oct. 2016.

[74] T. Xiong, H. Li, P. Qi, Z. Li, and S. Zheng, "Pre-decision for wideband spectrum sensing with sub-Nyquist sampling," *IEEE Trans. Veh. Technol.*, vol. PP, no. 99, pp. 1–1, Jan. 2017.

[75] P. Feng and Y. Bresler, "Spectrum-blind minimum-rate sampling and reconstruction of multiband signals," in *Proc. IEEE Int. conf. on Acoust., Speech and Signal Process. (ICASSP)*, vol. 3, Atlanta, GA, May 1996, pp. 1688–1691.

[76] Office of Commun. (Feb. 2015) *Programme Making and Special Events (PMSE)*. [Online]. Available: https://www.ofcom.org.uk/manage-your-licence/radiocommunication-licences/pmse/

[77] D. L. Donoho, M. Elad, and V. N. Temlyakov, "Stable recovery of sparse overcomplete representations in the presence of noise," *IEEE Trans. Inf. Theory*, vol. 52, no. 1, pp. 6–18, Jan. 2006.

[78] R. Chartrand and V. Staneva, "Restricted isometry properties and nonconvex compressive sensing," *Inverse Problems*, vol. 24, no. 035020, pp. 1–14, May 2008.

[79] J. Salt and H. Nguyen, "Performance prediction for energy detection of unknown signals," *IEEE Trans. Veh. Technol.*, vol. 57, no. 6, pp. 3900–3904, Nov. 2008.

[80] S. Atapattu, C. Tellambura, H. Jiang, and N. Rajatheva, "Unified analysis of low-SNR energy detection and threshold selection," *IEEE Trans. Veh. Technol.*, vol. 64, no. 11, pp. 5006–5019, Nov. 2015.

[81] N. Wang, Y. Gao, and X. Zhang, "Adaptive spectrum sensing algorithm under different primary user utilizations," *IEEE Commun. Lett.*, vol. 17, no. 9, pp. 1838–1841, Sept. 2013.

[82] S. Yoon, L. E. Li, S. C. Liew, R. R. Choudhury, I. Rhee, and K. Tan, "Quicksense: Fast and energy-efficient channel sensing for dynamic spectrum access networks," in *Proc. IEEE Int. conf. on Comput. Commun. (INFOCOM)*, Turin, Italy, Apr. 2013, pp. 2247–2255.

[83] Y. Ma, Y. Gao, A. Cavallaro, C. G. Parini, W. Zhang, and Y.-C. Liang, "Sparsity independent sub-Nyquist rate wideband spectrum sensing on real-time TV white space," *IEEE Trans. Veh. Technol.*, vol. PP, no. 99, pp. 1–1, Apr. 2017.

[84] Z. Xu, X. Chang, F. Xu, and H. Zhang, "$l_{1/2}$ regularization: A thresholding representation theory and a fast solver," *IEEE Trans. Neural Netw. Learn. Syst.*, vol. 23, no. 7, pp. 1013–1027, Jul. 2012.

[85] X. Zhou, R. Molina, F. Zhou, and A. K. Katsaggelos, "Fast iteratively reweighted least squares for l_p regularized image deconvolution and reconstruction," in *Proc. IEEE Int. conf. on on Image Process. (ICIP)*, Paris, France, Oct. 2014, pp. 1783–1787.

[86] J. Yang, J. Wright, T. S. Huang, and Y. Ma, "Image super-resolution via sparse representation," *IEEE Trans. Image Process.*, vol. 19, no. 11, pp. 2861–2873, Nov. 2010.

[87] R. M. Mersereau and S. J. Reeves, "Optimal estimation of the regularization parameter and stabilizing functional for regularized image restoration," *Opt. Eng.*, vol. 29, no. 5, pp. 446–454, May 1990.

[88] N. P. Galatsanos and A. K. Katsaggelos, "Methods for choosing the regularization parameter and estimating the noise variance in image restoration and their relation," *IEEE Trans. Image Process.*, vol. 1, no. 3, pp. 322–336, Jul. 1992.

[89] F. Cao, M. Cai, Y. Tan, and J. Zhao, "Image super-resolution via adaptive l_p $(0 < p < 1)$ regularization and sparse representation," *IEEE Trans. on Neural Networks. and Learning Syst.*, vol. 27, no. 7, pp. 1550–1561, Jul. 2016.

[90] X. Zhang, Y. Ma, and Y. Gao, "Adaptively regularized compressive spectrum sensing from real-time signals to real-time processing," in *Proc. IEEE Global Commun. Conf. (GLOBECOM)*, Washington, D.C., Dec. 2016.

[91] M. G. Kang and A. K. Katsaggelos, "General choice of the regularization functional in regularized image restoration," *IEEE Trans. Image Process.*, vol. 4, no. 5, pp. 594–602, May 1995.

[92] Z. Ye, G. Memik, and J. Grosspietsch, "Energy detection using estimated noise variance for spectrum sensing in cognitive radio networks," in *Proc. IEEE Wireless Commun. Netw. Conf. (WCNC)*, Las Vegas, NV, Mar. 2008, pp. 711–716.

[93] Y. Saad, *Iterative Methods for Sparse Linear Systems*. SIAM, 2009.

[94] National Instruments. (Oct. 2016). *LabVIEW System Design Software*. [Online]. Available: http://www.ni.com/labview/

[95] S. Dikmese, Z. Ilyas, P. Sofotasios, M. Renfors, and M. Valkama, "Novel frequency domain cyclic prefix autocorrelation based compressive spectrum sensing for cognitive radio," in *Proc. IEEE Int. conf. on Vehicular Technology (VTC-Spring)*, Nanjing, China, May 2016, pp. 1–6.

[96] S. Dikmese, Z. Ilyas, P. C. Sofotasios, M. Renfors, and M. Valkama, "Sparse frequency domain spectrum sensing and sharing based on cyclic prefix autocorrelation," *IEEE J. Sel. Areas Commun.*, vol. 35, no. 1, pp. 159–172, Jan. 2017.

[97] Y. Ma, X. Zhang, and Y. Gao, "Joint Sub-Nyquist Spectrum Sensing Scheme with Geolocation Database over TV White Space," *IEEE Trans. Veh. Technol.*, Dec.

2017 (To appear).

[98] Y. Wang, Z. Tian, and C. Feng, "Sparsity order estimation and its application in compressive spectrum sensing for cognitive radios," *IEEE Trans. Wireless Commun.*, vol. 11, no. 6, pp. 2116–2125, Jun. 2012.

[99] X. Zhang, Z. Qin, and Y. Gao, "Dynamic adjustment of sparsity upper bound in wideband compressive spectrum sensing," in *Proc. IEEE Int. conf. on Signal and Inf. Process. (GlobalSIP)*, Atlanta, GA, Dec. 2014, pp. 1214–1218.

[100] J. Jiang, H. Sun, D. Baglee, and H. V. Poor, "Achieving autonomous compressive spectrum sensing for cognitive radios," *IEEE Trans. Veh. Technol.*, vol. 65, no. 3, pp. 1281–1291, Mar. 2016.

[101] Y. Selén, H. Tullberg, and J. Kronander, "Sensor selection for cooperative spectrum sensing," in *Proc. IEEE Int. Symp. on Dynamic Spectrum Access Networks (DySPAN)*, Chicago, Oct. 2008, pp. 1–11.

[102] Z. Khan, J. Lehtomaki, K. Umebayashi, and J. Vartiainen, "On the selection of the best detection performance sensors for cognitive radio networks," *IEEE Signal Process. Lett.*, vol. 17, no. 4, pp. 359–362, Apr. 2010.

[103] A. S. Cacciapuoti, I. F. Akyildiz, and L. Paura, "Correlation-aware user selection for cooperative spectrum sensing in cognitive radio ad hoc networks," *IEEE J. Sel. Areas Commun.*, vol. 30, no. 2, pp. 297–306, Feb. 2012.

[104] Q.-T. Vien, H. X. Nguyen, R. Trestian, P. Shah, and O. Gemikonakli, "A hybrid double-threshold based cooperative spectrum sensing over fading channels," *IEEE Trans. Wireless Commun.*, vol. 15, no. 3, pp. 1821–1834, Nov. 2016.

[105] Q. Song and W. Hamouda, "Performance analysis and optimization of multiselective scheme for cooperative sensing in fading channels," *IEEE Trans. Veh. Technol.*, vol. 65, no. 1, pp. 358–366, Jan. 2016.

[106] X. Zhang, Y. Ma, and Y. Gao, "Autonomous compressive spectrum sensing approach for 3.5 GHz shared spectrum," in *Proc. IEEE Int. conf. on Signal and Inf. Process. (GlobalSIP)*, Washington, D.C., Dec. 2016.

[107] J. Matoušek, "On variants of the johnson-lindenstrauss lemma," *Random Struct. & Algorithms*, vol. 33, no. 2, pp. 142–156, Sep. 2008.

[108] Y.-C. Liang, Y. Zeng, E. C. Y. Peh, and A. T. Hoang, "Sensing-throughput tradeoff for cognitive radio networks," *IEEE Trans. Wireless Commun.*, vol. 7, no. 4, pp. 1326–1337, Apr. 2008.

[109] S. M. Mishra, A. Sahai, and R. W. Brodersen, "Cooperative sensing among cognitive radios," in *Proc. IEEE Int. Conf. on Commun. (ICC)*, Malaysia, Jun. 2006, pp. 1658–1663.

[110] L. Lu, X. Zhou, U. Onunkwo, and G. Y. Li, "Ten years of research in spectrum sensing and sharing in cognitive radio," *EURASIP Journal on Wireless Commun. and Netw.*, vol. 2012, no. 1, p. 28, Jan. 2012.

[111] X. Zhang, Y. Ma, Y. Gao, and S. Cui, "Real-time adaptively-regularized compressive sensing in cognitive radio networks," *IEEE Trans. Veh. Technol.*, vol. PP, no. 99, pp. 1–1, 2017.

[112] S. Dikmese, P. C. Sofotasios, M. Renfors, and M. Valkama, "Maximum-minimum energy based spectrum sensing under frequency selectivity for cognitive radios," in *Cognitive Radio Oriented Wireless Networks and Communications (CROWN-COM), 2014 9th International Conference on*, Oulu, Finland, Jun. 2014, pp. 347–352.

[113] A. Sahai and D. Cabric, "Spectrum sensing: fundamental limits and practical challenges," in *Proc. IEEE Int. Conf. Dyn. Spectr. Access Netw. (DySPAN)*, Baltimore, MD, Dec. 2005.

[114] Y. Pei, Y.-C. Liang, K. C. Teh, and K. H. Li, "Energy-Efficient Design of Sequential Channel Sensing in Cognitive Radio Networks: Optimal Sensing Strategy, Power Allocation, and Sensing Order," *IEEE J. Sel. Areas Commun.*, vol. 29, no. 8, pp. 1648–1659, Sep. 2011.

[115] M. R. Palattella, M. Dohler, A. Grieco, G. Rizzo, J. Torsner, T. Engel, and L. Ladid, "Internet of things in the 5G era: Enablers, architecture, and business models," *IEEE J. Sel. Areas Commun.*, vol. 34, no. 3, pp. 510–527, Feb. 2016.

[116] C. J. Miosso, R. von Borries, and J. Pierluissi, "Compressive sensing with prior information: Requirements and probabilities of reconstruction in l_0-minimization,"

IEEE Trans. Signal Process., vol. 61, no. 9, pp. 2150–2164, May 2013.

[117] N. Vaswani and W. Lu, "Modified-CS: Modifying compressive sensing for problems with partially known support," *IEEE Trans. Signal Process.*, vol. 58, no. 9, pp. 4595–4607, Feb. 2010.

[118] B. Nielson and D. R. Cox, *Asymptotic Techniques for Use in Statistics*, 1st ed. London; New York: Chapman and Hall/CRC, 1989.

[119] J. Chen and X. Huo, "Theoretical Results on Sparse Representations of Multiple-Measurement Vectors," *IEEE Trans. Signal Process.*, vol. 54, no. 12, pp. 4634–4643, Dec. 2006.

[120] J. A. Tropp, A. C. Gilbert, and M. J. Strauss, "Simultaneous sparse approximation via greedy pursuit," in *Proc. IEEE Int. conf. on Acoust., Speech and Signal Process. (ICASSP)*, Philadelphia, PA, Mar. 2005.

[121] J. F. Determe, J. Louveaux, L. Jacques, and F. Horlin, "On the exact recovery condition of simultaneous orthogonal matching pursuit," *IEEE Signal Process. Lett.*, vol. 23, no. 1, pp. 164–168, Jan. 2016.